

**Cytochromes P450 - from model compounds towards  
artificial hemoproteins**

**INAUGURALDISSERTATION**

zur

Erlangung der Würde eines Doktors der Philosophie

vorgelegt der

**Philosophisch-Naturwissenschaftlichen Fakultät  
der Universität Basel**



von

**Dominik Büttiker (Geb. Meyer)**

aus

**Basel, Schweiz**

**Basel 2007**



Genehmigt von der Philosophisch-Naturwissenschaftlichen Fakultät auf Antrag der Herren:

Prof. Dr. Wolf-Dietrich Woggon

Prof. Dr. Edwin Constable

Basel, den 22. Mai 2007

Prof. Dr. Hans-Peter Hauri (Dekan)



Für Selina



# Table of Contents

## Theoretical Part

<b>1</b>	<b>Introduction .....</b>	<b>1</b>
1.1	Heme Proteins .....	1
1.2	The P450 Super-Family .....	1
1.3	The Catalytic Cycle of Cytochromes P450.....	4
1.4	Model Compounds.....	7
1.5	Selected P450s and their Reactivity.....	10
1.5.1	C-C bond cleavage in P450 <sub>scc</sub> (CYP 11A1) and P450 <sub>Biol</sub> (CYP107H1) .....	10
1.5.2	P450 <sub>BM-3</sub> (CYP 102A1) and enzyme engineering.....	14
<b>2</b>	<b>Description of the Aims of this Work .....</b>	<b>17</b>
2.1	Establishment of a new Class of Model Compounds .....	17
2.2	Modification of the Natural Cofactor .....	18
<b>3</b>	<b>Results and Discussion .....</b>	<b>19</b>
3.1	Synthesis of the new Model Compounds.....	19
3.1.1	Support for the SO <sub>3</sub> <sup>-</sup> Strategy by DFT Calculations .....	19
3.1.2	Design and Synthetic Strategy .....	20
3.1.3	Synthesis.....	22
3.2	Characterisation of the new Model Compounds.....	28
3.2.1	Physical and Spectroscopic Properties .....	28
3.2.2	Iron(II)-state .....	31
3.2.3	CpdI Analogues ((porph <sup>•+</sup> )Fe <sup>IV</sup> =O) .....	32
3.3	Epoxidation of Alkenes.....	34
3.4	Demethylation of Amines .....	36
3.5	Cleavage of Diols.....	39
3.6	Nitric Oxide Binding.....	42
3.7	Modification of the Natural Cofactor .....	50
3.7.1	Design and Synthetic Strategy .....	50
3.7.2	First Findings and adapted Approaches .....	53
3.7.3	Chlorination of Mesoporphyrin Derivatives .....	54
3.8	Characterisation and Application of the modified Cofactor .....	58

3.8.1	Characterisation of Iron Complexes 92 and 93 .....	58
3.8.2	Sulfur Coordination.....	62
3.8.3	Reactivity .....	64
<b>4</b>	<b>Summary and Conclusions .....</b>	<b>65</b>

## Experimental Part

<b>5</b>	<b>Experimental Part .....</b>	<b>67</b>
5.1	General Remarks.....	67
5.1.1	Solvents and Reagents.....	67
5.1.2	Materials & Instruments.....	67
5.1.3	Chromatographic Methods .....	68
5.1.4	Spectroscopic Methods .....	69
5.1.5	Elemental Analysis.....	71
5.1.6	Electrochemical methods .....	71
5.2	Syntheses.....	72
5.2.1	Porphyrin Model Compound Synthesis .....	72
5.2.2	Synthesis of Substrates, Co-oxidants and References for Catalytic Experiments	82
5.2.3	Catalytic Experiments applying Model Compounds .....	86
5.2.4	Protoporphyrin Derivative Synthesis .....	88
5.2.5	Catalytic Experiments applying the Modified Cofactor .....	96

## Appendix

<b>6</b>	<b>Appendix .....</b>	<b>97</b>
6.1	Abbreviations.....	97
6.2	References.....	99
6.3	Curriculum Vitae .....	105
6.4	Publications and Presentations.....	106
6.5	Eidesstattliche Erklärung .....	108



## **Theoretical Part**



# 1 Introduction

## 1.1 Heme Proteins

All over aerobic life on earth heme proteins play an essential role in accomplishing a vast variety of physiological functions. A common feature of all of these proteins is an iron(III) protoporphyrin IX cofactor (heme *b* (figure 1)) in the active site.

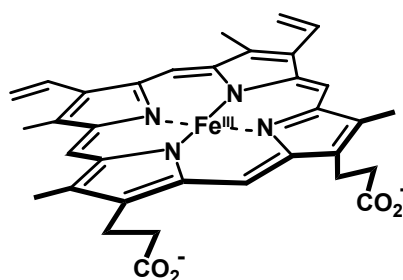


**Figure 1:** Iron (III) protoporphyrin IX (heme *b*)

The iron center of this moiety is coordinated by further ligands from the amino acid backbone varying from imidazole of Histidine in proteins such as *haemoglobin* and *myoglobin*, *peroxidases* and *cytochrome c Oxidase*, over tyrosine phenolate in *catalase* to cystein thiolate in *cytochromes P450*, *Chloroperoxidase* and *Nitric oxide Synthase*. In virtue of the nature of these additional ligands and the protein residues and architecture in the active site heme proteins gain their ability for exceptional diversity in functionality. Within the vast variety of enzymes mentioned, this work will mainly focus on the thiolate ligated enzyme family of *cytochromes P450* participating in oxidative transformation of substrates using molecular oxygen.

## 1.2 The P450 Super-Family

The discovery of cytochromes P450 started in the late 1950s when pigments of liver microsomes were isolated that displayed a strong absorption band at  $\lambda = 450$  nm in the visible spectrum for the reduced form in the presence of carbon monoxide.<sup>1,2</sup> This characteristic band also gave name to the “P450” and originates from the CO-complex of iron(II)-protoporphyrin IX in the active site. (figure 2)

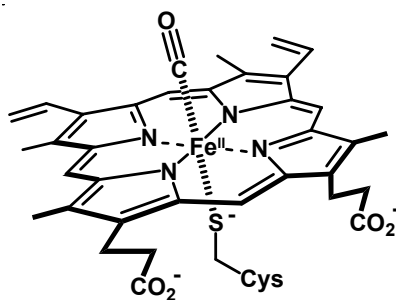


**Figure 2:** CO-complex of ferrous thiolate coordinated heme *b*

Ever since these findings a huge number of different P450 enzymes have been identified throughout all lifeforms,<sup>3</sup> from mammals, plants and fungi to bacteria, where they catalyse a huge variety of transformations. They therein vary strongly in substrate specificity from very selective P450s active in the biosynthesis of steroid hormones to P450s with a very broad substrate tolerance e.g. catalysing hydroxylation of exogenous substances in liver tissue thereby rendering them more water soluble and therefore better excretable.

P450s can catalyse reactions such as epoxidation of alkenes, heteroatom-dealkylation and -oxidation, hydrocarbon hydroxylation and carbon-carbon bond cleavage (*figure 3*).<sup>4</sup>

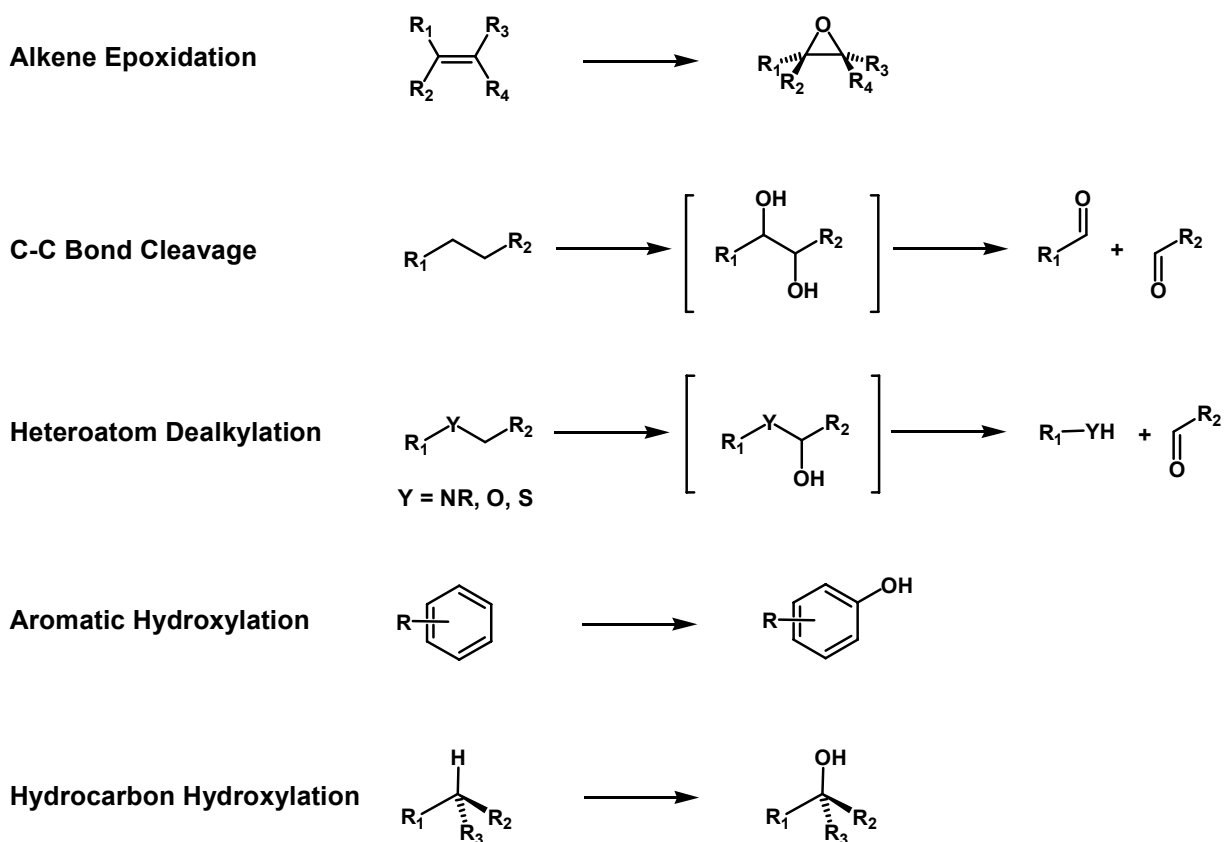
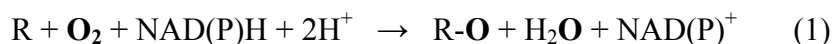


**Figure 3:** P450-catalysed reactions

In all these transformations, the P450s use molecular oxygen of which they incorporate only one oxygen atom into the substrate R (monooxygenase reaction). The required electrons for the generation of the active species (outlined in the catalytic cycle later on) are transferred from NAD(P)H to get an overall reaction as outlined in equation (1).



Cytochrome P450 have initially been classified according to the electron-transfer proteins which supply the oxygenase protein with electrons from NAD(P)H.<sup>5</sup>

**Class I:** most mitochondrial and bacterial P450s use a three protein arrangement in which electrons are transferred from NAD(P)H via a FAD containing flavoprotein reductase and an iron-sulfur ( $Fe_2S_2$ ) protein to the heme protein (*figure 4*). One of the best known and most studied members of this class is P450<sub>cam</sub>, a soluble cytosolic P450 isolated from soil bacterium *Pseudomonas Putida* which hydroxylates camphor stereoselectively as a first of several steps in energy supply. Being soluble and therefore handled rather easily compared to its membrane bound eukaryotic counterparts it has become the very prototype for P450s and has played a key role in elucidation of fundamental properties of P450s. It also was the first P450 to give a high-resolution X-ray structure.<sup>6</sup>

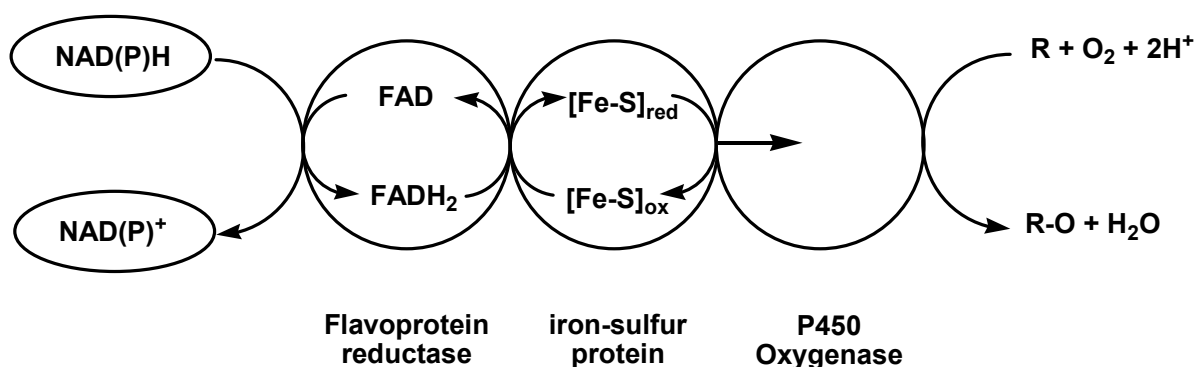


*Figure 4:* Electron transport in Class I P450s.

**Class II:** microsomal P450s are provided with electrons through a FAD- and FMN-containing reductase, where electrons from NAD(P)H are first transferred to FAD and afterwards consecutively donated to the oxygenase by FMN (*figure 5*). The first bacterial P450 characterized to be a class II P450 was P450<sub>BM-3</sub><sup>7</sup> isolated from *Bacillus megaterium*. In this enzyme the reductase- and heme-domain are fused as a self sufficient cytosolic fatty acid

hydroxylase. Due to similarity in the electron delivery system to mammal P450s, P50<sub>BM-3</sub> has become a well studied model system.<sup>8</sup>

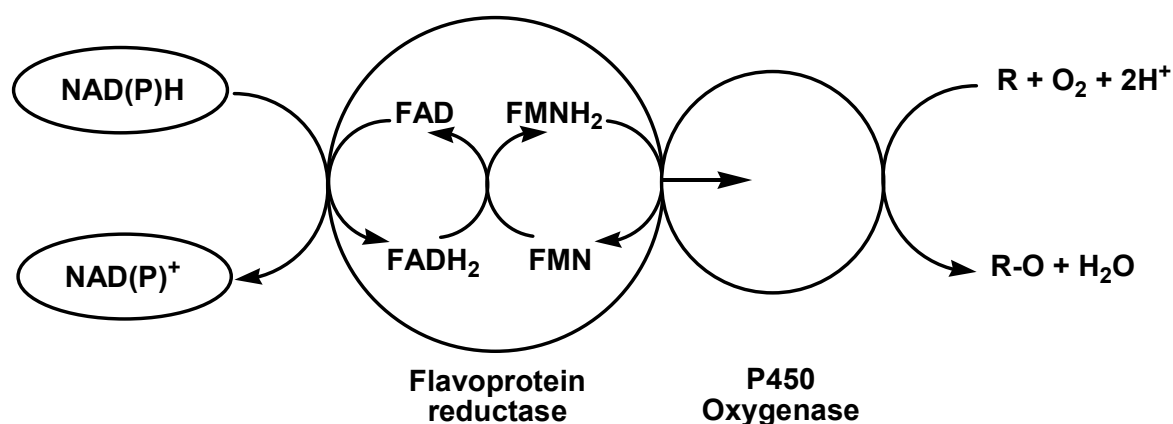


**Figure 5:** Electron transport in Class II P450s.

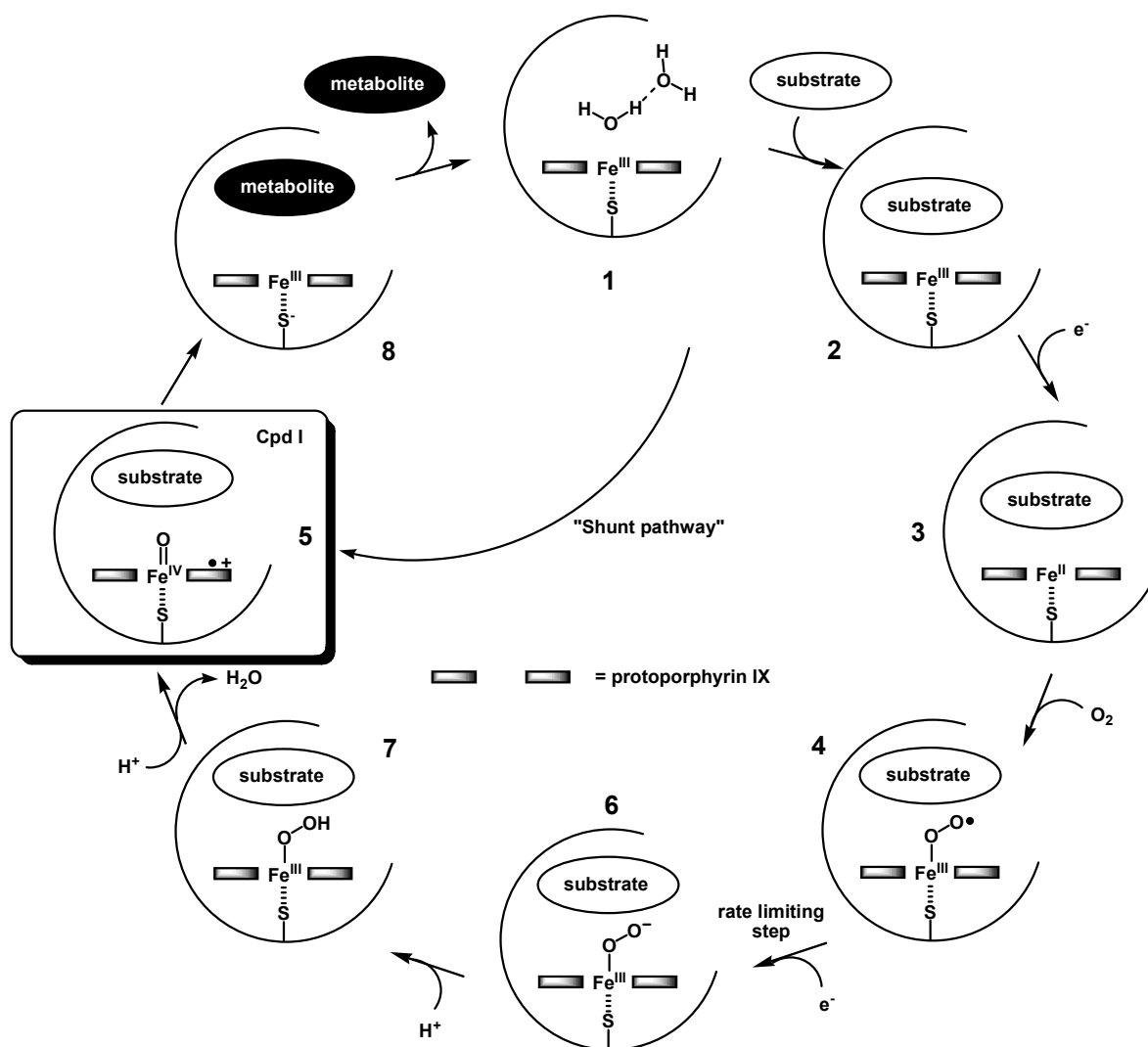
There are two more classes of P450s, **Class III** and **Class IV** which do not require any additional electron transport system as they react with peroxide-substrates in the first case (e.g. allen oxide synthase, thromboxane synthase)<sup>9,10</sup> or obtain their electrons from reduced pyridine-nucleotides in the latter (e.g. P450<sub>nor</sub>).<sup>11</sup>

Nomenclature of P450s was originally organized according to their physiological function. E.g. earlier mentioned P450<sub>cam</sub>, hydroxylating **cam**phor or a P450 involved in the cleavage of a side chain in steroid hormone synthesis called P450<sub>sec</sub> (**side chain cleavage**).

Nowadays,<sup>12</sup> P450s are classified according to the degree of similarity in their amino acid sequences. Going from the super-family (CYP) containing all known P450s, P450s branch into families ( $\geq 40\%$  similarity) and subfamilies ( $\geq 55\%$  similarity). Leading to systematical names such as e.g. CYP 11A1 for P450<sub>sec</sub> being member 1 of subfamily 11A of family 11.

### 1.3 The Catalytic Cycle of Cytochromes P450

Spectroscopic and crystallographic investigations on P450s (particularly on P450<sub>cam</sub>), as well as mechanistic studies applying labelled substrates and substrate analogues together with appliance of chemical model compounds have led to a consensus mechanism on the catalytic cycle of the cytochromes P450<sup>13</sup> displayed in *scheme 1*. Nevertheless several aspects of P450 mechanisms are still elusive and subject to broad debate.



**Scheme 1:** Catalytic cycle of cytochromes P450

The catalytic cycle is entered upon substrate binding to P450. This causes a shift in spin equilibrium from predominantly low spin in the resting state (1) to high spin in the substrate bound form (2). (The relative energy of orbitals and therefore spin state of the iron center atom strongly depends on coordinating ligands; see *figure 6* for a schematic illustration of possible electron distributions leading to different spin states in iron(III)-porphyrins.)

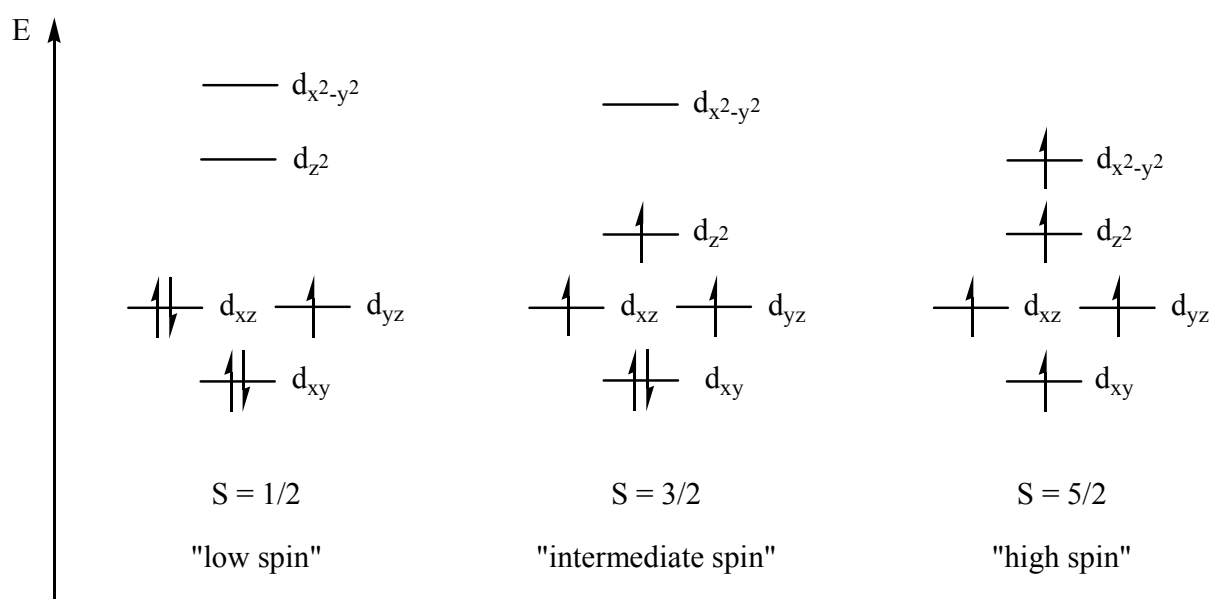


**Figure 6:** Possible distributions of the five d-electrons in Fe<sup>III</sup>-porphyrins leading to low spin (LS), intermediate spin (IS) or high spin (HS) configuration.

This modification in spin state alters the redox potential of the metal center from  $E_0 = -300$  to  $-170$  mV (vs. SHE), enabling electron transfer from the reductase and thus triggering the catalytic cycle. This remarkable tuning of redox potentials prevents entrance into the cycle and generation of active species in the absence of substrate.

In a second step one electron is donated to reduce the iron of the cofactor from the ferric (Fe<sup>III</sup>) to the ferrous (Fe<sup>II</sup>) form (3). Which can coordinate dioxygen to form a dioxygen adduct (4). Resonance Raman<sup>14</sup> and Mössbauer<sup>15</sup> spectroscopy both support the view of this intermediate as being a ferric superoxide (Fe<sup>III</sup>-O<sub>2</sub><sup>•-</sup>). The next step, donation of a second electron, being the rate limiting step in the catalytic cycle, all further intermediates have eluded direct detection so far and are hence still subject of debate. Studies on peroxidases have identified a green high valent iron oxo species, compound I (CpdI) (5) as the reactive species. Studies on P450s with external oxidants using the so-called “shunt pathway” (figure 7), as well as extensive studies on model compounds and theoretical approaches support a similar electrophilic species to be the active species in P450s. The latter is formed via double protonation of the intermediately formed iron (III)-peroxo complex (6) to form an iron (III) – hydroperoxo complex (7), also referred to as compound 0 (Cpd0), after the first protonation, and heterolytic cleavage of the O-O bond after second protonation to form water and (5). The



so formed reactive species then oxidizes the bound substrate, generating the metabolite and the ferric P450 (**8**) which can coordinate a new substrate and enter a new cycle.

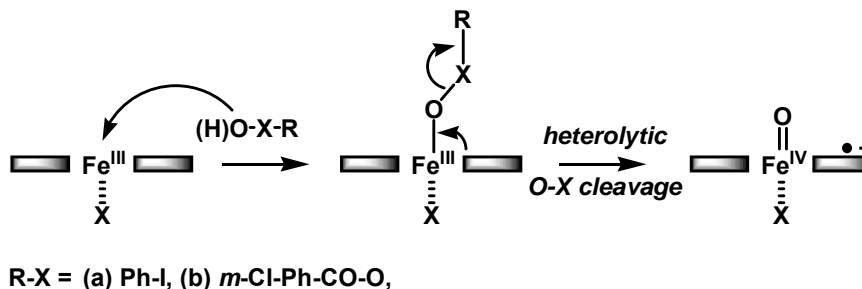


**Figure 7:** The shunt pathway of iron porphyrins applying oxidants such as (a) iodosobenzene or (b) *m*CPBA

The nature of the active species CpdI has been thoroughly studied and has been generally accepted to be an iron(IV)-oxo species having a positive charge (radical cation) on the aromatic ring of the porphyrin. Nevertheless CpdI is not the only possible active species and e.g. experimental findings<sup>16,17</sup> in hydrocarbon hydroxylation reactions, one of the most sophisticated and chemically interesting reactions of P450s, have provoked a “two oxidant” mechanism, where participation of Cpd0 as second oxidant together with CpdI was claimed to explain the obtained results. However further theoretical<sup>18,19</sup> as well as model compound studies<sup>20</sup> have shown that a “two state” mechanism referring to different spin states of CpdI can explain the earlier findings. Nevertheless in other P450-catalysed reactions, such as the aromatization of steroids by P450<sub>aromatase</sub>, nucleophilic iron(III)-peroxo species are indeed believed to participate in the reaction mechanism.

## 1.4 Model Compounds

As adumbrated in the above descriptions the appliance of chemical model compounds has been a valuable tool to investigate the properties of the P450s. Omitting the inherent complexity and lability of the natural system, these model systems are much more readily handled and studied. Therefore a large number of different model compounds have been developed over the years addressing different aspects in the field of P450 research (*figure 8*).<sup>21</sup>

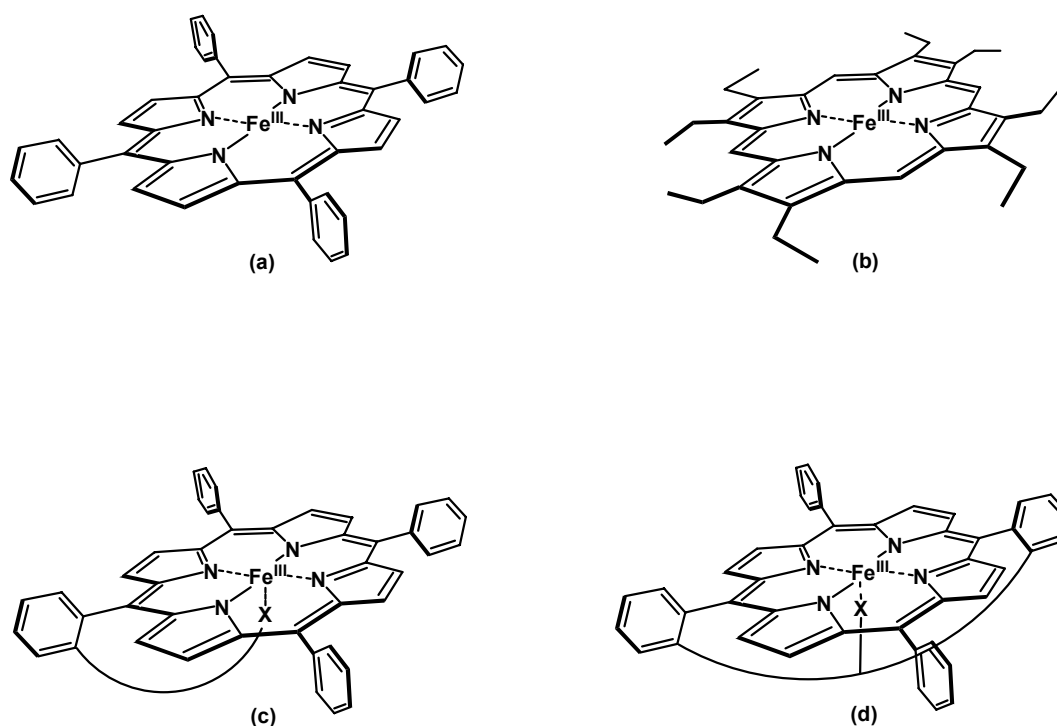


**Figure 8:** Different types of P450 model compounds.

They range from rather simple tetra-aryl- (a) and octa-alkyl-metal-porphyrins (b) to more elaborated models such as tailed (c) or strapped (d) metal-porphyrins. Each of these types of model compounds has its advantages and disadvantages, dependent on their field of application. The simpler compounds (a) and (b) are much easier obtained in shorter and higher yielding synthesis and are therefore often used in the field of catalysis. One of their major drawbacks in mimicking the natural system lies in the uncertainty of their axial ligands. In the tailed porphyrins, a covalently linked fifth ligand is introduced to ensure confident axial ligation; nevertheless these complexes still suffer from so-called “on-off” movement of the ligand<sup>22</sup> and possible oligomer formation.

Amending the drawback mentioned before, the fifth ligand then is effectively fixed in the strapped complexes, where it is forced into coordination via a bridge moiety spanning the porphyrin core. These compounds therefore resemble the natural system more closely albeit demanding more tedious preparation. The Woggon group has contributed earlier to the field of model compounds synthesizing doubly bridged (**9**)<sup>23</sup> and bridged (**10**)<sup>24</sup> iron porphyrins (*figure 9*) carrying a thiolate ligand coordinating to iron (Fe<sup>III</sup>...S<sup>-</sup>), thus preventing ligand exchange phenomena. For the time being, these active site analogues have been the first

complexes to resemble both spectroscopic and chemical features of Cytochromes P450. Investigations and optimisation of such model compounds has since then been an integral part in the research of the group.

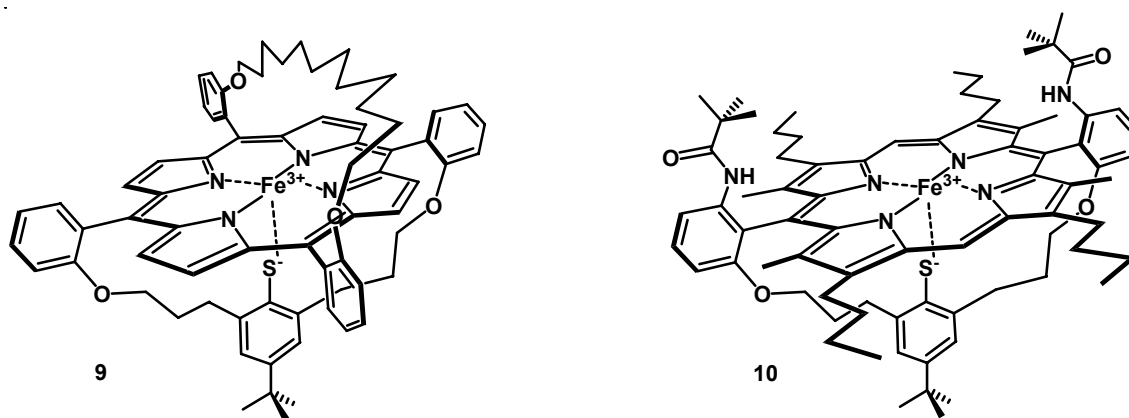


**Figure 9:** Earlier model compounds by the Woggon group.

Interestingly, the redox potentials of the above thiolate model compounds are considerably more negative than that of the natural system (e.g.  $E_0 = -630$  mV vs. SCE for **10** versus  $E_0 = -170$  mV vs. SHE, =  $-411$  mV vs. SCE for substrate bound P450<sub>cam</sub>).

From X-ray analysis of several P450s (*figure 10*)<sup>25</sup> these modified electronic properties in the natural system were deduced to result from reduced charge density on the fifth ligand due to H-bonding of sulfur to the amino acid backbone.

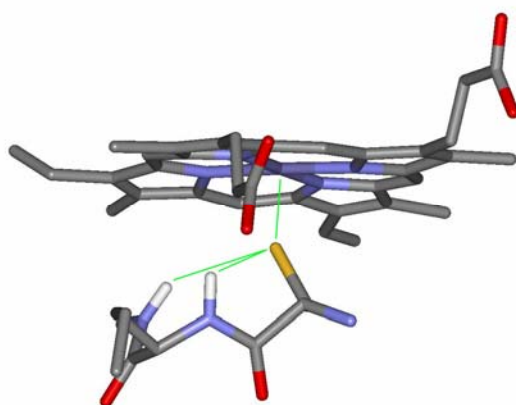


**Figure 10:** H-bonding of sulfur to the amino acid backbone in P450<sub>cam</sub>.

This effect has been studied by Nakamura et al<sup>26</sup> on free thiolate ligands coordinating to octaethyl porphyrins. In their system, they found the redox potential to shift to more positive values upon introduction of motives enabling H-bonding to sulfur (*figure 11*).

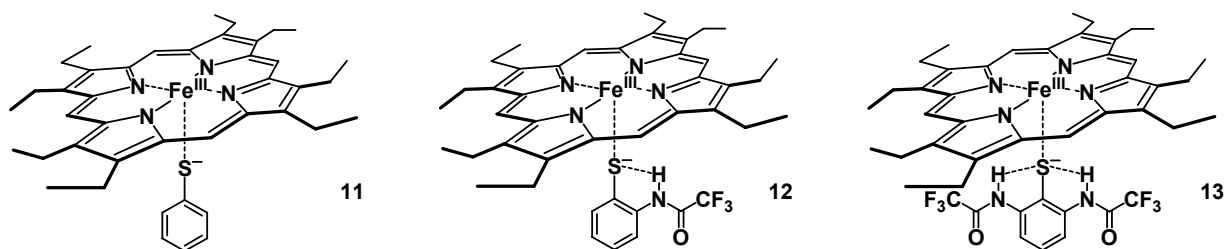


**Figure 11:** Model compounds of Nakamura et al.

Redox potentials in  $\text{CH}_2\text{Cl}_2$  shifted from  $-680$  mV (vs. SCE) for (11) to  $-520$  mV after introduction of one H-bond (12) and further to  $-350$  mV after introduction of a second one (13). Because of the non-covalent attachment of the fifth ligand, these compounds are very elegant for analytical purposes but are not suitable for catalytic reactions.

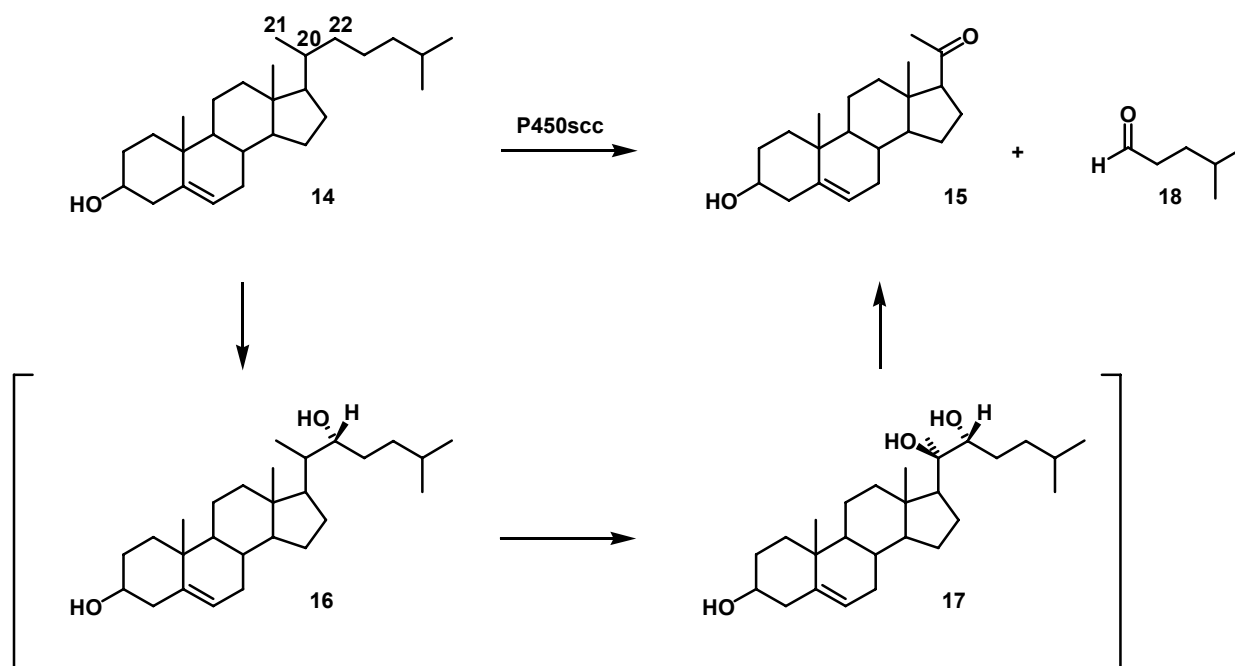
## 1.5 Selected P450s and their Reactivity

As implied, the P450s represent quite a variety of enzymes, each displaying its own, unique properties. Being of central interest in this work, selected P450s will be discussed in closer detail in this section.

### 1.5.1 C-C bond cleavage in P450<sub>SCC</sub> (CYP 11A1) and P450<sub>Biol</sub> (CYP107H1)

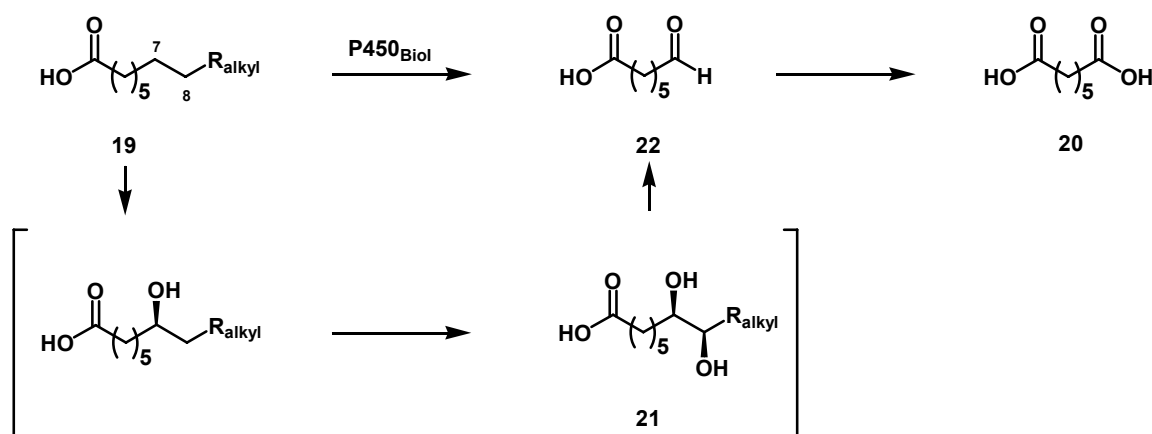
A remarkable reaction in the P450 catalogue is the cleavage of nonactivated carbon-carbon bonds. Such reactivity has been observed with P450<sub>SCC</sub>, a mammal adrenal Class I P450,<sup>27</sup> which catalyses the first and rate determining step in steroid hormone biosynthesis; the conversion of cholesterol (14) to pregnenolone (15) (*scheme 2*). The mechanism by which this P450 effects this transformation has been studied extensively. In going from 14 to 15, P450<sub>SCC</sub> uses 3 equivalents of NADPH and 3 equivalents of  $\text{O}_2$ .<sup>28</sup> Although several possible pathways have been suggested,<sup>29</sup> a stepwise mechanism has been brought forward to best rationalise the experimental findings and has been broadly accepted, where cholesterol is hydroxylated first at  $\text{C}_{22}$  to form 22(R)-Hydroxycholesterol (16) and second at  $\text{C}_{20}$  forming a vicinal diol,

20(R),22(R)-dihydroxycholesterol (**17**). In the last and mechanistically most interesting step, this diol is cleaved to form the products pregnenolone (**15**) and 4-methylpentanal (**18**).



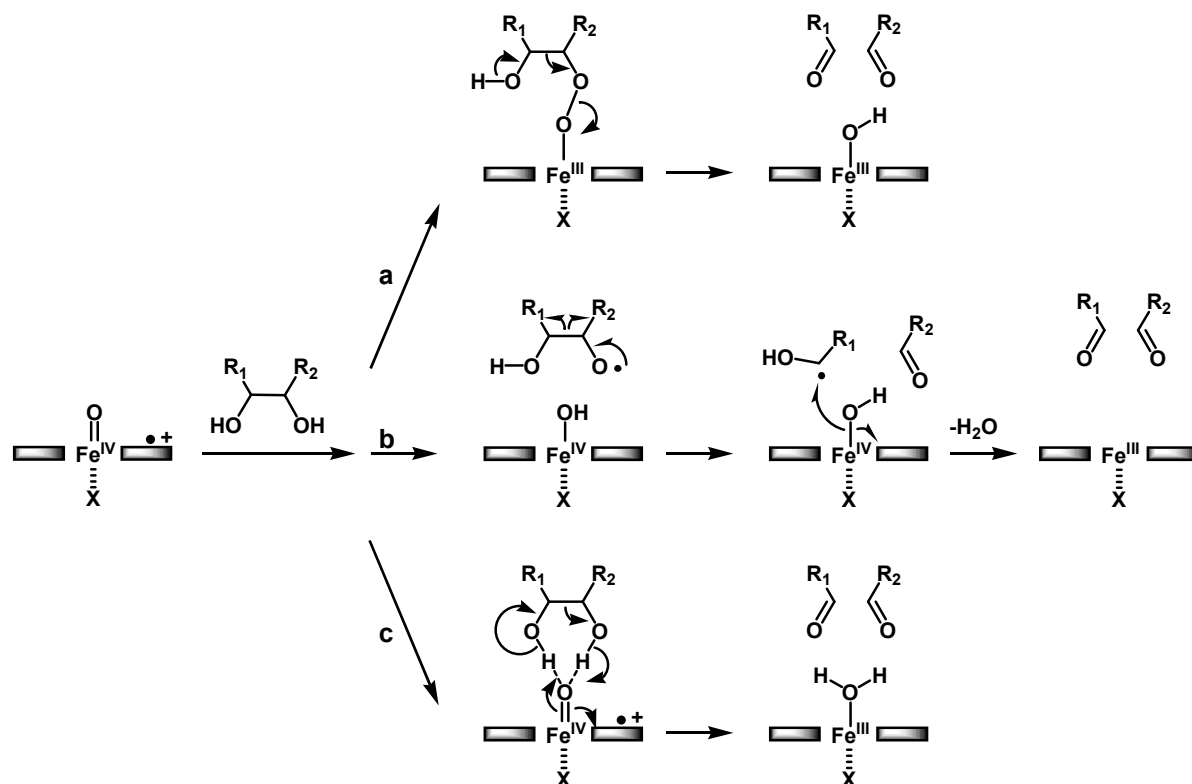
**Scheme 2:** Transformation of cholesterol to pregnenolone by  $P450_{scc}$ .

A more recently discovered enzyme,<sup>30,31</sup>  $P450_{Biol}$  involved in the biosynthesis of biotin in *Bacillus subtilis*, has been the first prokaryotic P450 found to follow a similar mechanism in the cleavage of acyl carrier protein (ACP)-coupled or free long chain (C-14 to C-18) fatty acids (**19**) to form pimelic acid (**20**) via the *threo*-7,8-diol (**21**) (the initially produced aldehyde (**22**) observed at short reaction times is converted to the corresponding acid by aerial oxidation under enzyme turnover conditions (*scheme 3*)).



**Scheme 3:** Fatty acid C-C bond cleavage in  $P450_{Biol}$

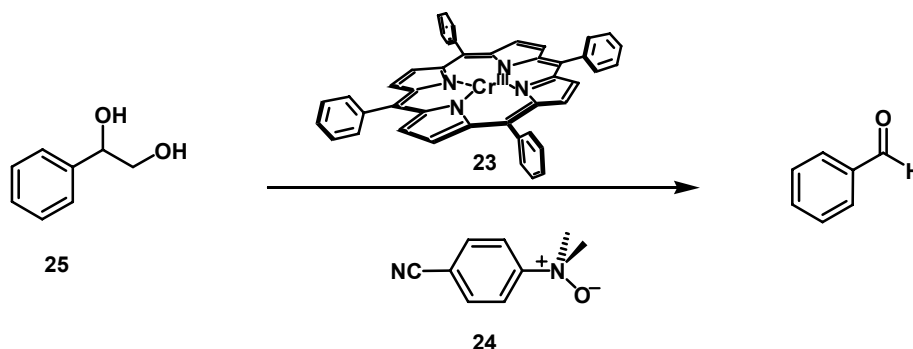
Despite the fascinating features of this transformation, its complexity renders it almost impossible to be studied in model systems. As hydroxylation reactions applying model compounds are very low yielding, a sequence of three consecutive steps cannot be expected to be realised. As the first two steps represent “standard” hydrocarbon hydroxylation, the most studied P450 transformation, the last step, diol cleavage, captures the main focus of interest. For the natural system a number of diol cleavage mechanisms can be proposed (*scheme 4*). As further oxidation of the carbon atoms carrying the alcohol functions (C<sub>22</sub> in the cholesterol case) is excluded due to the fact that their hydrogens are retained in the cleavage product, the most likely mechanism is one in which the hydroxyl moieties are activated in some fashion, followed by decomposition with C-C bond cleavage. This can for example be rationalised by formation of a peroxy-intermediate (path a), by H<sup>•</sup>-abstraction (path b) or in a concerted way (path c).



**Scheme 4:** Mechanistic proposals for the final step in C-C bond cleavage a) by peroxy-intermediate, b) by H<sup>•</sup>-abstraction and c) concerted.

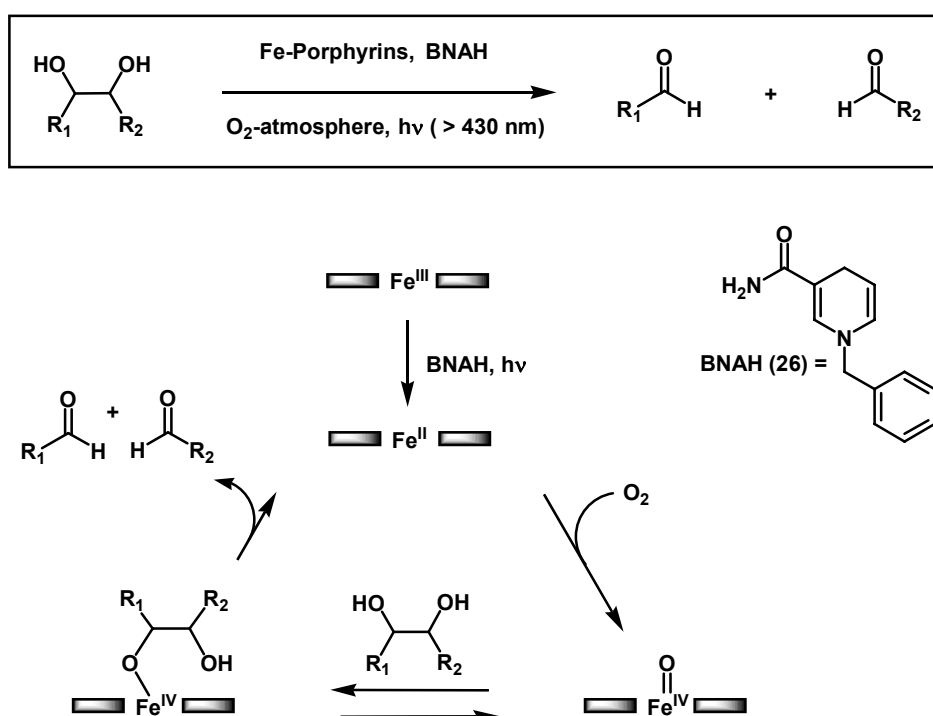
Only few examples of diol cleavage using metal porphyrins have been brought forward over the years.

Murray and Sligar<sup>32</sup> have reported a model system for diol cleavage applying chloro(5,10,15,20-tetraphenylporphinato)chromium(III) (Cr(TPP)Cl) (**23**) and the exogenous oxidant 4-cyano-N,N-dimethylaniline-N-Oxide (CN-DMANO) (**24**) in the cleavage of 1-Phenyl-1,2-ethanediol (**25**) (scheme 5).



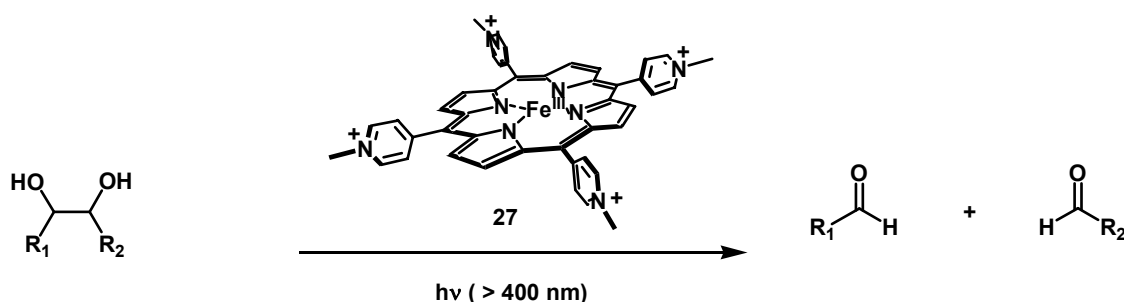
**Scheme 5:** Diol cleavage by **23**.

Okamoto et al<sup>33,34</sup> developed a biomimetic approach where they used iron porphyrins in presence of an NAD(P)H mimic 1-benzyl-3-carbamoyl-1,4-dihydropyridine (BNAH) (**26**) and molecular oxygen under the irradiation of visible light to cleave various vicinal diols (scheme 6). From kinetic interpretation of product formation together with electrochemical experiments<sup>35</sup> they brought up a proposed catalytic cycle for their system, where the diol coordinates to an iron(IV)-porphyrin obtained upon reduction of the corresponding iron(III)-porphyrin by BNAH and subsequent reaction with O<sub>2</sub>.



**Scheme 6:** Okamoto System for cleavage of diols and proposed mechanism.

In 1991 Ito<sup>36,37</sup> presented purely photochemical cleavage of vicinal diols in the presence of water-soluble Iron porphyrins (e. g. **27**, *scheme 7*).

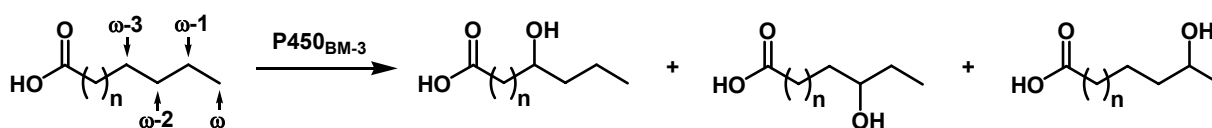


**Scheme 7:** Photochemical cleavage of diols.

Despite these contributions several features of diol cleavage remain elusive. *Murray* and *Sligar* used chromium instead of the natural iron center atom and therefore their system deviates rather far from the natural system. The same concerns account for the photochemical diol cleavage. The most elaborated model system, that of *Okamoto* et al, has given one view on how diol cleavage might be performed. Nevertheless, the applied model compounds lack appropriate ligation and taken together with the complexity of the system, there are plural possible mechanistic pathways deviating from the situation in the enzyme case. As a conclusion, further investigations, in particular appliance of simple, reliable model systems on diol cleavage would contribute to better understanding of C-C bond cleavage, one of the reactions that illustrate best the power of P450 oxidative transformations.

### 1.5.2 P450<sub>BM-3</sub> (CYP 102A1) and enzyme engineering

As mentioned earlier P450<sub>BM-3</sub> isolated from *Bacillus megaterium* was the first bacterial P450 characterized to be a class II P450. Although its precise physiological function remains elusive, the enzyme was shown to catalyse hydroxylation of saturated long chain fatty acids near their  $\omega$ -terminus (typically  $\omega$ -1, to  $\omega$ -3) (*scheme 8*).



**Scheme 8:** Hydroxylation of long chain ( $n=10-13$ ) fatty acids by P450<sub>BM-3</sub>.



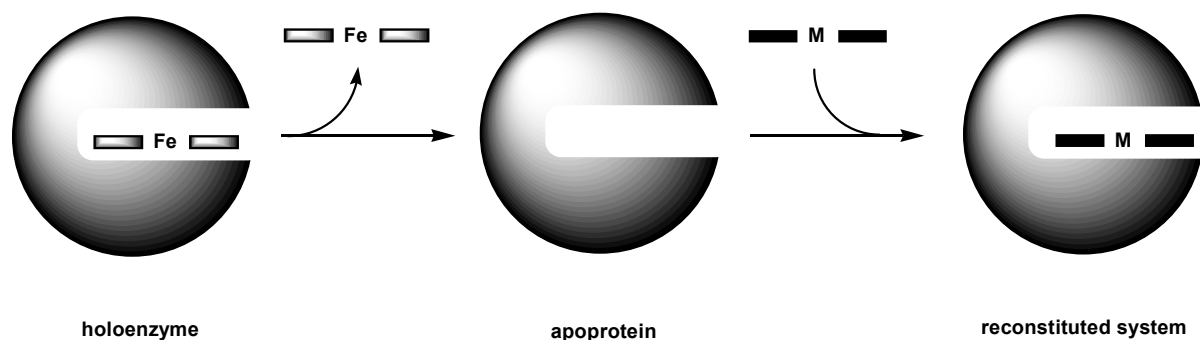
The reductase domain (BMR) of soluble P450<sub>BM-3</sub> is covalently linked to the C-terminus of the heme-domain (BMP). Due to its solubility (in contrast to mammal P450s being membrane bound) and its single 119-kDa polypeptide structure, it is relatively easily purified, analysed and overexpressed.<sup>8,38</sup> It has been recombinantly expressed in *E. coli* as a whole fused protein and as separated BMR and BMP domains. Crystal structures of both substrate free and substrate bound BMP have been obtained.<sup>39,40</sup> Rational mutagenesis has been applied for better understanding its catalytic function and electron transfer processes.

But P450<sub>BM-3</sub> is more than just a model for mammal P450s. Having the highest catalytic activity determined for any P450 ( $\sim 17\,000\text{ min}^{-1}$  with arachidonate)<sup>41</sup> it is also of great biotechnological interest for the production of high-value oxygenated organic molecules. Regio- and stereospecific enzyme-mediated transformations are an interesting and clean alternative to traditional organic chemistry. Therefore protein engineering has been employed to alter and improve the properties of P450<sub>BM-3</sub> to render it an even more cost-effective and attractive catalyst for biotechnological processes. With the field still being in its relative infancy, rational mutagenesis, forced evolution and random mutagenesis and functional selection have already generated a series of mutants with interesting properties such as changed regio- and substrate selectivity,<sup>42,43</sup> improved stability in organic solvents<sup>44</sup> and compatibility to other, cheaper reductants than NAD(P)H.<sup>45,46</sup> In this way, newly designed enzymes with enhanced properties for short chain alkanolic acid- or even alkane hydroxylation<sup>47</sup> and selective epoxidation of polyunsaturated hydrocarbons<sup>48</sup> have been obtained. Furthermore, BMP has been mutated to form a self-sufficient peroxide-driven hydroxylase<sup>49</sup> and further improved for thermostabilization.<sup>50</sup>

All of the above efforts have focused on changes in the architecture of the amino-acid backbone surrounding the cofactor. In general further strategies to alter the properties of heme proteins are feasible, going from exchange of axial ligands of the cofactor to modifications on the cofactor itself, including exchange of the metal center atom and modification of the porphyrin moiety surrounding it. The exchange of axial ligands has been studied with several enzymes<sup>51</sup> showing the importance of its properties to behaviour of the whole system and enabling conversion of one class of enzymes to behaviour similar to another class (e.g. modification of axial *Cys* in P450<sub>cam</sub> to *His* inducing much greater peroxidase activity).

While modification of the axial ligand might simply be seen as an extension of amino acid mutagenesis, modification of the cofactor itself represents an additional new tool to tailor enzyme properties. One basic prerequisite for applicability of this tool is the possibility to

remove the natural cofactor from the holoenzyme to obtain a cofactor free apoprotein and ability of the apoprotein to subsequently properly incorporate the desired new cofactor (*scheme 9*).



**Scheme 9:** Exchange of cofactor in P450s.

This basic principle has been shown to work for both P450<sub>cam</sub><sup>52</sup> and P450<sub>scc</sub><sup>53</sup> where enzymes obtained after removal and subsequent reincorporation of protoheme have been shown to restore spectroscopic properties and reactivity identical to the unprocessed system. The same technique can also be applied to P450<sub>BM-3</sub>.<sup>54,55</sup> Incorporation of unnatural cofactors in different heme proteins has been used in a series of studies to gain information on the influence of the peripheral architecture of the porphyrin on heme orientation and physiological properties. Simplified detection of dynamics has been achieved by incorporation of spectroscopically active species into the cofactor (e.g. fluorine substituents for <sup>19</sup>F NMR characterisation).<sup>56</sup> Stabilisation of active intermediate analogues has been accomplished by metal exchange (e.g. Fe vs. Mn)<sup>57</sup> to gain closer insight into the catalytic cycle and the electron supplying system. All these examples show that cofactor modification is a valuable tool in enzyme engineering and together with amino acid mutagenesis a rich arsenal for tailoring new P450 based biotechnological catalysts is in principle available and applicable to e.g. P450<sub>BM-3</sub>.

## 2 Description of the Aims of this Work

The body of this work is split in two parts accounting for two projects elaborated during its development. One concerns the further development of model compounds for cytochromes P450 and their appliance in P450-catalysed reactions, the other one investigates modifications on the natural cofactor, heme *b*, for obtaining new cofactors with altered properties in the field of enzyme engineering.

### 2.1 Establishment of a new Class of Model Compounds

As already mentioned, the Woggon group has been contributing to the field of P450 model compounds with a notable body of work.<sup>58</sup> In this context the synthesis and characterisation of members of a new class of model compounds was envisioned, where the thiolate ligand (*figure 12a*) of the bridge moiety in earlier model compounds (e.g. **9** and **10**) is exchanged for a sulfonate group (*figure 12b*).

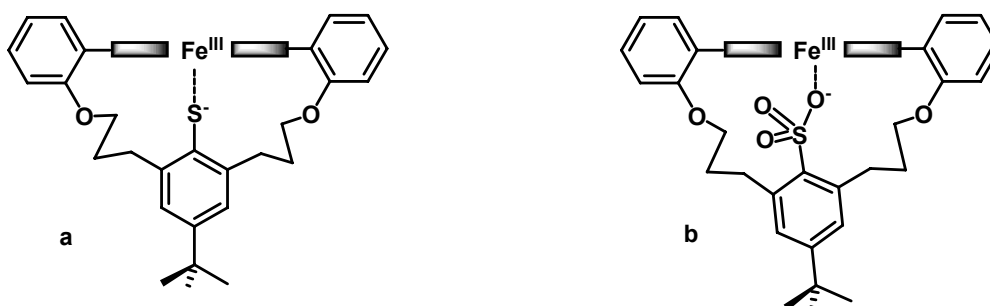


**Figure 12:** Thiolate a) vs. sulfonate b) coordination in Fe-porphyrin model compounds.

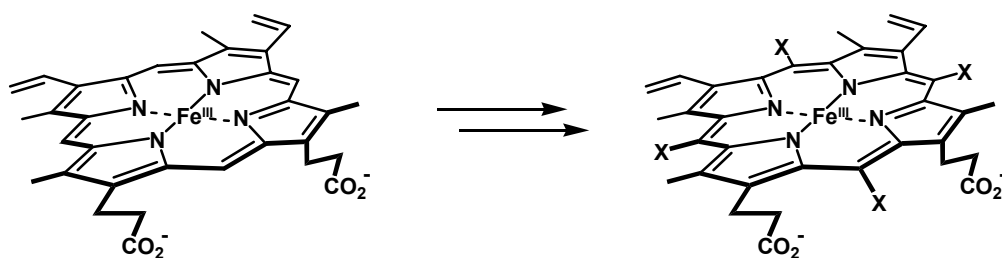
This change bears technical advantages with the  $\text{SO}_3^-$  group being much more stable towards oxidative conditions than the thiolate  $\text{S}^-$ . This makes handling much easier and ensures one single coordinating species althrough catalytic reactions using oxidants such as *m*CPBA. More importantly though it was designed to reflect the earlier introduced reduced charge density on the fifth ligand in the natural system.

Distribution of the negative charge over the three oxygens of a sulfonate moiety should result in a similar reduction of charge density on the fifth ligand, being predicted to be one of the sulfonate oxygen atoms, and therefore shift the redox potential to more positive values than in the thiolate model compounds, towards the value for the substrate bound form of P450s and H-bonded model compounds (13).

Having the new model compounds in hand, the goal would then be to investigate their reactivity in P450-catalysed reactions with special focus on finding a system for the cleavage of vicinal diols and drawing conclusions therefrom on the active species in this reaction.

## 2.2 Modification of the Natural Cofactor

The second project of this work focuses on modifications of the natural cofactor heme *b*. As has been deduced earlier, such modifications present a valuable tool for tuning the properties of enzymes in biotechnology and might help to further elucidate features of P450s. The general concept was to retain the original substituents as far as possible and to introduce further groups in the originally unsubstituted *meso*-positions (*scheme 10*).



**Scheme 10:** Modification of the cofactor in *meso*-position.

This strategy was chosen in order to retain the possibility for interaction with the amino acid backbone via the original substituents and to allow at the same time tuning of the electronic and steric effects of the cofactor by introduction of different substituents (**X**). Finally, after reconstitution of the enzyme system, the modified cofactors were expected to show behaviour different from the unmodified system dependent on the newly introduced substituents (**X**).

## 3 Results and Discussion

### 3.1 Synthesis of the new Model Compounds

#### 3.1.1 Support for the $\text{SO}_3^-$ Strategy by DFT Calculations

In a collaboration with Shaik et al.,<sup>59</sup> DFT calculations were applied to gain information on the properties of the conceived system and to address the question of properness of a model compound bearing sulfonate coordination instead of a thiolate as in the natural system.

In these studies it was found that for two CpdI models,  $\text{MeSO}_3^-$  coordinated **A** and  $\text{PhSO}_3^-$  coordinated **B** (figure 13), the iron center atom coordinated to one of the oxygen atoms indeed represents an energetic minimum, in which as anticipated only part of a negative charge (-0.45 for **A**, -0.38 for **B**) is located on the actual fifth ligand, whereas the rest of the charge is distributed over the two other oxygen atoms.

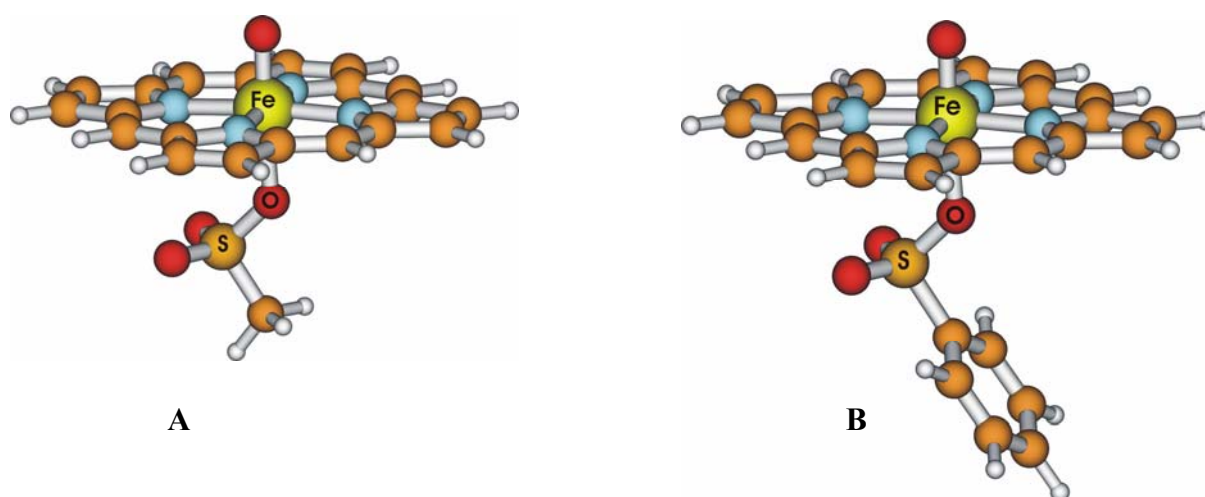
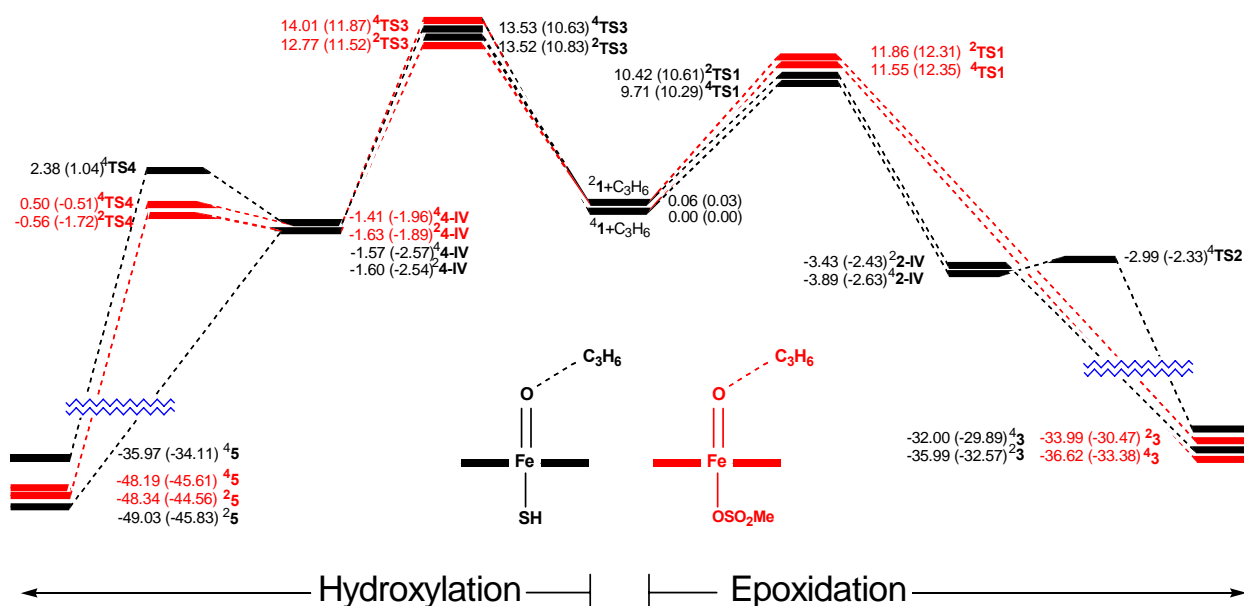


**Figure 13:** Calculation Model compounds **A** (left) and **B** (right).

Further calculations were performed to compare reactivity of  $\text{SO}_3^-$  vs.  $\text{S}^-$  coordinated models in both hydroxylation (left part) and epoxidation (right part) of propene (scheme 11).



**Scheme 11:** Superimposed high spin (HS) and low spin (LS) energy profiles for the reaction of  $\text{SO}_3^-$  and  $\text{S}^-$  coordinated CpDI models with propene. The reactants are placed in mid-diagram. The energies (in kcal/mol) are given relative to the separated reactants.

From superimposition of energy profiles for the calculated reaction pathways of both species it was deduced that overall the  $\text{SO}_3^-$  coordinated species shows very similar reactivity to the  $\text{S}^-$  case. Closer detailed examination shows a slight increase in preference for hydroxylation versus epoxidation when going from  $\text{S}^-$  to  $\text{SO}_3^-$  and a more concerted pathway for  $\text{SO}_3^-$  reaction especially in the epoxidation case. This should render the new model compounds slightly more stereoselective reagents. Other than those differences, the profiles show almost perfect superimposition, disclosing the fundamental similarity between the two reagents.

### 3.1.2 Design and Synthetic Strategy

In the light of the above discussion two members of a new family of model compounds **28** and **29** (figure 14) were elaborated in our laboratories.

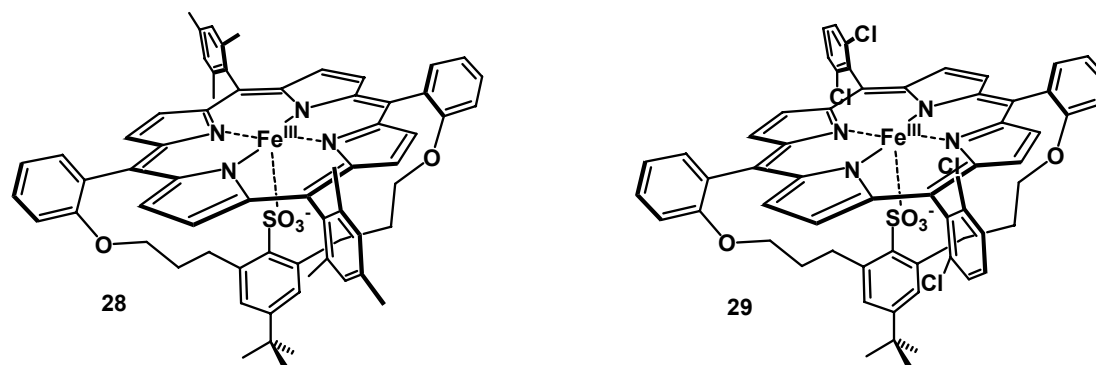
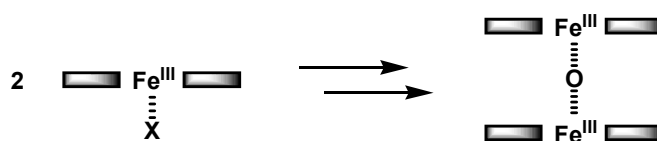


**Figure 14:** Elaborated model compounds.

The common features are a tetra-aryl-porphyrin moiety covalently linked to a bridge moiety carrying the  $\text{SO}_3^-$  group for ligation to the iron center atom. Aryl substituents in the *meso*-position were chosen because of several advantages of such substitution. A) the free *meso*-positions are oxidatively labile and primary site of attack in the destruction of the porphyrin moiety. Substitution therefore hampers destruction of the model compounds under oxidative conditions and therefore improves stability. B) introduction of appropriate substituents on the *meso*-phenyls can be used to influence the reactivity of the models. By introduction of electron-withdrawing or -donating groups the electron density in the aromatic system can be altered and thereby the redox potential of the new compounds can be tuned. C) steric demand of the aryl moieties prevents undesirable formation of so called  $\mu$ -oxo dimers<sup>60</sup> (scheme 12).

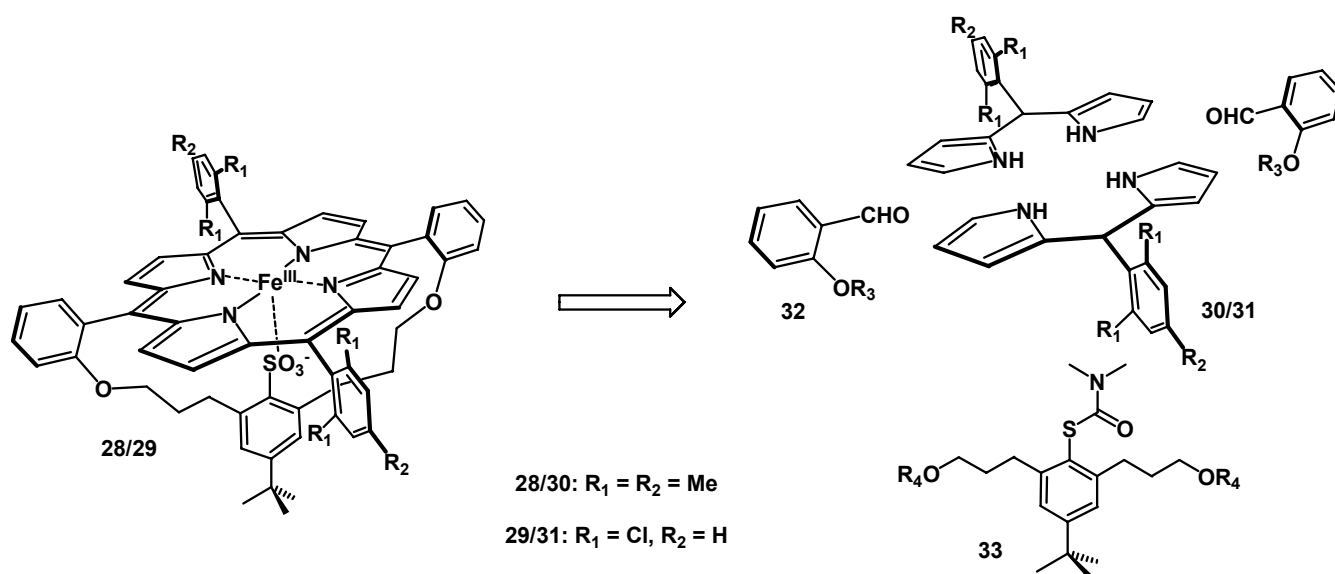


**Scheme 12:**  $\mu$ -oxo dimer formation.

The bridge moiety was adopted from earlier design for sulfur ligation in the group<sup>61</sup> and therefore expected to have the correct length for spanning the porphyrin and appropriate ligation. The *tert*-Butyl group on the aromatic ring of this moiety was introduced both for synthetic reasons<sup>61</sup> and to increase steric congestion, thereby forcing the sulfonate into coordination.

The two model compounds differ in their substituents on the *meso*-phenyl moieties. **28** carries two mesityl-substituents, representing rather innocent, slightly electron donating alkane substituents. In contrast to this, in **29** each of these two phenyl moieties is substituted with two chlorines in *ortho* position, leading to a more electron deficient system. Therefore it was predicted, that **29** should display a more positive redox potential than **28** and that the corresponding CpdI analogue should therefore display higher reactivity.

Retrosynthetic analysis of the model compounds (*scheme 13*) implied condensation of a dipyrromethane **30/31** with the appropriate aldehyde **32** and coupling of a protected bridge moiety **33**.



*Scheme 13*: Retrosynthetic analysis of model compounds **28** and **29**.

### 3.1.3 Synthesis

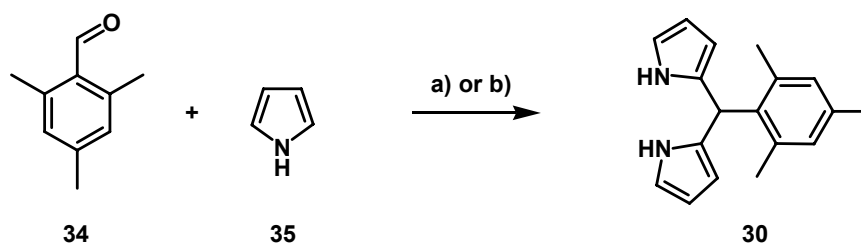
The synthesis and appliance of the new family of model compounds has been brought together by a couple of members of the group. Model Compound **29** has first been obtained by Leifels<sup>62</sup> and synthesized and applied both in the work of Sbaragli<sup>63</sup> and this work. **28** on the other hand was first synthesized and characterized in the present work. Synthetic methodology and optimisation was adopted from earlier work in the group and performed in collaboration with the other group members.



The synthesis was performed in a convergent manner. As outlined in the retrosynthetic analysis the target molecule was obtained by assembly of the main components **30** to **33**. the aldehyde **32** was commercially available, whereas **30/31** and **33** had to be synthesized. The following route is described for the mesityl-model **28** but applies to both model compounds.

### 3.1.3.1 The Dipyrromethane

The first building block, the *meso*-substituted dipyrromethane **30**,<sup>64</sup> was obtained upon reaction of the appropriate benzaldehyde **34** with a 40 to 80 fold excess of freshly distilled pyrrole **35** used as the solvent (*scheme 14*). This reaction was catalysed by both Brønsted- (TFA) and Lewis acids (BF<sub>3</sub>·Et<sub>2</sub>O) and the desired dipyrromethane was obtained in similar yields for both (30%) upon workup and chromatography. As the product is sensitive to daylight, all preparations were performed under the exclusion of light.

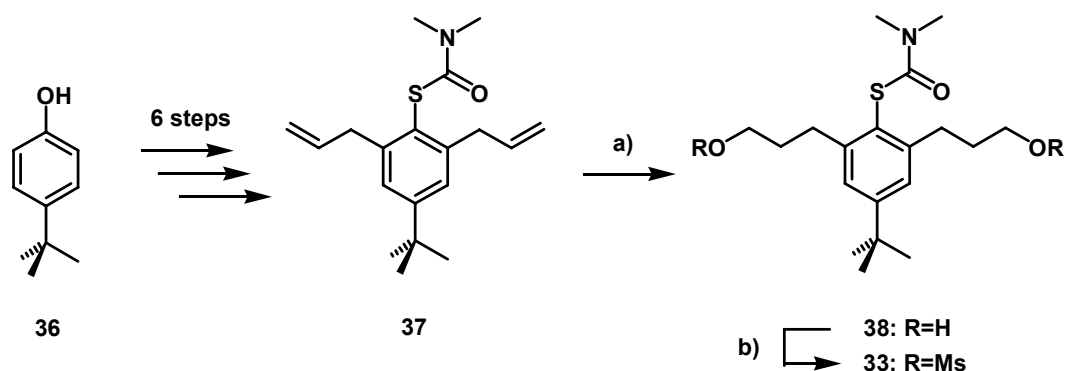


*Scheme 14:* Synthesis of dipyrromethane **30** applying a) 0.1 eq. of TFA, b) 0.3 eq. of BF<sub>3</sub>·Et<sub>2</sub>O.

### 3.1.3.2 The Bridge Moiety

The design and synthesis of the sulfur protected bridge moiety (*scheme 15*) starting from commercially available 4-(*tert*-butyl)phenol (**36**) had already been established in the group.<sup>65,62</sup> obliged to this, synthesis could be started from intermediate **37** of which larger quantities were on stock (the earlier steps are therefore not discussed in detail here).

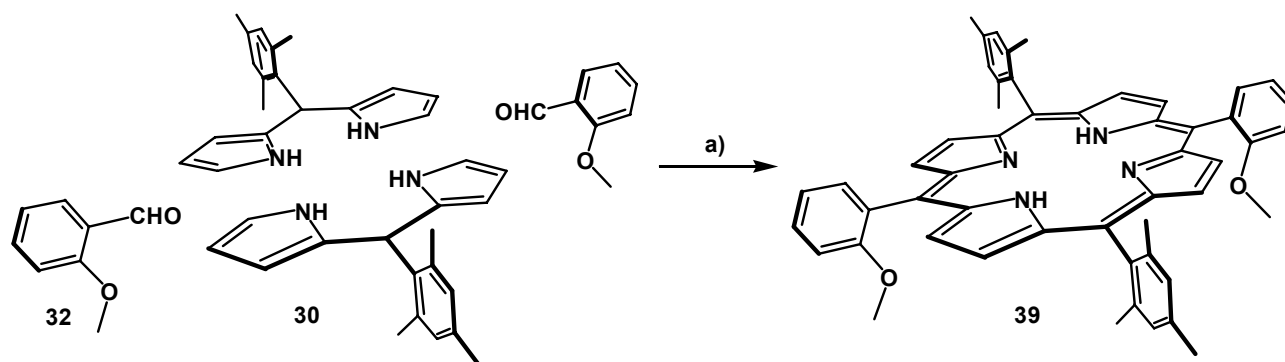
In a first step a) **37** was converted in 87% to the corresponding alcohol **38** by hydroboration using BH<sub>3</sub>·SMe<sub>2</sub>. In a second step b) **38** was then transformed with Methanesulfonylchloride (MsCl) to the mesylate **33** in 92%, which represents the desired moiety for coupling to the porphyrin.



**Scheme 15:** Synthesis of protected bridge **33** by a) hydroboration of **37** (1.  $\text{BH}_3\cdot\text{SMe}_2$  in THF at r.t., 2. NaOH,  $\text{H}_2\text{O}_2$ ) and b) mesylation ( $\text{MsCl}$ ,  $\text{Et}_3\text{N}$ ,  $\text{CH}_2\text{Cl}_2$ ) of **38**.

### 3.1.3.3 The Porphyrin

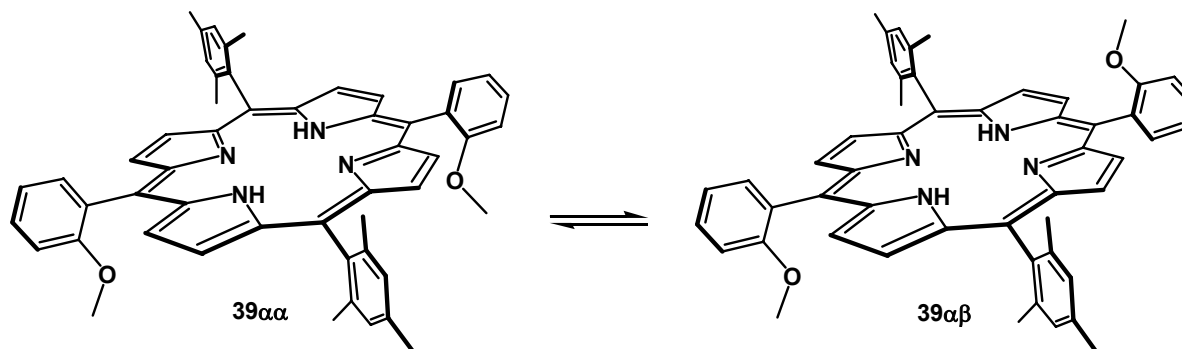
Condensation of the dipyrromethane **30** with the aldehyde **32** (scheme 16) in a MacDonald type 2 + 2 condensation<sup>66</sup> was performed according to optimized conditions<sup>67</sup> for minimization of so called scrambling leading to porphyrin products with different undesired *meso*-substitution pattern.



**Scheme 16:** Porphyrin condensation: a) TFA,  $\text{CH}_2\text{Cl}_2$ , then DDQ.

A 1 : 1 ratio of **30** and **32** was condensed by TFA under high dilution (10 mM) at r.t. in  $\text{CH}_2\text{Cl}_2$ . The so obtained porphyrinogenic species (a chlorin) displaying a UV/Vis absorption at 477 nm was then oxidized to full conjugation by addition of 2,3-Dichloro-5,6-dicyano-*p*-benzoquinone (DDQ) and the change in UV/Vis absorption (from 477 to 418 nm) was controlled for complete conversion. The porphyrin **39** was obtained in 27% as a mixture of

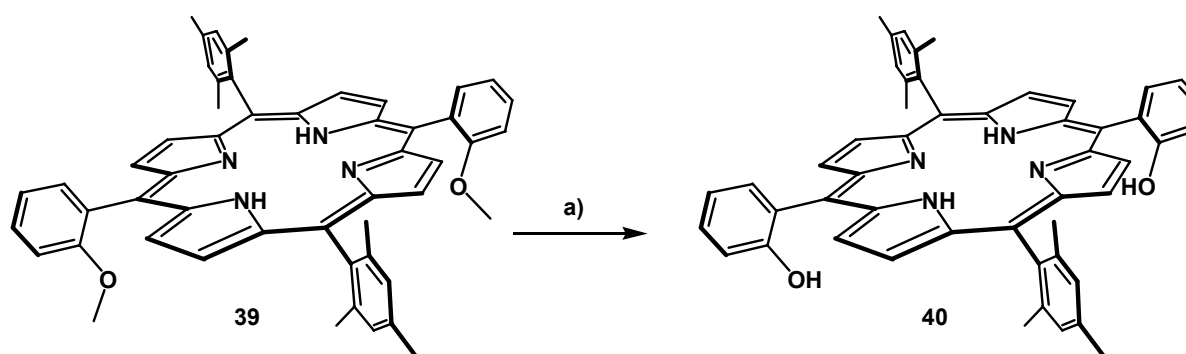
two atropisomers (**39 $\alpha\alpha$**  and **39  $\alpha\beta$**  in *scheme 17*) which showed slow interconversion at r.t. (as observed from both NMR and TLC experiments).



**Scheme 17:** The two atropisomers of **39**. In the  $\alpha\alpha$ -isomer (left), both methoxy groups of the two *meso*-phenyl substituents are located on the same side of the porphyrin plane. In the  $\alpha\beta$ -isomer they occupy different sides.

Only the  $\alpha\alpha$  isomer is appropriately oriented for correct coupling of the bridge moiety in a later step. But as interconversion was observed even at r.t., the two atropisomers were taken together for further synthesis.

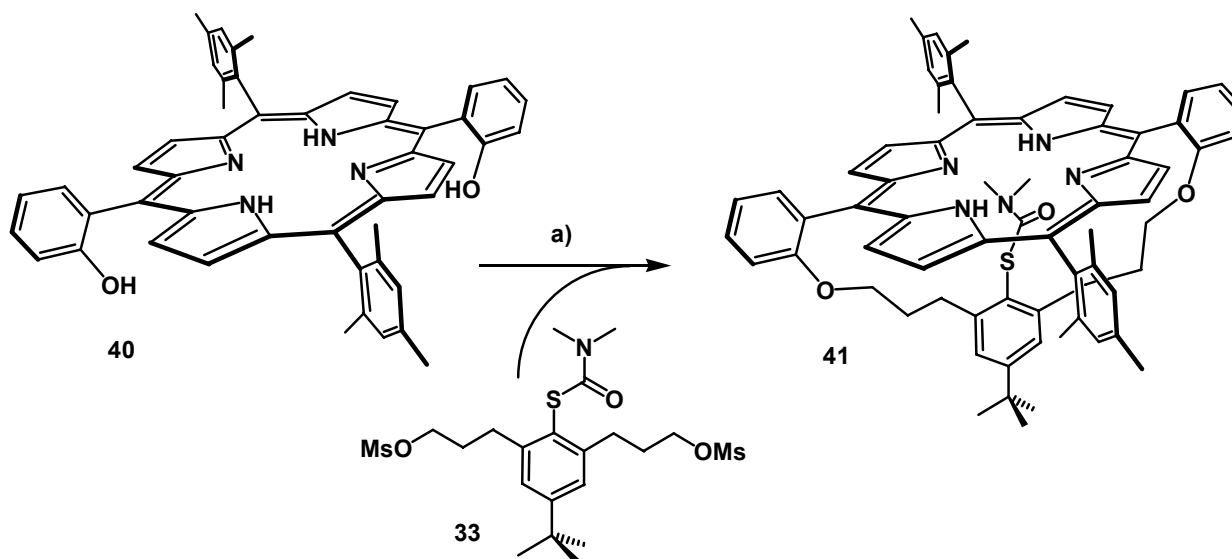
In the next step, **39** was demethylated to the corresponding bisphenol **40** by  $\text{BBr}_3$ <sup>68</sup> (*scheme 18*). Here again a mixture of two atropisomers interconverting at r.t. was obtained in 79% yield.



**Scheme 18:** Demethylation of **39**, a)  $\text{BBr}_3$ ,  $\text{CH}_2\text{Cl}_2$ , r.t., only one atropisomer is shown.

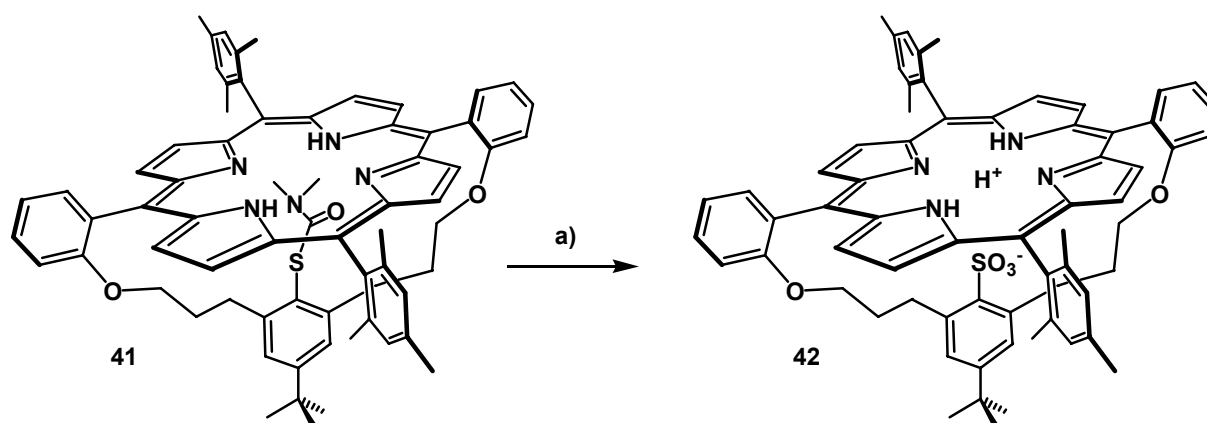
For the bridge coupling step (*scheme 19*) conditions were chosen such that reaction of one molecule of **40** with one molecule of the bridge moiety **33** was preferred. This was achieved

by diluted conditions and slow addition of **33** via syringe pump. In addition elevated temperatures (80 °C) were applied to ensure interconversion of the atropisomers of **40**. Under such conditions and the addition of Cs<sub>2</sub>CO<sub>3</sub>, 75% of **41** were obtained.



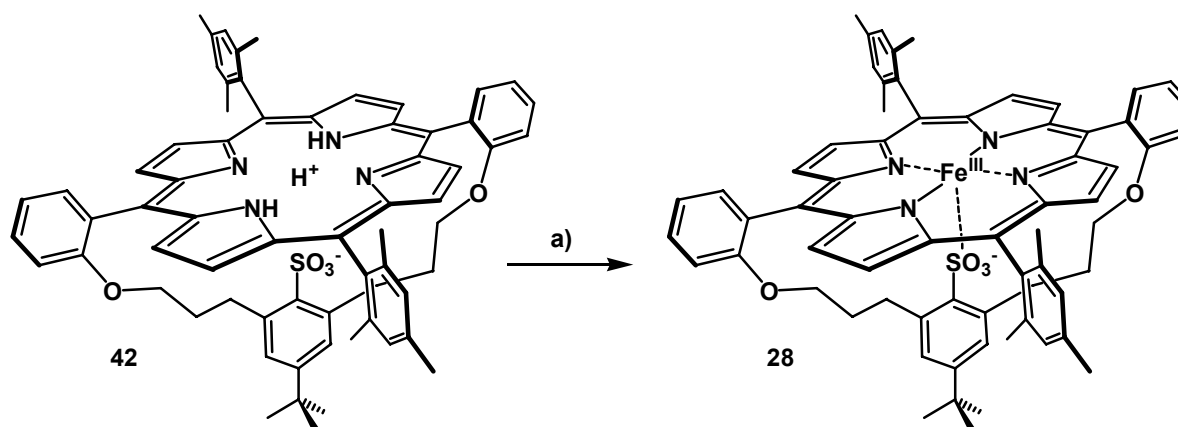
**Scheme 19:** Bridge coupling to **40** by a) slow addition of **33** at 80 °C in the presence of Cs<sub>2</sub>CO<sub>3</sub> in DMF.

From earlier work on thiolate model compounds<sup>61,69</sup> it was known that upon deprotection of the sulfur moiety the compounds had to be handled under strictly anaerobic conditions to prevent sulfur oxidation. As such oxidation was just the desired reaction in the case of the new family of model compounds, no such precautions were necessary in the deprotection step. Even more, although different sulfur oxidation procedures were tested before or after iron insertion,<sup>63</sup> the best results were obtained when the deprotection was simply run under O<sub>2</sub> atmosphere (*scheme 20*). Only trace amounts of thiolate product were observed under such conditions, the main product being sulfonate-porphyrin **42**. As a side product, partially oxidized SO<sub>2</sub>-porphyrin **43** was obtained. After separation, the latter could be further oxidized to the desired sulfonate **42** by oxidation with Bu<sub>4</sub>NHSO<sub>5</sub>,<sup>70</sup> such that **42** could be obtained in an overall yield of 55%.



**Scheme 20:** Deprotection of sulfur under aerobic conditions a) KOMe, dioxane, O<sub>2</sub>-atmosphere, reflux.

The final step towards the model compound was then the insertion of iron. This was accomplished by heating a toluene solution of **42** with FeBr<sub>2</sub> under addition of 2,6-Lutidine as a base (*scheme 21*). Although an iron(II) salt is used for iron insertion, the product obtained in 86% is the corresponding more stable iron(III)-porphyrin **28**.



**Scheme 21:** Iron insertion into sulfonate-porphyrin **42**: a) FeBr<sub>2</sub>, 2,6-Lutidine, toluene, reflux.

## 3.2 Characterisation of the new Model Compounds

### 3.2.1 Physical and Spectroscopic Properties

With the new model compounds synthesized, their properties were investigated by different analytic methods.<sup>71</sup> From slow diffusion crystallisation in THF/heptane suitable crystals for X-ray analysis could be obtained in both cases.<sup>72</sup> The so obtained structures (*figure 15*) validate both the synthetic procedures and the DFT calculation results, as indeed in both cases iron is coordinated by one of the oxygens of the  $\text{SO}_3^-$  group. Interestingly, the more electron poor **29** has a THF molecule coordinating as a sixth ligand, whereas the structure of **28** obtained under similar conditions shows a five coordinated species. The analysis further shows a slightly strained system for both cases with the iron positioned out of plane towards the  $\text{SO}_3^-$  ligand especially dominant for the five coordinated structure of **28**.

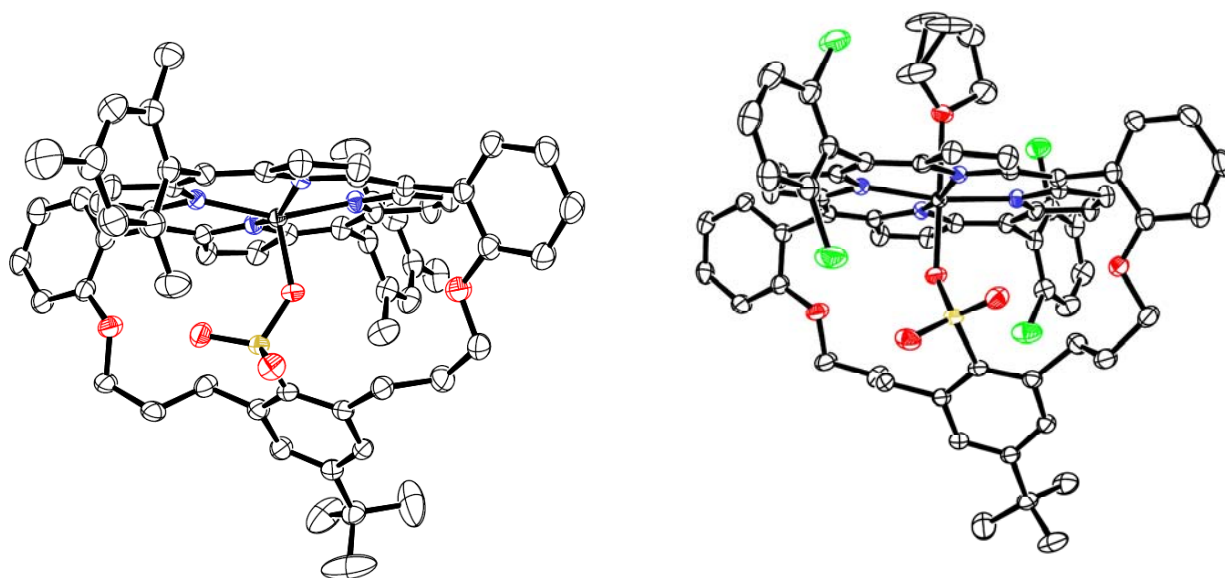


*Figure 15:* ORTEP representation of model compounds **28** (left) and **29** (right) crystallised from THF/heptane

The structural properties imply high-spin iron(III) systems, which correlates very well with the cw-EPR spectra obtained in toluene at 94K (*figure 16*) displaying characteristic signals for axial high spin iron(III) systems ( $g = 5.67, 2.03$  for **28**;  $5.51, 2.00$  for **29**<sup>63</sup>).

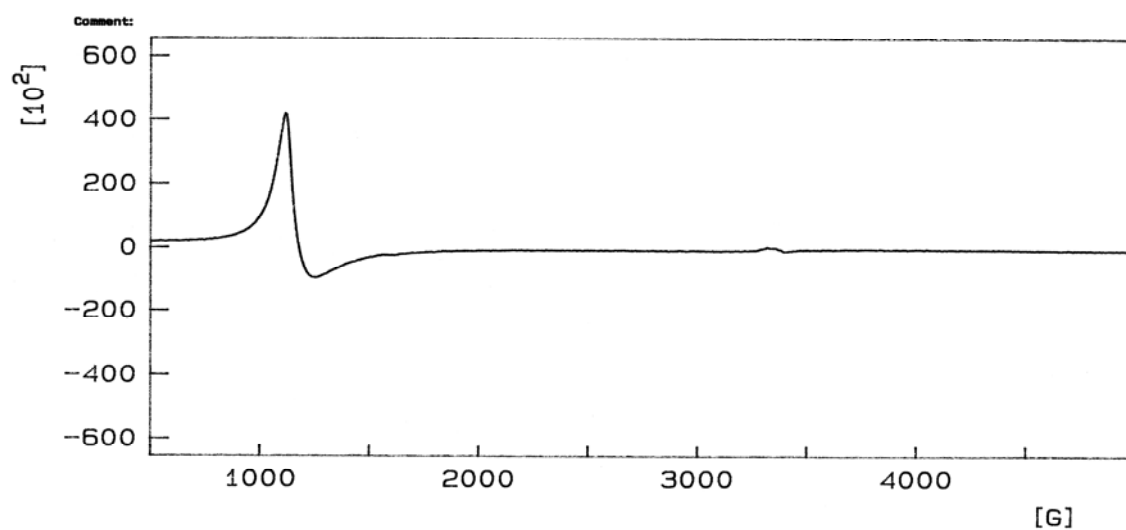


**Figure 16:** cw-EPR spectrum of **28** in toluene at 94K

The UV/Vis spectra of both compounds in  $\text{CHCl}_3$  are very similar (*figure 17*) with a Soret band (the most dominant absorption in the electronic spectra of porphyrins) at 416 nm and further absorptions at higher wavelengths, the so called Q-bands, at 512, 581 and 670 nm for **28** and 513, 590 and 656 nm for **29**.

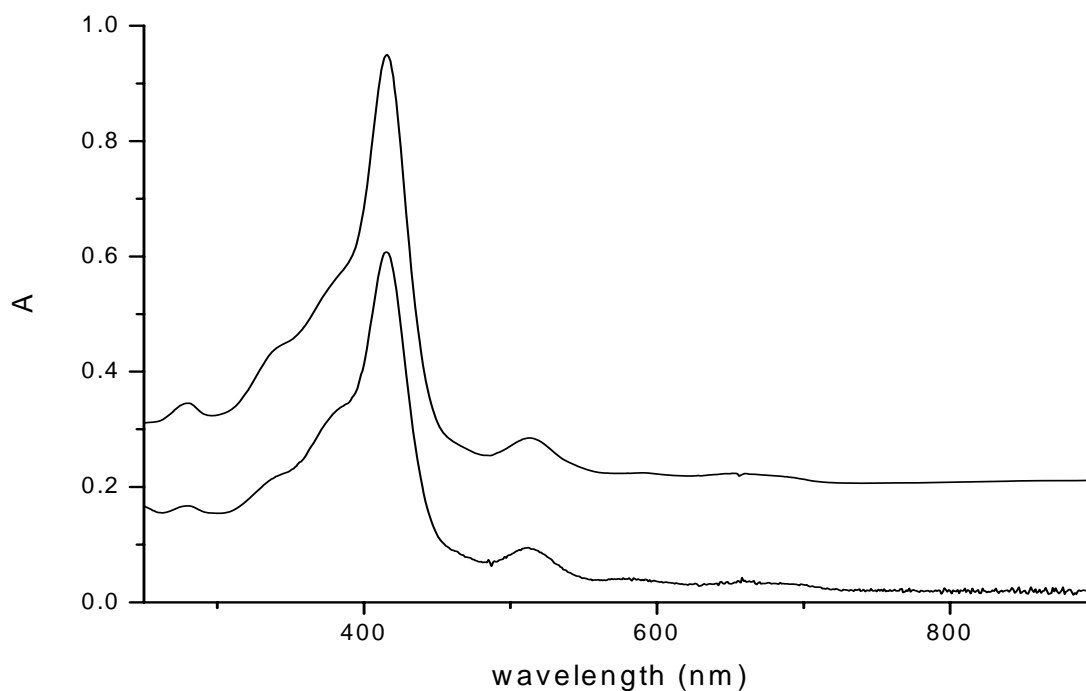


**Figure 17:** UV/Vis spectra of **28** (lower trace) and **29** (upper trace) in  $\text{CHCl}_3$ .

Cyclovoltammetry in LiBr saturated DMF (0.1M in LiClO<sub>4</sub>) gave redox potentials for both compounds versus ferrocene as an internal standard. The obtained values showed the influence of the dichloro-phenyl substituents in **29** to indeed cause a shift to more positive potential of ~ 80 mV for the (Fe<sup>III</sup>/Fe<sup>II</sup>) transition compared to mesityl substitution in **28**. Measurements for **29** and its S<sup>-</sup> analogue in the same solvent system had already implied a shift of ~300 mV to more positive values for SO<sub>3</sub><sup>-</sup> ligation.<sup>62</sup> This trend was confirmed by calculating the obtained potentials vs. ferrocene towards SCE<sup>73,74</sup> to obtain values of -290 mV (±20 mV) for **28** and -210 mV (±20 mV) for **29**. These values, particularly that of **28**, are in the same region as the E<sub>o</sub> value of the E·S complex of P450<sub>cam</sub> (-411 mV) and hydrogen-bonding model compound **13** (-350 mV). Omission of LiBr (used to ensure defined coordination of iron) slightly shifted potentials for more negative values: -340 mV for **28** and -280 mV for **29** and enabled measurement of the first oxidation potential (Fe<sup>III</sup>/Fe<sup>IV</sup>) for both models (*figure 18*) which again show a positive shift of ~ 90 mV when going from **28** (920 mV) to **29** (1010 mV).

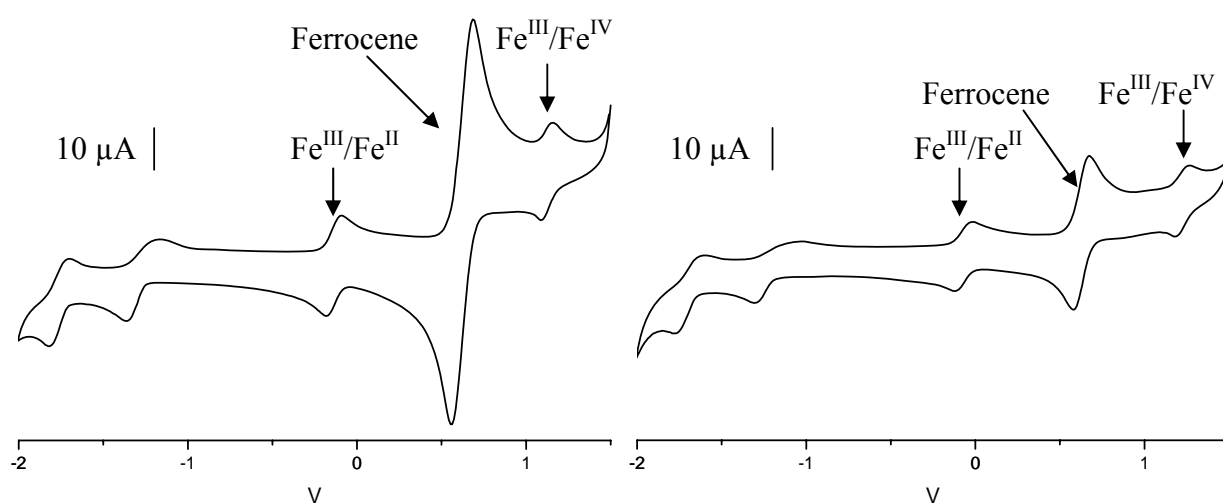


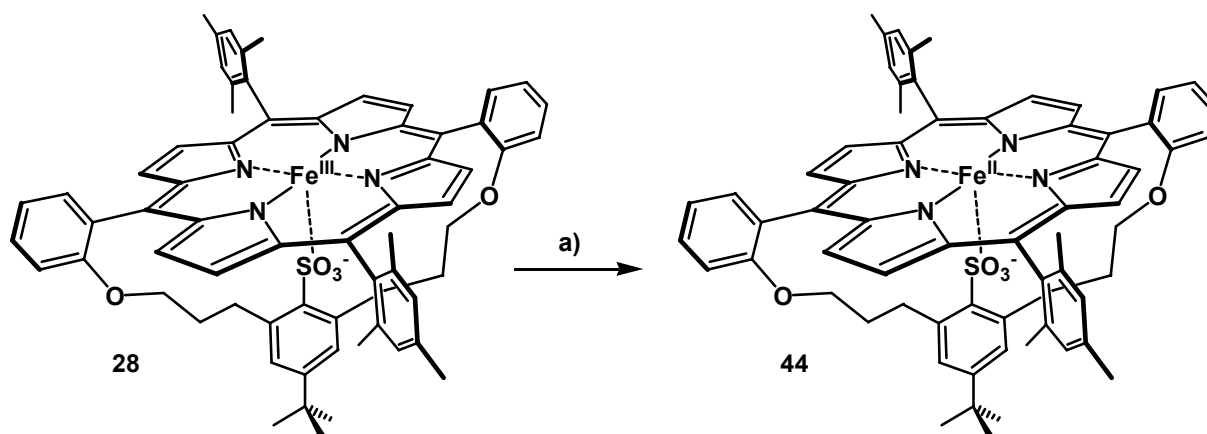
**Figure 18:** Cyclovoltammograms of 0.62 mM **28** (left) and 0.59 mM **29** (right) in 0.1 M LiClO<sub>4</sub> solution in DMF with ferrocene as an internal standard. Scan rate 200 mVs<sup>-1</sup>.

The positive shift from earlier S<sup>-</sup> model compounds with E<sub>o</sub> more negative than -600 mV (vs. SCE) in some cases to the new SO<sub>3</sub><sup>-</sup> coordinated models with E<sub>o</sub> ~ -300 mV (vs. SCE) validates the principle of predicted influence of reduced charge density on the fifth ligand in the latter case.



### 3.2.2 Iron(II)-state

Treating a degassed toluene solution of **28** with an excess ( $\geq 3$  eq.) of KH/18-crown-6 or  $\text{Na}_2\text{S}_2\text{O}_4$ /15-crown-5 solutions, a shift of the Soret band from 416 to 422 nm and an increase in absorption intensity was observed. EPR samples taken from these solutions only showed strongly decreased iron(III) high spin signals (probably from traces of nonreduced **28**), which were completely restored after bubbling with air. These findings suggest the newly formed species to be the reduced iron(II) compound (**44**) of **28** (scheme 22).



**Scheme 22:** Reduction of **28** by KH or  $\text{Na}_2\text{S}_2\text{O}_4$  to obtain iron(II) compound **44**.

The procedure leading to **44** had to be monitored closely by UV/Vis-spectroscopy because if a too large excess of reducing agent was added a further species with  $\lambda_{\text{max}} = 440$  nm was observed, the EPR spectrum of which showed a mixture of species, including a sharp  $g = 2.00$  signal indicating organic radicals.

Further support for the nature of **44** and correct assignment of electronic spectra was obtained by spectrovoltammetric measurements in DMF displaying a shift and increase of the Soret band (420 nm to 425 nm) similar to the first species observed by KH reduction (**44**) when applying negative potentials (-500 mV) (see *figure 19*).

Saturation of toluene solutions of **44** with CO gas did not cause any further shift of the Soret band. The CO-complex of **44**, if formed, is thus believed to have the same  $\lambda_{\text{max}}$  as **44**, which is in good agreement with results for a potential iron(II)-CO complex of **29** ( $\lambda_{\text{max}} = 422$  nm in  $\text{THF}^{62}$ ) studied by Leifels.

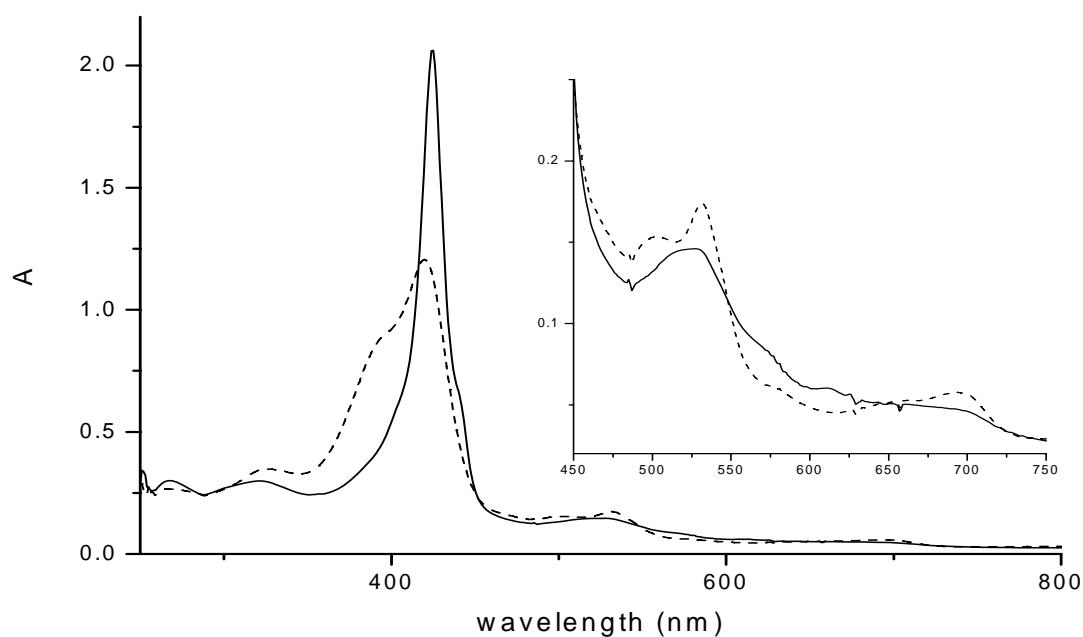


**Figure 19:** Spectra obtained by spectroelectrochemistry of **28** in 0.1 M LiClO<sub>4</sub> solution in DMF. Dashed line: +400 mV: iron(III) spectrum; solid line: -500 mV: iron(II) spectrum. Inset: 450–750 nm region.

### 3.2.3 CpdI Analogues ((porph<sup>•+</sup>)Fe<sup>IV</sup>=O)

As displayed in *figure 7*, oxidants such as *m*CPBA or iodosobenzene (PhIO) can be applied to obtain the oxidation state analogue to the active species in the natural system, CpdI. Preliminary work on identification of such a species was performed under UV/Vis conditions in CH<sub>2</sub>Cl<sub>2</sub> at -50 °C. Indeed upon addition of 1.5 eq. *m*CPBA to a precooled solution of **28**, a new species with the desired spectral properties (a blue shifted Soret band at 408 nm of reduced intensity and a broad absorption at 600-700 nm characteristic of a radical cation on the porphyrin ring) (**45**) was obtained (*figure 20*). The so obtained spectrum is in excellent agreement with published data for simpler porphyrin systems in the CpdI-state.<sup>75,76</sup>

More elaborated techniques were applied in a collaboration with van Eldik et al to obtain closer insight into formation and reactivity of the iron-oxo species of **28** and **29**.<sup>77</sup> They applied low temperature, rapid scan stopped-flow techniques to obtain spectroscopic and kinetic information on the formation of the (porph<sup>•+</sup>)Fe<sup>IV</sup>=O species (**45**) and (**46**) of **28** and **29** respectively. Mixing acetonitrile solutions of **28** and **29** with an excess of *m*CPBA at -35 °C resulted in formation of **45** and **46**.

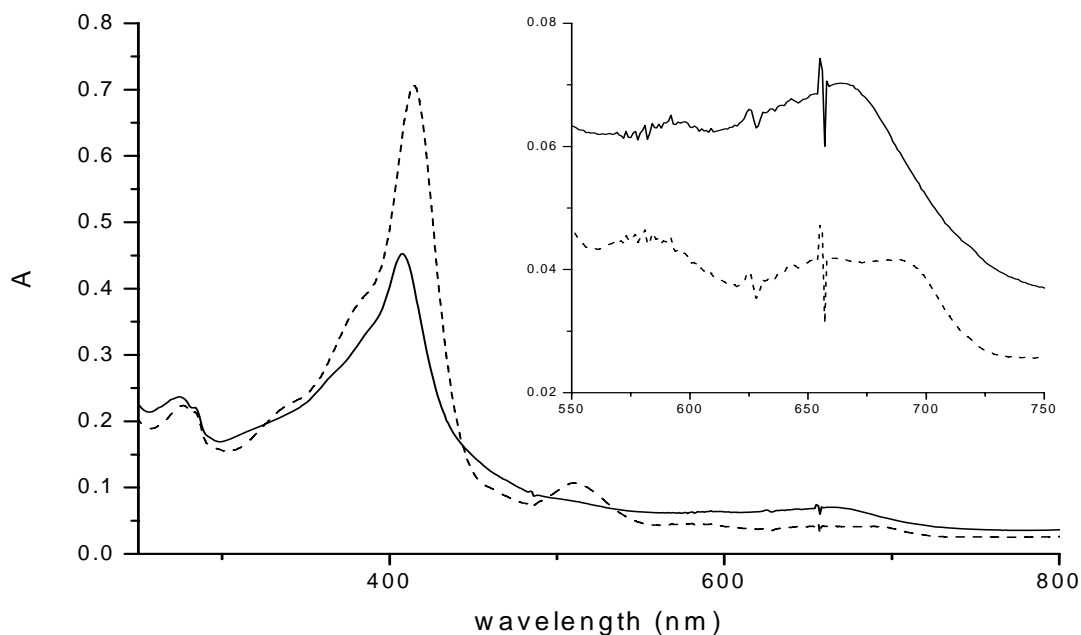
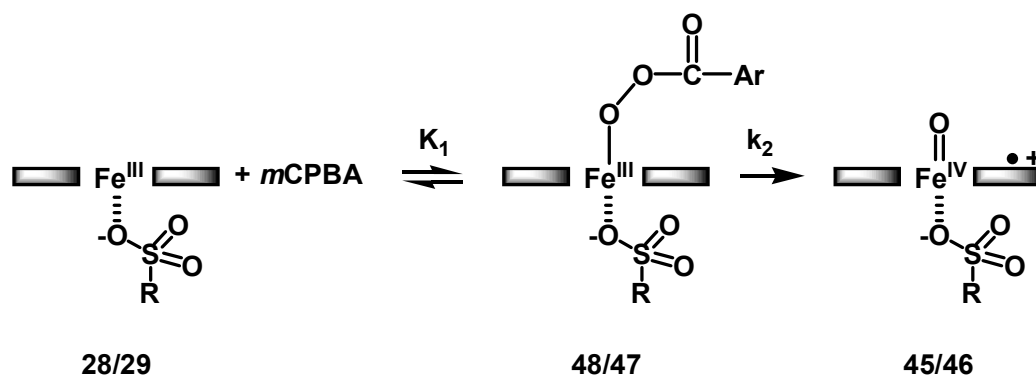


**Figure 20:** UV/Vis change after addition of 1.5 eq. of *m*CPBA to a  $\text{CH}_2\text{Cl}_2$  solution ( $8 \mu\text{M}$ ,  $-50 \text{ }^\circ\text{C}$ ) of **28**. dashed line: spectrum 30 sec after addition, full line: 25 min after addition. Inset: 550-750 nm region.

For **29**, rate saturation for high concentrations of *m*CPBA was obtained. Detailed spectral analysis implied a two step sequence where in a first equilibrium ( $K_1 = 4.4 \pm 0.5 \times 10^3 \text{ M}^{-1}$ ) the corresponding acylperoxy-iron(III) intermediate (**47**) is transiently formed and breaks down to form **46** ( $k_2 = 2.4 \pm 0.1 \text{ s}^{-1}$  at  $-35 \text{ }^\circ\text{C}$ ) (scheme 23).



**Scheme 23:** Reaction sequence for the formation of  $(\text{porph}^{\bullet+})\text{Fe}^{\text{IV}}=\text{O}$  species **45** and **46** from **28** and **29**.

No indication for a corresponding acylperoxy intermediate (**48**) could be observed in the reaction of **28** which forms **45** directly without rate saturation (figure 21). The formation of an intermediate **47** can be attributed to the electron withdrawing properties of the porphyrin

substituents, stabilising **47**<sup>78</sup> whereas electron donation in **28** triggers the rate of O-O cleavage and therefore reduces the lifetime of a potential intermediate **48**.

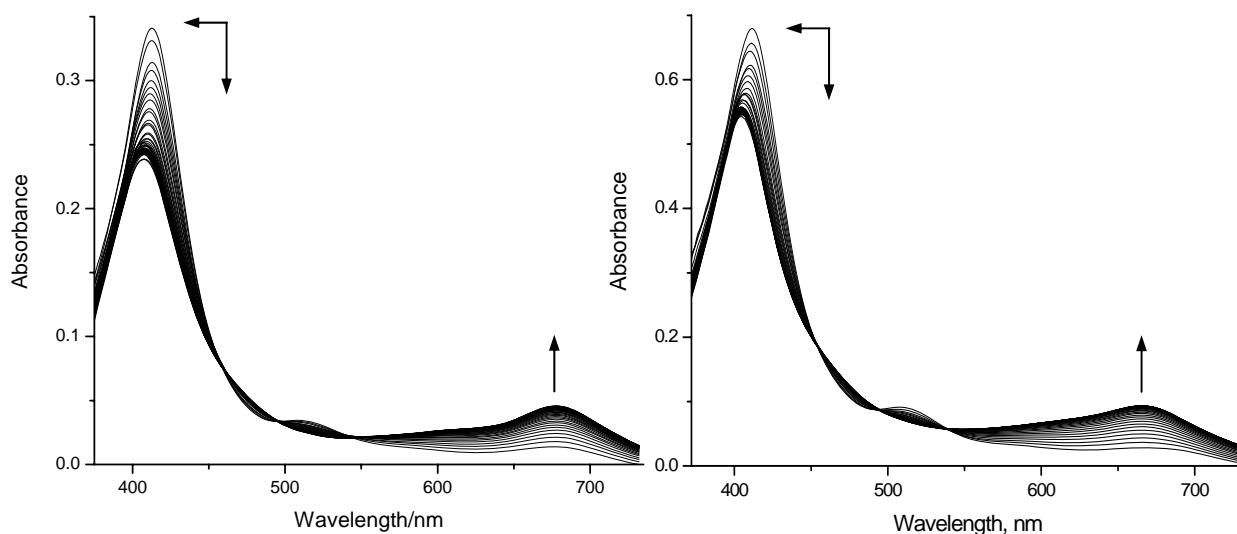


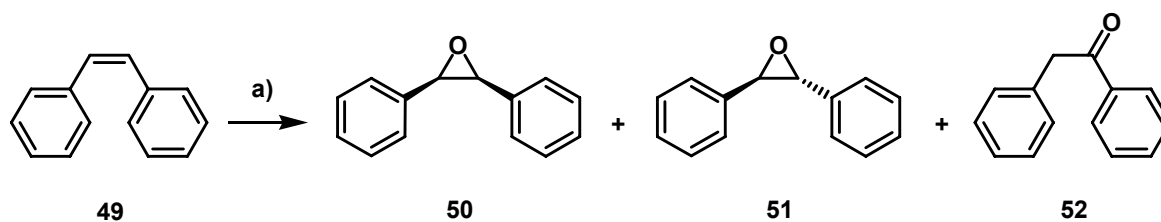
**Figure 21:** Rapid-scan spectra recorded for the formation of (porph\*)Fe<sup>IV</sup>=O in the reaction of **29** (left) and **28** (right) with *m*CPBA. Experimental conditions: (left) [**29**] = 4.3 x 10<sup>-6</sup> M, [*m*CPBA] = 5.4 x 10<sup>-5</sup> M, MeCN, -35 °C. (right) [**28**] = 8.7 x 10<sup>-6</sup> M, [*m*CPBA] = 8.7 x 10<sup>-5</sup> M, MeCN, -30 °C.

The obtained results showed that both new model compounds can form a reactive species similar to the natural system, this being a prerequisite to apply them to P450-catalysed reactions such as epoxidation of alkenes, hydrocarbon hydroxylation, diol cleavage and demethylation of amines.<sup>79</sup>

### 3.3 Epoxidation of Alkenes

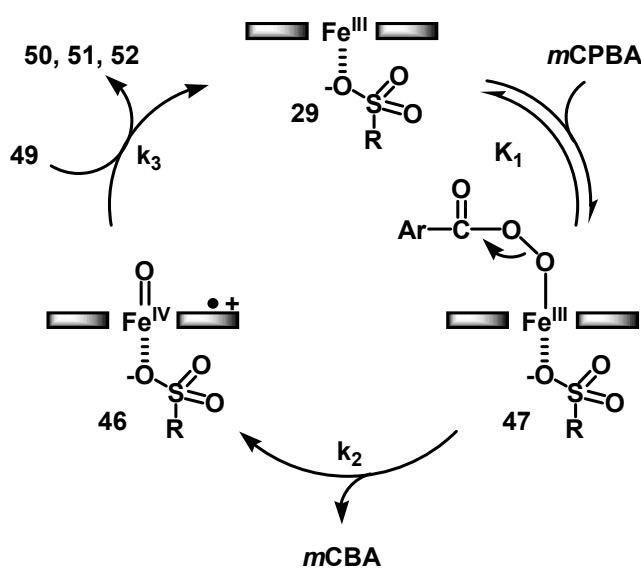
As alkene epoxidation is a well-known reaction performed by many P450 analogues, it was used to establish the new model compounds as enzyme reaction mimetics. First epoxidation experiments applying **29** performed by Leifels<sup>62</sup> demonstrated that **29** was capable to catalyse epoxidation of a variety of substrates with high turn over numbers (TON) using PhIO as a ‘O’-source (e.g. TON = 1810 for the epoxidation of *cis*-stilbene (**49**) in *scheme 24*). This high reactivity towards epoxidation was then used in collaboration with van Eldik et al to obtain insight into the catalytic cycle (*scheme 25*) of this reaction.<sup>77</sup> Mixing solutions of the preformed reactive species **46** at -35 °C with variable amounts of *cis*-stilbene (**49**) resulted in the regeneration of the original spectrum of **29** after an induction period dependent on the

amounts of *m*CPBA and *cis*-stilbene added. Higher amounts of *m*CPBA in the mixture elongated the induction period, whereas addition of a larger excess of **49** led to a decrease.



**Scheme 24:** Epoxidation of **49** to form a mixture of *cis*-stilbene epoxide **50**, *trans*-stilbene epoxide **51** and deoxybenzoin **52**. a) **29**/PhIO.

The previous findings imply a catalytic cycle performed during this induction period, where **46** is reformed after reaction with **49** fast enough to be the dominant spectroscopically observed species under these conditions (acetonitrile,  $-35\text{ }^{\circ}\text{C}$ ). This was confirmed by control experiments in our laboratories, where samples taken during the induction period already showed major formation of oxidation products, as assigned by GC-FID analysis. Product formation further increased in the course of the reaction to obtain 40-50% of oxidation products with respect to applied *m*CPBA. (control reactions performed under similar conditions omitting **29** showed no formation of epoxidation products even after elongated reaction times).

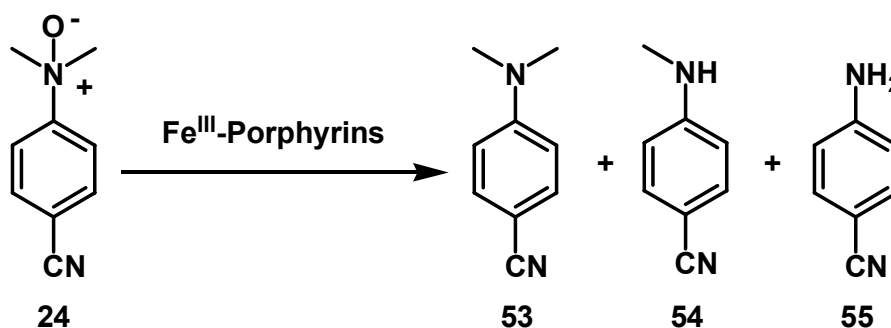


**Scheme 25:** Catalytic cycle for the epoxidation of *cis*-stilbene by **29** in the presence of *m*CPBA

From spectral changes after the induction period the rate for the epoxidation reaction could be determined ( $k_3 = 7.0 \pm 0.2 \text{ M}^{-1} \text{ s}^{-1}$  at  $-35 \text{ }^\circ\text{C}$ ) which, when extrapolated to  $20 \text{ }^\circ\text{C}$  ( $\sim 411 \text{ M}^{-1} \text{ s}^{-1}$ ) is in the same range as rates obtained for kinetic studies on other model systems,<sup>80</sup> ranging from  $90$  to  $320 \text{ M}^{-1} \text{ s}^{-1}$ . In summary, the above findings in epoxidation reactions establish the new model compounds, particularly **29**, as valuable catalysts able to mimic oxygenation reactivity of cytochromes P450.

### 3.4 Demethylation of Amines

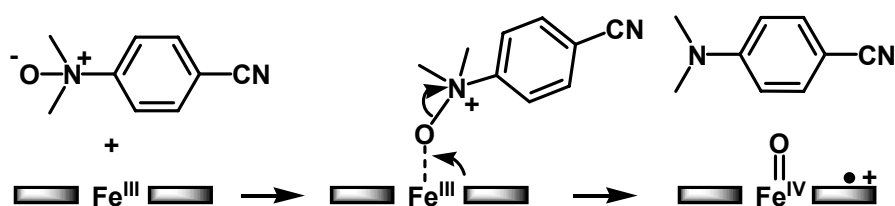
Bruice et al have established<sup>81,82</sup> and thoroughly studied model systems for the amine dealkylation reaction of cytochromes P450 using N-Oxides of aniline derivatives, in particular *p*-cyano-N,N-dimethylaniline N-Oxide (**24**) as an 'O'-source for a number of iron porphyrins.<sup>83-88</sup> The amine **53** arising from O-donation of the N-oxide to the iron porphyrin takes the role of the substrate, being demethylated to *p*-cyano-N-methylaniline (**54**) under the reaction conditions. The latter can react further to form *p*-cyano-aniline (**55**) in a second demethylation step (*scheme 26*).



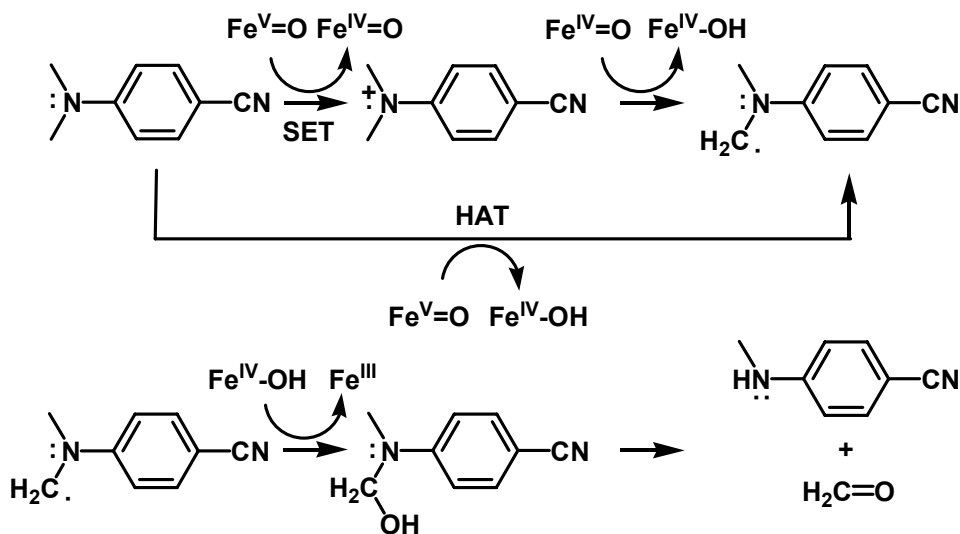
*Scheme 26*: N-Dealkylation system established by Bruice et al.

Bruice et al have studied this phenomenon in thorough detail. As transfer of oxygen from **24** to the iron porphyrin was found to be rate-determining, the active species could not unambiguously be designated directly. Nevertheless there is a strong indication towards intermediate CpDI analogue formation. First, the demethylation of **53** can be catalysed by iron porphyrin/PhIO systems to yield the same products. The upper system can further be applied to epoxidation of alkenes and even hydrocarbon hydroxylation with yields similar to reactions catalysed by 'O'-donation of PhIO under the same conditions. When the reactive intermediates were trapped by either a one electron acceptor trap 2,4,6-tri-*tert*-butylphenol

(TBPH) or an “oxene” acceptor 2,3-dimethyl-2-butene the only products formed were 100% of **53** and the corresponding oxidized trap (the stable radical TBPH<sup>•+</sup> in the first case and the epoxide in the latter). Also, N-oxide probes have been applied to enzymatic dealkylation reactions using P450s and therein showed mechanistic similarity to dealkylation reactions on the corresponding amines by the natural oxidant system (NAD(P)H, O<sub>2</sub>) as concluded from appliance of isotopically labelled compounds.<sup>89,90</sup> All these findings support a mechanistic pathway containing formation of a (porph<sup>•+</sup>)Fe<sup>IV</sup>=O species (*scheme 27a*).



a) formation of the reactive CpDI species and **53** by ‘O’-donation of **24**



b) reaction of **53** with the reactive CpDI species

**Scheme 27:** Reaction mechanism of demethylation of **53** in a iron-porphyrin/**24** system: a) formation of the reactive iron oxo species by heterolytic cleavage of the N-O bond after coordination of **24** to iron. b) the two possible mechanisms of N-dealkylation via single electron transfer (SET) or Hydrogen atom transfer (HAT) leading to demethylated product **54**.

For the dealkylation of amines in general two different mechanisms are plausible. The first by initial electron abstraction to form the nitrogen radical cation (SET pathway in *scheme 27b*).

After deprotonation of a vicinal carbon this then results in a carbon radical that combines with the iron bound oxygen to give a hemiaminal which forms the demethylated product (e.g. **54** from **53**) and the corresponding aldehyde (e.g. formaldehyde from demethylation). The second mechanism (HAT pathway in *scheme 27b*) is more closely related to the “classical” hydrocarbon hydroxylation mechanism, where the iron-oxo species directly abstracts a hydrogen atom from the vicinal carbon atom to form the carbon radical, which in analogy to the first mechanism recombines with the iron bound oxygen to form the hemiaminal and the subsequent demethylated products. Although the first, single electron transfer (SET) mechanism is more broadly accepted there is considerable experimental work favouring the second, hydrogen atom transfer (HAT) mechanism.<sup>91,92</sup>

Interestingly, Bruice et al found that product distribution depended on the electronic properties of the applied porphyrins. The more electron deficient [*meso*-tetrakis(2,6-dichlorophenyl)porphyrinato]iron(III)chloride ((Cl<sub>8</sub>TPP)FeCl)<sup>86</sup> gives rise to a larger fraction of the mono-demethylated product **54** when compared to the more electron rich [*meso*-tetrakis(2,6-dimethylphenyl)porphyrinato]iron(III)chloride ((Me<sub>8</sub>TPP)FeCl)<sup>85</sup> showing more diverse product distribution (*table 1*). When applying their system to our new model compounds a similar trend was observed for the more electron deficient **29** versus more electron rich **28** (*table 1*). These results can be interpreted in terms of higher reactivity of an intermediately formed iron-oxo species in the more electron poor porphyrins ((Cl<sub>8</sub>TPP)FeCl and **29**) which is in good agreement with their more positive oxidation potentials. Upon formation of the iron-oxo species the simultaneously formed amine **53** has to be replaced to obtain demethylation products different from **54** such as **55** resulting from demethylation of **54** being present in solution. It appears that high reactivity of the iron-oxo species in the more electron poor models admits such exchange to a smaller extent than their more electron rich counterparts.

model compound	<b>53</b> (in %)	<b>54</b> (in %)	<b>55</b> (in %)
(Cl <sub>8</sub> TPP)FeCl	40	60	0
(Me <sub>8</sub> TPP)FeCl	53	24	3
<b>29</b>	37	58	5
<b>28</b>	39	35	10

**Table 1:** Yields of products in N-dealkylation reactions calculated relative to added N-oxide.

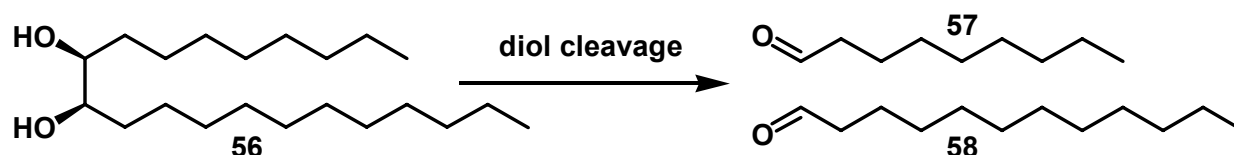
The same rationale can be applied to the observation that the (Me<sub>8</sub>TPP)FeCl/**24** system allowed alkene epoxidation for a variety of substrates, whereas for (Cl<sub>8</sub>TPP)FeCl/**24** the



epoxidation yields were lower and only observed for the most competitive substrates. Therefore demethylation of **53** provided a good tool to investigate the relative reactivity of **28** versus **29** under catalytic conditions.

### 3.5 Cleavage of Diols

As implemented earlier, one goal of this work was to find a suitable system for the biomimetic cleavage of vicinal diols. A first starting point was the choice of appropriate diols. Diols with aromatic substituents (e.g. **25**) used in earlier attempts were discarded, as the enhanced reactivity of the benzylic positions in these diols does not correspond properly to the diols in nonactivated positions cleaved in the natural systems. To further reduce interference of diol substituent functionalities with the desired cleavage reaction a simple long chain diol, 9,10-heneicosan-diol (**56**) was chosen as a candidate (*scheme 28*) as it was readily obtained by osmium-catalysed dihydroxylation<sup>93</sup> from commercially available *cis*-9-heneicosen and its unequal lengthed hydrocarbon substituents would lead to two different aldehydes after cleavage, C-9 pelargonaldehyde (Nonanal) (**57**) and C-12 lauraldehyde (dodecanal) (**58**) both readily analysed by GC-FID and GC-MS. The expected one to one appearance of two products gives more analytical information on the observed reaction than a similar symmetric system.



*Scheme 28*: Diol cleavage of 9,10-heneicosan-diol **56** under formation of the two aldehydes **57** and **58**.

For diol cleavage model systems the choice of an appropriate oxidant is crucial. For example, PhIO which is used for many other catalyses is unsuitable due to intrinsic reactivity of hypervalent iodine species towards diols in the absence of any additional catalyst. Furthermore, when applying *m*CPBA to our model system, considerable blank reactions were observed. Nevertheless addition of iron porphyrin quadrupled the amount of cleavage products (1.6%) when compared to the blank reaction (0.4%).

The H<sub>2</sub>O<sub>2</sub>-urea adduct is a convenient reagent to introduce non-aqueous H<sub>2</sub>O<sub>2</sub> into the catalytic system. Indeed diol cleavage was observed by appliance of this ‘O’-donor, with **29**

being more reactive than **28** (table 2). Reactivity in the H<sub>2</sub>O<sub>2</sub> system might not only arise from CpdI analogues but also from iron-peroxo species (Cpd0). Both blank reaction in absence of the catalysts and participation of possible Cpd0 analogues were finally avoided by applying the N-Oxide 'O'-donor system of Bruice et al mentioned earlier. Although for both iron porphyrins N-dealkylated compounds remained the major products, yields of diol cleavage products could be increased by modification of the N-oxide to its morpholine derivative **59** (figure 22). Omission of the electron withdrawing *p*-cyano-substituent on the aromatic ring in **60** again led to lower yields of diol cleavage, a trend reported by Bruice for epoxidation reactions applying dimethylaniline N-oxide versus **24** (demethylation of dimethylaniline N-oxide is significantly faster than the competing reactions). Both **59** and **60** were synthesized via the corresponding tertiary amines **61** and **62** (see exp. part).

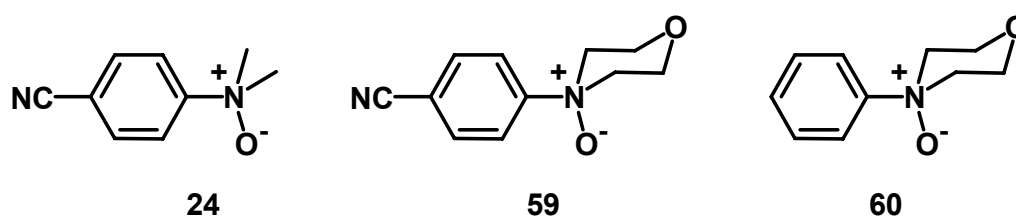


Figure 22: N-Oxides applied in diol cleavage catalysis

Co-oxidant	Model compound <b>28</b>	Model compound <b>29</b>
H <sub>2</sub> O <sub>2</sub> -urea	0.3 % aldehydes <0.1 % acids	3 % aldehydes 0.5 % acids
<b>24</b>	1 % aldehydes <0.1 % acids	0.2 % aldehydes <sup>a</sup>
<b>59</b>	4 % aldehydes 1 % acids	0.8 % aldehydes <sup>a</sup>
<b>60</b>	0.9 % aldehydes <sup>b</sup>	0.8 % aldehydes <sup>b</sup>

Table 2: Diol cleavage results applying different co-oxidants. Conditions: [porph] = 1.5 x 10<sup>-3</sup> M, [co-oxidant] = 1.5 x 10<sup>-2</sup> M, [56] = 1.5 x 10<sup>-2</sup> M in CH<sub>2</sub>Cl<sub>2</sub> at r.t. a) no detectable concentrations of acids were observed. b) control experiments for acid detection have been omitted.

For all reactions listed in table 2, omission of either co-oxidant or porphyrin led to no detectable formation of diol cleavage products. Unreacted diol could be recovered from the

reactions in 85-95% as the corresponding acetal. In analogy to the natural system in case of P450<sub>Biol</sub>, the model reactions aside the aldehydes gave rise to the corresponding acids, which were detected as their methylester<sup>94</sup> and the yield of which is also given in *table 2*. both the aldehydes and the acids were formed in a one to one ratio of C-9/C-12 products. Increase of diol concentration from diol/N-oxide/porphyrin 10/10/1 (as in *table 2*) to 100/10/1 resulted in a 1.2 fold increase in diol cleavage product, whereas slower addition of N-oxide over a longer period had only minor influence on diol cleavage versus dealkylation. Further improvement of diol cleavage/dealkylation selectivity could be envisioned by further modification of the substituents on the N-oxide to reduce reactivity of the corresponding amine towards the reactive iron oxo-species. This might be achieved by either further increase of steric demand to aid dissociation after 'O'-donation (a principle employed in the change of **24** to **59**) or by stronger electron withdrawing character of the substituents leading to amines with lower reactivity (as indicated from **60** vs. **59**).

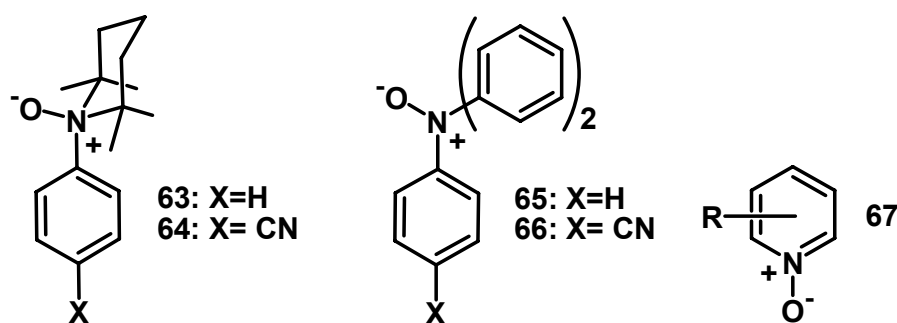


**Figure 23:** Candidates of further optimisation of N-oxide properties for appliance to diol cleavage reactions.

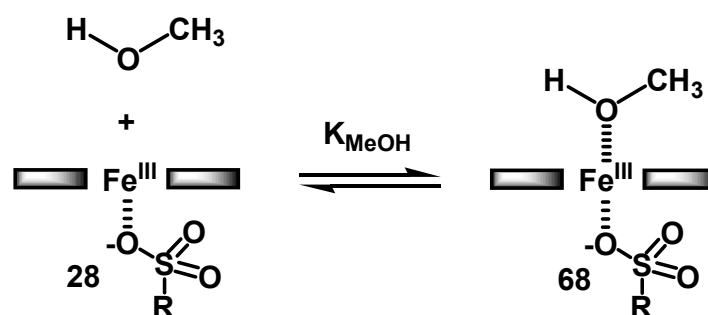
Compounds **63-66** (*figure 23*) are examples for such strategies employed, none of which could be applied to catalysis unfortunately as synthesis did not result in stable N-oxides for any of them. Aromatic N-oxides such as pyridine N-oxide and its derivatives (**67**) showed no reactivity towards the diol cleavage system. Therefore a possible N-oxide with better diol cleavage vs. dealkylation selectivity than **59** to date remains elusive.

As yields of diol cleavage products strongly depend on the applied N-oxide it is plausible to imply a scenario similar to the one discussed earlier for amine dealkylation, where the diol and the amine compete for the same reactive species formed from 'O'-donation of the N-oxide to the iron porphyrin. This scenario is also supported from differences in cleavage product yields comparing **28** and **29**. As in dealkylation reactions, the more reactive intermediate formed from **29** allows exchange of substrate to a far lower extend and therefore results in lower yields of diol cleavage products. Considering all these findings it is persuasive

to advance intermediately formed Cpdl analogues **45** and **46** as active species responsible not only for epoxidation and hydrocarbon hydroxylation but also for cleavage of vicinal diols. A similar situation is suggestive in the natural system thereby supporting the unique role of Cpdl in the field of P450 catalysis. Furthermore the simple catalytic system in hand opens the path for future investigations in the field of biomimetic diol cleavage.

### 3.6 Nitric Oxide Binding

Nitric oxide (NO) has multiple protective, deleterious and regulatory effects in biology.<sup>95</sup> It plays a role in trapping of oxidative radical species, in immune response to pathogen invasion and as a neurotransmission regulator. Metal centers, in particular iron are major targets in bioregulation by NO.<sup>96</sup> Interaction of NO with the metal centers of enzymes changes their reactivity by either enhancement or inhibition. In the context of involvement of heme enzymes in the biochemistry of NO, understanding of its interaction with iron porphyrins is of profound interest. In collaboration with van Eldik et al model compound **28** was therefore studied on its behaviour towards NO<sup>97</sup> and compared to interactions with P450<sub>cam</sub> studied earlier by the van Eldik group.<sup>98</sup> To investigate the influence of the iron coordination sphere, studies were conceived to be performed in both apolar, noncoordinating solvent (toluene), where the model compound displays a five-coordinate complex resembling the E'S complex of P450<sub>cam</sub>, and in MeOH, where a solvent molecule is assumed to be coordinated to iron, forming a six ligand complex **68** (scheme 29), comparable to the P450<sub>cam</sub> resting state (P450<sub>cam</sub>RS).



**Scheme 29:** Coordination of MeOH to **28** as a sixth ligand.

Indeed the UV/Vis spectrum of **28** in MeOH differs drastically from that in toluene ( $\lambda_{\text{max}} = 416 \text{ nm}, 512 \text{ nm}$ ) showing a split Soret band with  $\lambda_{\text{max}} = 396$  and  $416 \text{ nm}$  and a Q-band at  $532$

nm. From titrations of toluene solutions of **28** with MeOH (*figure 24*), the van Eldik group was able to obtain the equilibrium constant  $K_{\text{MeOH}}$  for the coordination of MeOH to **28**, which is rather small and equals  $0.20 \pm 0.05 \text{ M}^{-1}$  at  $25 \text{ }^\circ\text{C}$ .

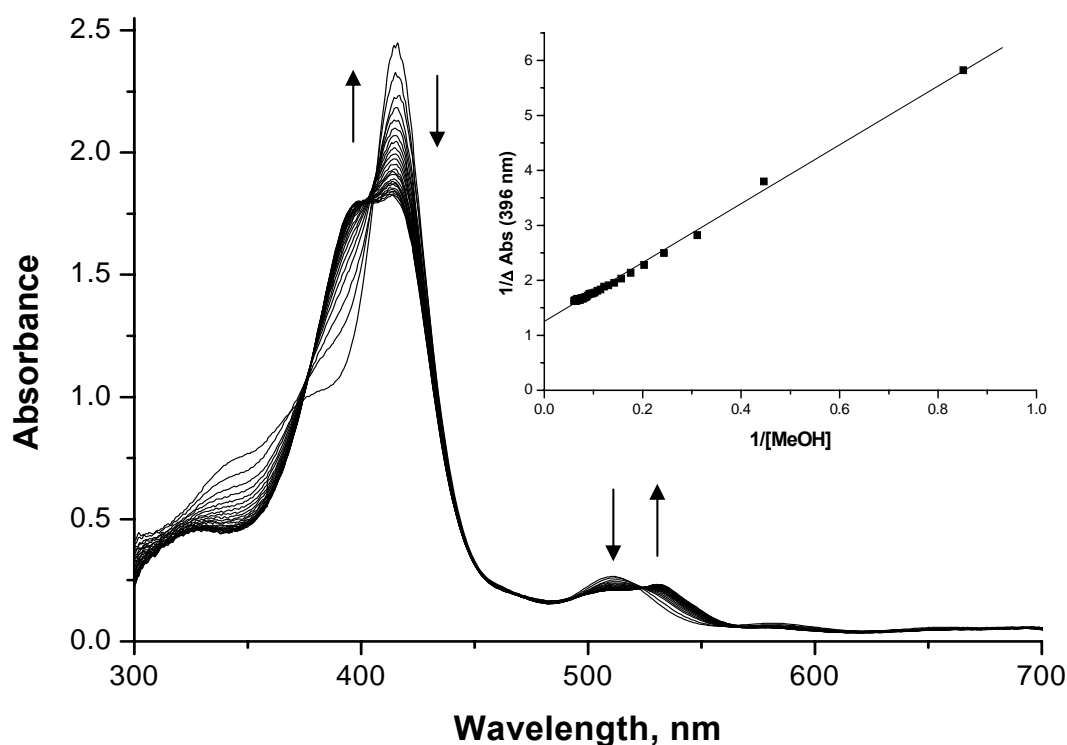


**Figure 24:** Spectral changes recorded during titration of  $1.01 \times 10^{-5} \text{ M}$  **28** in toluene with methanol at  $25 \text{ }^\circ\text{C}$ . *Inset:* Plot of  $(\Delta \text{Abs})^{-1}$  at 396 nm vs.  $[\text{MeOH}]^{-1}$  to determine the equilibrium constant  $K_{\text{MeOH}}$ .

cw-EPR investigations in our group showed that upon addition of MeOH to toluene solutions of **28** for a MeOH/toluene ratio up to 2/1 the spin state of iron does not change, the only changes in the spectrum being a slight broadening and shift of the high spin signal at  $g = 5.8$  to 5.6. Although the matrix prevented an adequate analysis for pure MeOH, the recorded spectrum still adumbrates a high spin iron(III) species. This means MeOH coordination does not change the spin state of iron, with **68** still being high spin iron(III). Only when MeOH was exchanged for saturated KOMe/MeOH, the spectrum obtained (*figure 25*) displayed dominant signals of the low-spin iron(III) methoxylat-complex ( $g = 2.42, 2.15$  and  $1.93$ ). Therefore one main difference between six-coordinated **68** and the resting state of  $\text{P450}_{\text{cam}}$  is the spin state of iron being high spin iron(III) in the former and predominantly low spin iron(III) in the latter.

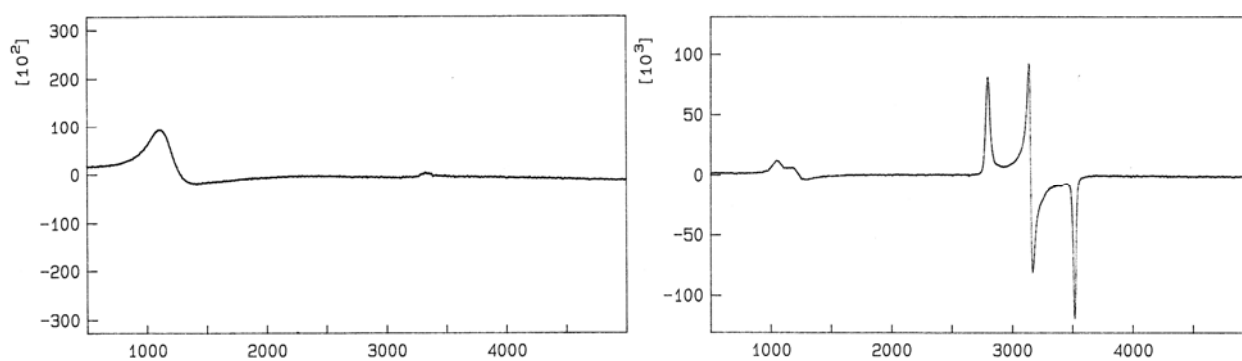


**Figure 25:** (left) cw-EPR spectrum of **28** in MeOH/Toluene 2/1 at  $T = 100$  K, (right) cw-EPR spectrum of **28** in KOMe-MeOH/Toluene 1/2 at  $T = 93$  K.

Nitric oxide, which has one unpaired electron located in the  $\pi^*$  orbital can coordinate to metals in a range from that of a nitrosyl cation ( $\text{NO}^+$ , *figure 26a*) which binds to the metal with a M-N-O bond angle of  $\sim 180^\circ$  and where considerable charge transfer to the metal leads to a formally reduced  $\text{M}^{n-1}$  state, to that of a nitroxyl anion ( $\text{NO}^-$ , *figure 26b*), where M is formally  $\text{M}^{n+1}$  and for which a M-N-O bond angle of  $\sim 120^\circ$  is expected.<sup>95</sup> The nature of binding between NO and the metal center is reflected in the IR spectra of the corresponding complexes, showing a  $\nu_{\text{N-O}}$  of  $\sim 1850$   $\text{cm}^{-1}$  in the nitrosyl cation case and of  $\sim 1670$   $\text{cm}^{-1}$  in the nitroxyl anion case. Further insight into the electronic structure of metal-NO complexes can be obtained by EPR.



**Figure 26:** Illustration of the possible character of metal porphyrin-NO complexes. a) nitrosyl cation b) nitroxyl anion case.

Iron(III)-porphyrin NO complexes have been analysed by both X-ray crystallography and IR spectroscopy. They show an almost linear coordination of NO ( $\text{Fe-N-O} \sim 175^\circ$ ) and IR signals indicative of nitrosyl cation coordination ( $\nu_{\text{N-O}} \sim 1820\text{-}1870$   $\text{cm}^{-1}$ ). Similar IR signals were obtained from NO-coordinated P450 enzymes; P450<sub>nor</sub> and P450<sub>cam</sub> showing  $\nu_{\text{N-O}}$  of 1853 and 1806  $\text{cm}^{-1}$  respectively.

Saturation of a toluene solution of **28** with NO resulted in UV/Vis changes from 416 nm (Soret) and 512 nm (Q-bands) to 432 and 542 nm (*figure 27a*).

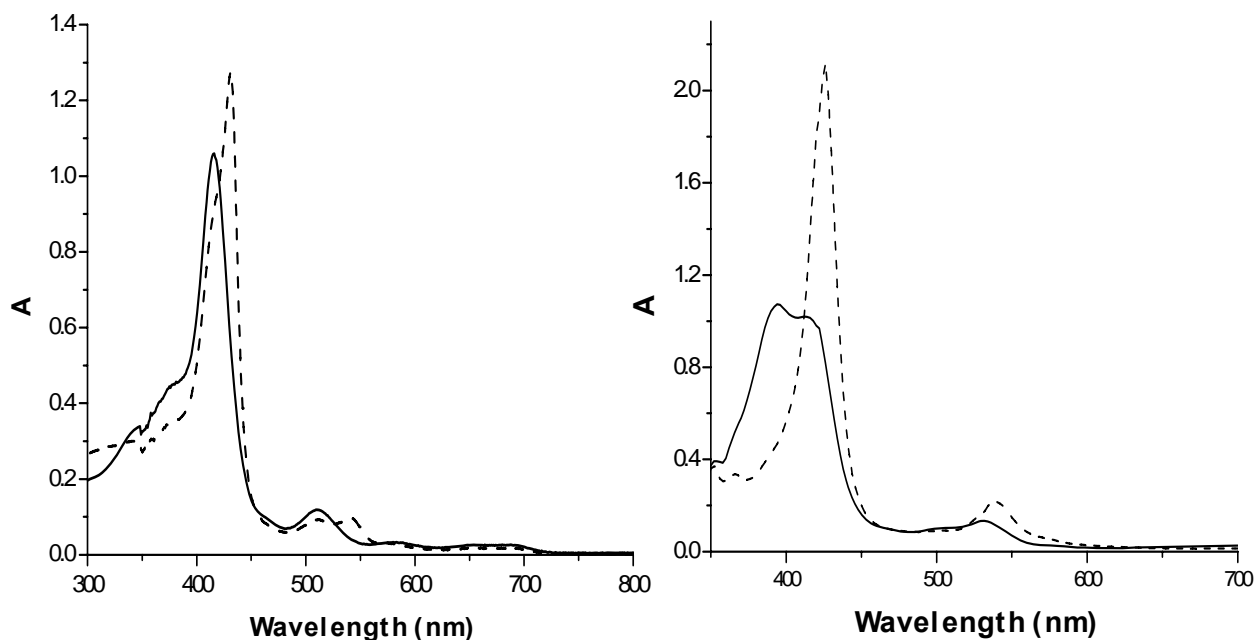


**Figure 27:** a) (left): Electronic absorption spectra of **28** before (solid line) and after saturation with NO (dashed line) in toluene solution at  $\sim 20$  °C. b) (right): Electronic absorption spectra of **68** before (solid line) and after saturation with NO (dashed line) in methanol solution at  $\sim 0$  °C.

FTIR characterisation revealed a sharp band at  $1833\text{ cm}^{-1}$  in the difference spectrum of **28**(NO) and **28**, which is in good agreement with above mentioned values for  $\nu_{\text{N-O}}$ . cw-EPR spectroscopic analysis after saturation of a degassed toluene solution of **28** with NO showed complete disappearance of the high spin signal at  $g = 5.8$  and appearance of a weaker signal at  $g = 1.98$ , which was assigned to originate from excess NO present in solution by comparison with a spectrum obtained from NO saturated toluene (*figure 28*) showing a very similar signal at  $g = 1.99$ . Therefore the species obtained from NO coordination to **28** appears to be EPR silent, which supports indication of a low spin “iron(II)-nitrosyl cation” species in agreement with the FTIR results.

NO ligation appears to be completely reversible, as the original UV/Vis spectrum could be regained upon removal of NO under a stream of argon. In a similar experiment, the  $g = 5.8$  high spin iron(III) EPR signal could be recovered after bubbling argon through a NO-induced “EPR silent” sample of **28**.

Similar behaviour was observed when a methanol solution of **68** was saturated with NO, UV/Vis maxima shifting from 396/416 (Soret) and 532 nm to 424 and 542 nm for **28(NO)** (*figure 27b*) in a reversible fashion.

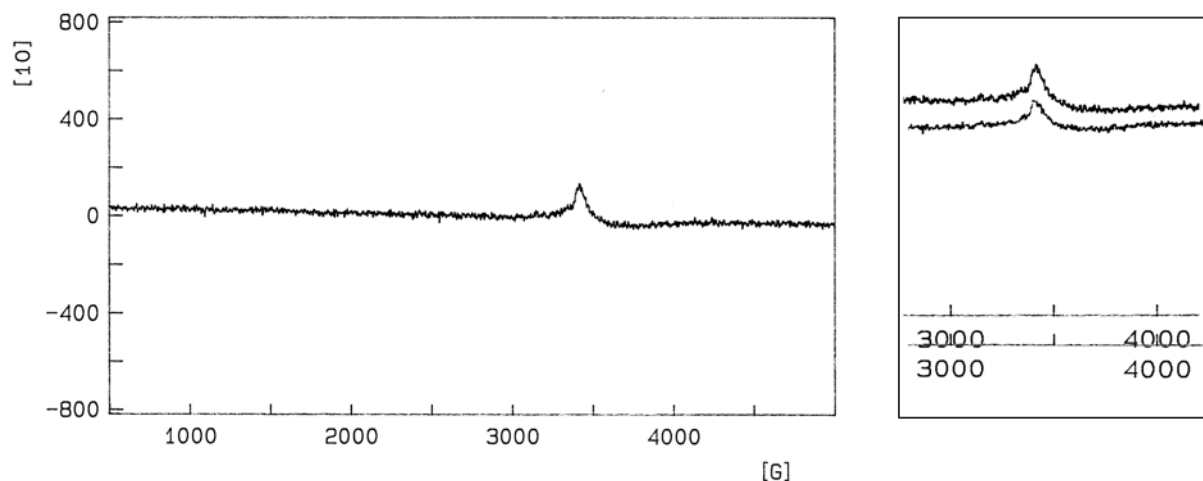
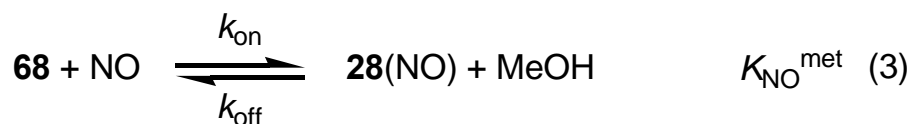
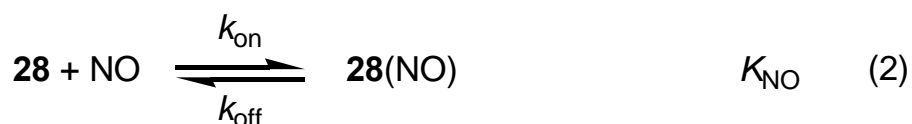


**Figure 28:** (left) cw-EPR spectrum obtained after saturation of a toluene solution of **28** with NO gas,  $T = 93$  K. (right) overlay of the  $g = 1.98$  signal in the sample of **28(NO)** on the left (upper trace) with the spectrum obtained from a NO saturated solution of toluene at  $T = 97$  K (lower trace).

The above findings are consistent with an equilibrium described in equation (2) for toluene and equation (3) for methanol.



Van Eldiks group has employed extensive low-temperature stopped-flow and laser flash photolysis techniques under variation of NO concentrations, temperature and pressure to thoroughly study both equilibria and in that way obtained detailed information on the kinetic and thermodynamic parameters of NO coordination. These could then be interpreted and compared to the same parameters obtained from NO coordination to P450<sub>cam</sub> (*table 3*).



	<b>28</b> (toluene)	E:S P450 <sub>cam</sub>	<b>68</b> (methanol)	P450 <sub>cam</sub> RS
$k_{\text{on}}$ (M <sup>-1</sup> s <sup>-1</sup> ) <sup>a</sup>	(1.80 ± 0.05)·10 <sup>6</sup>	(3.2 ± 0.5)·10 <sup>6</sup>	(0.6 ± 0.05)·10 <sup>5</sup>	(3.20 ± 0.02)·10 <sup>5</sup>
$\Delta H^{\ddagger}_{\text{on}}$ (kJ mol <sup>-1</sup> )	4 ± 2	14.1 ± 0.1	14 ± 1	92 ± 1
$\Delta S^{\ddagger}_{\text{on}}$ (J mol <sup>-1</sup> K <sup>-1</sup> )	-111 ± 6	-73.1 ± 0.4	-107 ± 3	+169 ± 4
$\Delta V^{\ddagger}_{\text{on}}$ (cm <sup>3</sup> mol <sup>-1</sup> )	-25 ± 1	-7.3 ± 0.2	-21 ± 4	+28 ± 2
$\Delta G^{\ddagger}_{\text{on}}$ (kJ mol <sup>-1</sup> ) <sup>a</sup>	37 ± 2	35.9 ± 0.1	46 ± 1	42 ± 1
$k_{\text{off}}$ (s <sup>-1</sup> ) <sup>a</sup>	(1.25 ± 0.01)·10 <sup>4</sup>	1.93 ± 0.02	2249 ± 167	0.35 ± 0.02
$\Delta H^{\ddagger}_{\text{off}}$ (kJ mol <sup>-1</sup> )	58 ± 1	83.8 ± 0.7	44 ± 5	122 ± 4
$\Delta S^{\ddagger}_{\text{off}}$ (J mol <sup>-1</sup> K <sup>-1</sup> )	+29 ± 5	+41 ± 2	-34 ± 22	+155 ± 15
$\Delta V^{\ddagger}_{\text{off}}$ (cm <sup>3</sup> mol <sup>-1</sup> )	+7 ± 3	+24 ± 1	+7 ± 3	+31 ± 1
$\Delta G^{\ddagger}_{\text{off}}$ (kJ mol <sup>-1</sup> ) <sup>a</sup>	50 ± 1	71.6 ± 0.7	54 ± 5	76 ± 4
$K_{\text{NO}}$ (M <sup>-1</sup> ) <sup>a</sup>	122 ± 10	(1.2 ± 0.4)·10 <sup>6</sup>	27 ± 3	(9.0 ± 0.2)·10 <sup>5</sup>
$\Delta H^{\circ}$ (kJ mol <sup>-1</sup> )	-71 ± 3	-69.7 ± 0.8	-59 ± 4	-30 ± 5
$\Delta S^{\circ}$ (J mol <sup>-1</sup> K <sup>-1</sup> )	-197 ± 10	-114 ± 2	-169 ± 13	+14 ± 19
$\Delta V^{\circ}$ (cm <sup>3</sup> mol <sup>-1</sup> )	-39 ± 2	-31.3 ± 1.2	-28 ± 1	+3 ± 3
$\Delta G^{\circ}$ (kJ mol <sup>-1</sup> ) <sup>a</sup>	-12 ± 3	-35.7 ± 0.7	-9 ± 4	-34 ± 4

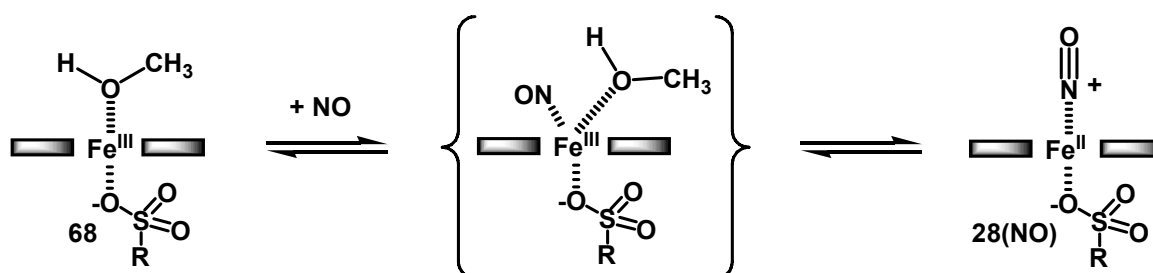
**Table 3:** Comparison of the rate and equilibrium constants, as well as thermodynamic and kinetic parameters for NO Binding to **28**, **68**, the E:S complex of P450<sub>cam</sub> and the P450<sub>cam</sub> resting state. a) at 25 °C.

Interpretation of the above parameters suggest a close similarity in the mechanism for binding of NO to **28** and E:S P450<sub>cam</sub>, where an encounter complex is formed prior to Fe-NO bond formation, according to equation (4). The rate for the ‘on’-reaction is very similar in both cases, the mechanism being dominated by Fe-NO-bond formation with a concomitant change of iron spin state from high to low spin.

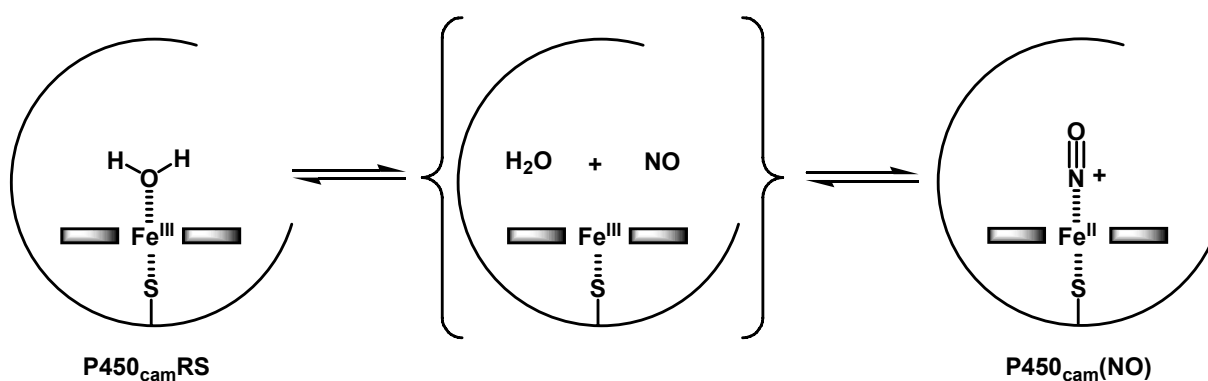


In contrast to the consistency of  $k_{\text{on}}$ , the ‘off’-reaction in the model case is a factor of 10<sup>4</sup> faster than in the enzyme case (a trend generally observed for binding of NO to model compounds),<sup>96,99</sup> which is also reflected in the dramatic decrease of the equilibrium constant  $K_{\text{NO}}$  for the model and emphasises the unique properties of the enzyme environment to stabilise coordination of NO to iron. The reaction towards NO in both the model- and enzyme case is slowed down significantly by the presence of a sixth ligand on iron (**68**/P450<sub>cam</sub>RS) which has to be removed for coordination of NO. In contrast to the similar behaviour of **28** to

E:S P450<sub>cam</sub>, the reactions of **68** and P450<sub>cam</sub>RS show completely divergent parameters. For **68** the obtained values indicate an associative interchange (I<sub>a</sub>) mechanism with a relatively strong contribution from the entering NO molecule (*scheme 30a*), whereas the reaction of P450<sub>cam</sub>RS is dominated by dissociation of a water molecule in a dissociative ligand substitution (*scheme 30b*).



a) associative interchange mechanism pathway for the reaction of NO with **68**



b) dissociative ligand substitution in P450<sub>cam</sub>RS

**Scheme 30:** Divergent mechanisms for NO coordination to a) **68** or b) P450<sub>cam</sub>RS.

This disparate mechanistic behaviour of **68** and P450<sub>cam</sub>RS can be explained in terms of the difference in their spin state of iron, being high spin in the earlier and predominantly low spin in the latter. Again NO dissociation is much slower in the enzyme case, where the Fe<sup>II</sup>-NO<sup>+</sup> complex is more efficiently stabilized by H-bonding and coulomb interactions with the water molecules in close vicinity when compared to similar but weaker interactions with less rigidly organised solvent molecules in methanol.

In summary, **28** in aprotic solvents is an appropriate model for NO coordination of substrate bound P450<sub>cam</sub> displaying completely reversible binding of NO in mechanistic analogy to the

enzyme case. The appliance of **68** on the other hand indicates the importance of iron spin state on the reaction mechanism. Results of both model systems finally emphasise the unique role of the enzyme pocket in stabilising NO coordination of heme proteins.

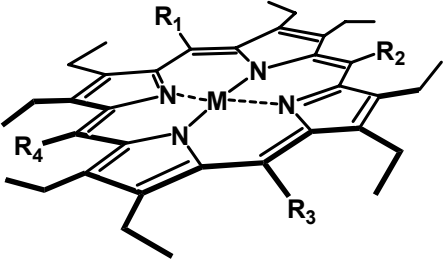
## 3.7 Modification of the Natural Cofactor

### 3.7.1 Design and Synthetic Strategy

As already observed in the case of the new family of model compounds introduced earlier, substituents in the *meso*-positions influence the behaviour of the porphyrin macrocycle. Introduction of electron withdrawing substituents both in *meso*- and  $\beta$ -positions of porphyrins has been applied to obtain more electron poor and therefore more reactive metal catalysts in oxidation reactions.<sup>100,101</sup> Thus, tetra-phenyl-porphyrins with electron poor *meso*-phenyl substituents (e.g. 2,6-dichloro- or pentafluoro-phenyl) have been further halogenated (perfluorination, -chlorination) in  $\beta$  – positions leading to increased activities of the so obtained porphyrin catalysts. Furthermore substitution hampers oxidative destruction of the catalysts, therefore not only enhancing their reactivity but also increasing their stability under catalytic conditions.

When designing new cofactors for P450 enzyme catalysis, one has to find a consensus between modification of properties and maintenance of structural similarity to the original cofactor. Therefore, as outlined in the aims of this work, the existing substituents in the  $\beta$  – positions were planned to be conserved as far as possible and new substituents were intended to be introduced in the originally free *meso*-position (*scheme 10*). To obtain more reactive variants, these substituents were envisioned to be electron withdrawing such as nitro groups ( $X = \text{NO}_2$ ) or halogens ( $X = \text{F}, \text{Cl}, \text{Br}$ ), but in principle the substitution strategy could also be extended towards electron donating groups. In this way more electron rich cofactors would be obtained, which might be applied in stabilisation of CpdI in the catalytic cycle of the P450s and therefore in rendering it spectroscopically analysable.

Modification of porphyrins in *meso*-position has already been studied for a rather long time, with e.g. Fischer et al<sup>102</sup> examining chlorination and bromination of a variety of porphyrins (including mesoporphyrin) as early as the beginning of the 20<sup>th</sup> century. In the 1960s, Stephenson et al<sup>103</sup> reported on sequentially chlorinated derivatives of octa-ethyl-porphyrin (**69**) (**70-72**, *figure 29*) and studied the influence of substituents on their electronic spectra.



	R <sub>1</sub>	R <sub>2</sub>	R <sub>3</sub>	R <sub>4</sub>	M
<b>69</b>	H	H	H	H	2H
<b>70</b>	Cl	H	H	H	2H
<b>71</b>	Cl	H	Cl	H	2H
<b>72</b>	Cl	Cl	Cl	Cl	2H

	R <sub>1</sub>	R <sub>2</sub>	R <sub>3</sub>	R <sub>4</sub>	M
<b>73</b>	H	H	H	H	Zn
<b>74</b>	NO <sub>2</sub>	H	H	H	Zn
<b>75</b>	NO <sub>2</sub>	NO <sub>2</sub>	H	H	Zn
<b>76</b>	NO <sub>2</sub>	H	NO <sub>2</sub>	H	Zn
<b>77</b>	NO <sub>2</sub>	NO <sub>2</sub>	NO <sub>2</sub>	H	Zn
<b>78</b>	NO <sub>2</sub>	NO <sub>2</sub>	NO <sub>2</sub>	NO <sub>2</sub>	Zn
<b>79</b>	F	H	H	H	2H
<b>80</b>	F	F	H	H	2H
<b>81</b>	F	H	F	H	2H
<b>82</b>	F	F	F	H	2H
<b>83</b>	F	F	F	F	2H

**Figure 29:** Substitution pattern of different octa-ethyl-porphyrin derivatives by Stephenson and Dolphin.

	Soret (nm)	Q-bands (nm)			
<b>69</b>	401	499	534	566	618
<b>70</b>	406	507	540	578	620
<b>71</b>	411	514	548	586	637
<b>72</b>	446	550	597	634	712

*a)* : electronic spectra of Cl-substituted octa-ethyl-porphyrins in CHCl<sub>3</sub>

	E <sub>1/2</sub> ox (1 <sup>st</sup> )	E <sub>1/2</sub> red (1 <sup>st</sup> )	Soret (nm)	Q-bands (nm)	
<b>73</b>	0.87	-1.47	402	490	532
<b>74</b>	1.01	-1.02	401	497	534
<b>75/76</b>	1.16	-0.78	404	503	539
<b>77</b>	1.31	-0.50	413	510	547
<b>78</b>	1.49	-0.28	426	520	561

*b)* : redox potentials and electronic spectra of NO<sub>2</sub>-substituted Zn-octa-ethyl-porphyrins

	Soret (nm)	Q-bands (nm)			
<b>69</b>	401	499	534	566	618
<b>79</b>	401	498	532	566	621
<b>80/81</b>	398	497	529	572	627
<b>82</b>	398	498	529	577	631
<b>83</b>	400	466/501	531	584	642

*c)* : electronic spectra of F-substituted octa-ethyl-porphyrins in CHCl<sub>3</sub>

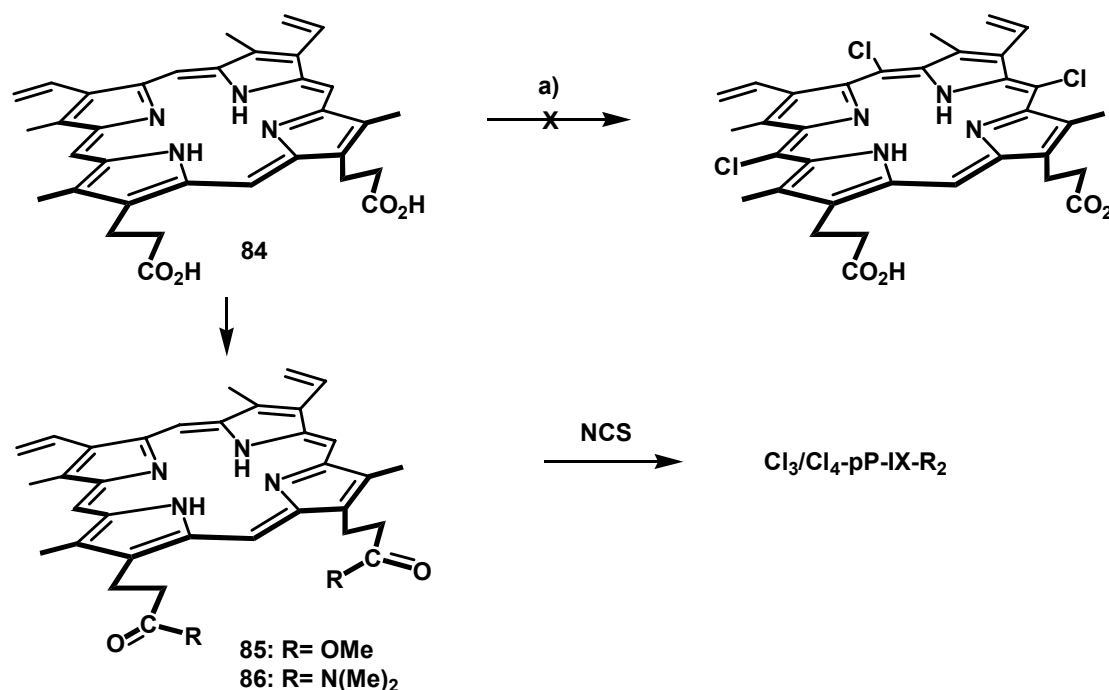
**Table 4 a-c:** Influence of the substitution pattern of different octa-ethyl-porphyrin derivatives.

The introduction of chlorines resulted in a bathochromic shift of both the Soret and Q-bands (*table 4a*). A similar trend was observed by Dolphin et al<sup>104</sup> in the 1980s for sequential nitration of the same compound. Furthermore he measured the redox potentials of the corresponding Zn-complexes (**73-78**, *figure 29*) and observed a shift to more positive values upon nitration (*table 4b*). Nitration was also applied in the late 1990s in the Woggon group by Forrer<sup>105</sup> to modify the redox potentials of model compounds. In all these contributions it was shown that not only electronic, but also steric factors of the newly introduced substituents influence the behaviour of the new compounds. Upon increase of steric strain the porphyrins lose their flat topology and adopt nonplanar conformations. This effect is more strongly pronounced in the free bases, whereas coordination of a metal can decrease nonplanarity and also reduce the shift in the electronic spectra. It can be deduced that the bathochromic shift upon substitution is dominated by nonplanarity and therefrom resulting decrease of the HOMO-LUMO gap of the porphyrin.<sup>106</sup> Reduction of steric influences was obtained for introduction of fluorine,<sup>107</sup> showing no bathochromic shift for different substituted derivatives of **69** (**79-83**, *table 4c*).

Considering the above findings, two strategies can be envisioned for the design of the modified cofactors. Fluorine-substitution would generate derivatives where altered properties mainly are resulting from different electronic properties, whereas substitution with other larger groups, e.g. chlorine, influences both steric and electronic factors. For a first exploration the chlorine-substituted derivatives of protoheme were chosen, particularly under considerations of practical advantages over fluorine-substituted derivatives in their synthesis. It can be envisioned that steric effects can have both advantageous and disadvantageous influences on a future biocatalytic system. An increase of steric demand might e.g. facilitate product dissociation from the active site or alter substrate specificity but at the same time can prevent appropriate arrangement of substrates or even inhibit incorporation of the new cofactor into the apoprotein. In a first construct it was therefore intended to explore a derivative where only three of the four *meso*-positions are chlorinated. The latter was envisioned to show less steric strain than its four-substituted counterpart but to still exhibit enough electron withdrawing character to enable the desired increased reactivity. In principal for a non-completely substituted compound there exist different possible regioisomers. It was anticipated though, that the  $\gamma$ -*meso*-position flanked by the two carboxyl groups might display lower reactivity and therefore lead to one predominant tri-substituted species where this position is still unsubstituted.

### 3.7.2 First Findings and adapted Approaches

First chlorination experiments were performed during the diploma thesis of Soydaner<sup>108</sup> on protoporphyrin IX (**84**) (pP-IX, *scheme 31*). The iron free porphyrin was chosen because iron complicates both behaviour and analysis of the corresponding compounds. Chlorination reactions from earlier studies, applying rather harsh conditions (e.g. conc. HCl / 3% H<sub>2</sub>O<sub>2</sub> in AcOH)<sup>102,103</sup> in his hands did not lead to any desired chlorination products (path **a** in *scheme 31*). Furthermore behaviour of the free acid functions of **84** was found to be cumbersome for handling. Therefore further studies were performed on the dimethylester (**85**) and the di-N,N-dimethyl-amide (**86**) of pP-IX. In addition their corresponding Zn-complexes were also prepared and investigated in the same reactions, the concept being that firstly metal coordination should change reactivity of the porphyrin and secondly Zn-insertion is known to facilitate separation of obtained product mixtures. With these approaches, Soydaner reported his best results for chlorination of **86** using N-chloro-succinimide (NCS), where a mixture of products with different grade of chlorination was obtained (mainly Cl<sub>3</sub> and Cl<sub>4</sub> products as judged from MALDI-TOF-MS analysis).

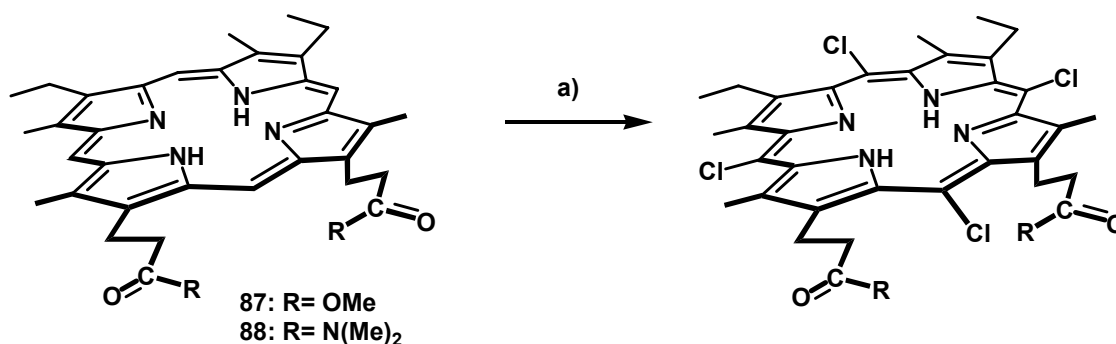


**Scheme 31:** First findings and adaptation of strategies in chlorination reactions on pP-IX.

Taking over from there it was possible to purify several fractions of NCS chlorination products to an extent where structural analysis by  $^1\text{H-NMR}$  was enabled. Unfortunately, analysis implied that the vinyl groups were major site of attack, such that these functionalities are incompatible even with these rather mild chlorination conditions.

### 3.7.3 Chlorination of Mesoporphyrin Derivatives

Taking into account the previous results, it was decided to proceed by appliance of the mesoporphyrin analogues (**87**) and (**88**) of **85** and **86**, where the vinyl groups are exchanged for ethyls (*scheme 32*). Utilisation of this subtle difference from the natural cofactor is legitimated by the fact that several reports confirm correct incorporation of mesoheme into heme-proteins<sup>109,110</sup> without major modification of their properties.



*Scheme 32:* Chlorination reactions of mesoporphyrin derivatives **87** and **88**. a) NCS

Reaction of **87** and **88** with NCS in  $\text{CH}_2\text{Cl}_2$  at r.t. under exclusion of light were found to be sufficiently slow to allow their tracking with HPLC techniques. Consumption of starting material ( $\lambda_{\text{max}} = 394$  nm) was associated with formation of new peaks appearing in consecutive order of  $\lambda_{\text{max}} = 401$ , 406 and finally 446 nm. This correlates very well with the bathochromic shift observed by Stephenson et al for “Cl<sub>1</sub>-“ **70**, “Cl<sub>2</sub>-“ **71** and “Cl<sub>4</sub>-“ **72**. Furthermore semi- and preparative HPLC separation allowed ESI-MS analysis of the  $\lambda_{\text{max}} = 406$  nm products and supported their Cl<sub>2</sub>-assignment. Detailed analysis of the final  $\lambda_{\text{max}} = 446$  nm products (*vide infra*) confirmed their Cl<sub>4</sub>-structure. Although in an early attempt the above techniques allowed observation of a species with  $\lambda_{\text{max}} = 432$  nm and the appropriate mass (ESI-MS analysis) indicative of a Cl<sub>3</sub>-species as a minor component in a mixture of the earlier compounds, multiple repetitions of the experiment did not afford any further observation of a



similar product. It seems, that under chlorination conditions the Cl<sub>3</sub>-product is chlorinated further to the final Cl<sub>4</sub>-product rather rapidly, thereby prohibiting accumulation. It was therefore concluded to proceed with the much more accessible Cl<sub>4</sub>-product, furthermore supported by the fact that the assigned Cl<sub>3</sub>-species also seems to display considerable nonplanarity, as judged from the electronic spectrum.

Initial experiments were performed on derivative **88**, as its amide functions are more resistant to experimental conditions than the ester groups of **87**. Indeed, the chlorinated product could be obtained in good yield, but appliance of several different purification techniques for the latter failed to separate the product from impurities evident by <sup>1</sup>H-NMR measurements. Furthermore, deprotection conditions to obtain the desired free acid seemed to demand conditions too harsh for maintaining the integrity of the rest of the molecule both for the free base Cl<sub>4</sub>-**89** or the corresponding iron complex **90**. It was therefore decided to further investigate the chlorination of dimethylester **87**, which was found to proceed analogous to the amide case, and furthermore allowed better purification due to its more apolar character. In that way, a pure tetrachlorinated compound **91** could be obtained, albeit at initially very low yield (~ 3%), which could be improved to ~20% by appliance of TMS-diazomethane/MeOH upon termination of chlorination. The so obtained compound was thoroughly analysed and characterized. HPLC analysis ensured its purity from other porphyrinogenic compounds. ESI-MS analysis showed the correct mass ( $m/z = 731$ ,  $[M+H]^+$ ) with the expected isotopic distribution for incorporation of four chlorines (calculated by MWC V. 6.3 for Windows).<sup>111</sup>

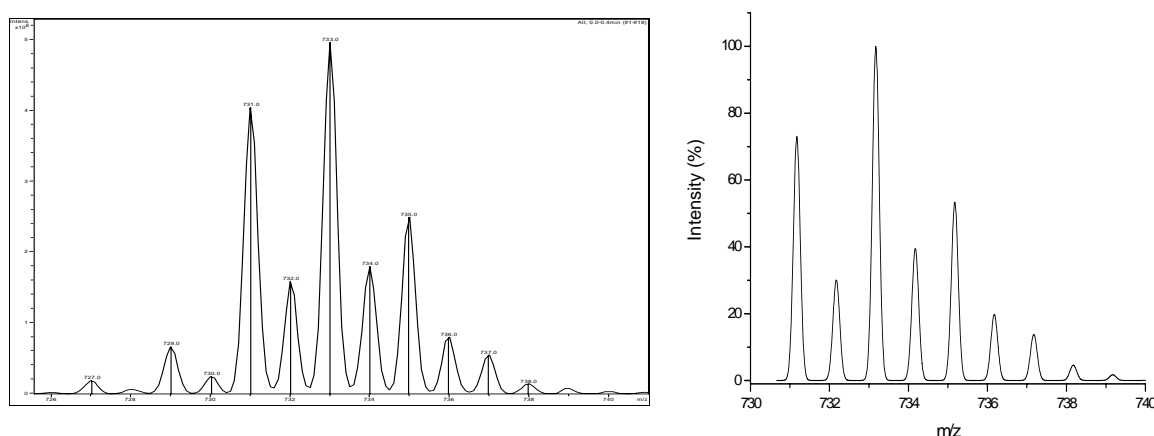
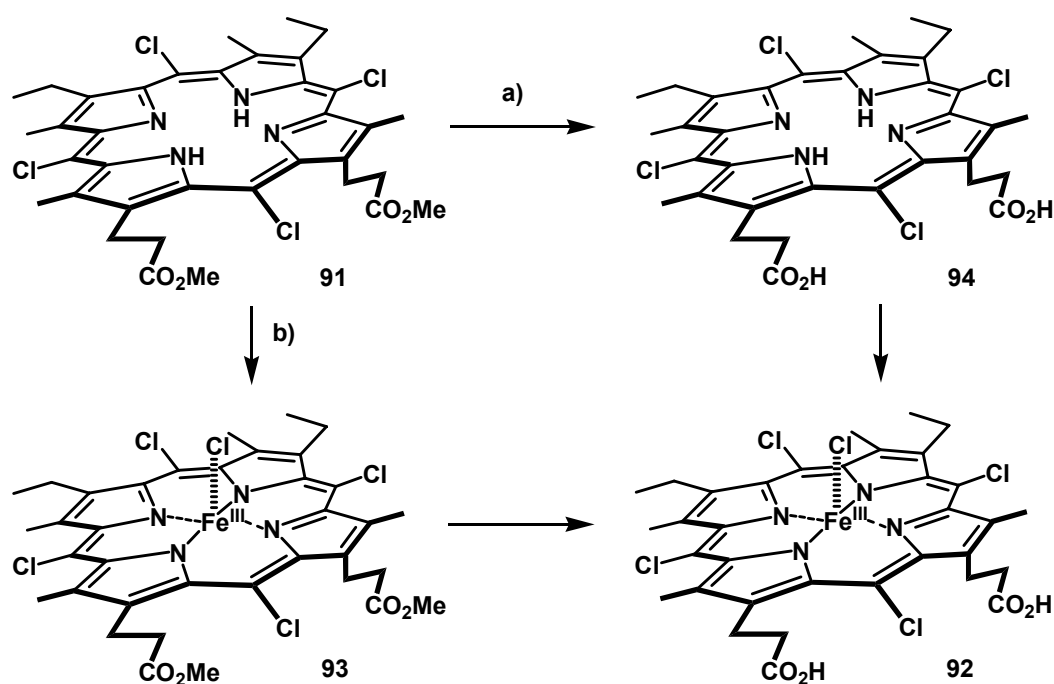


**Figure 30:** Comparison of the isotopic distribution of the product peak  $m/z = 731$ ,  $[M+H]^+$  of **91** obtained by ESI-MS measurement (left) with the pattern predicted by calculation (right).

*Meso*-selectivity of chlorination was proven by  $^1\text{H-NMR}$  characterisation, where no signals are observed above 5 ppm for **91**, whereas in the corresponding unchlorinated starting material **87** the *meso*-Hs show characteristic signals at 10-11 ppm. All the other proton signals of the starting material find their counterparts in the spectrum of the product, therefore ensuring exclusive *meso*-chlorination. The UV/Vis spectrum shows a considerable bathochromic shift for the Soret band from 397 nm for **87** to 441 nm for **91** in THF.

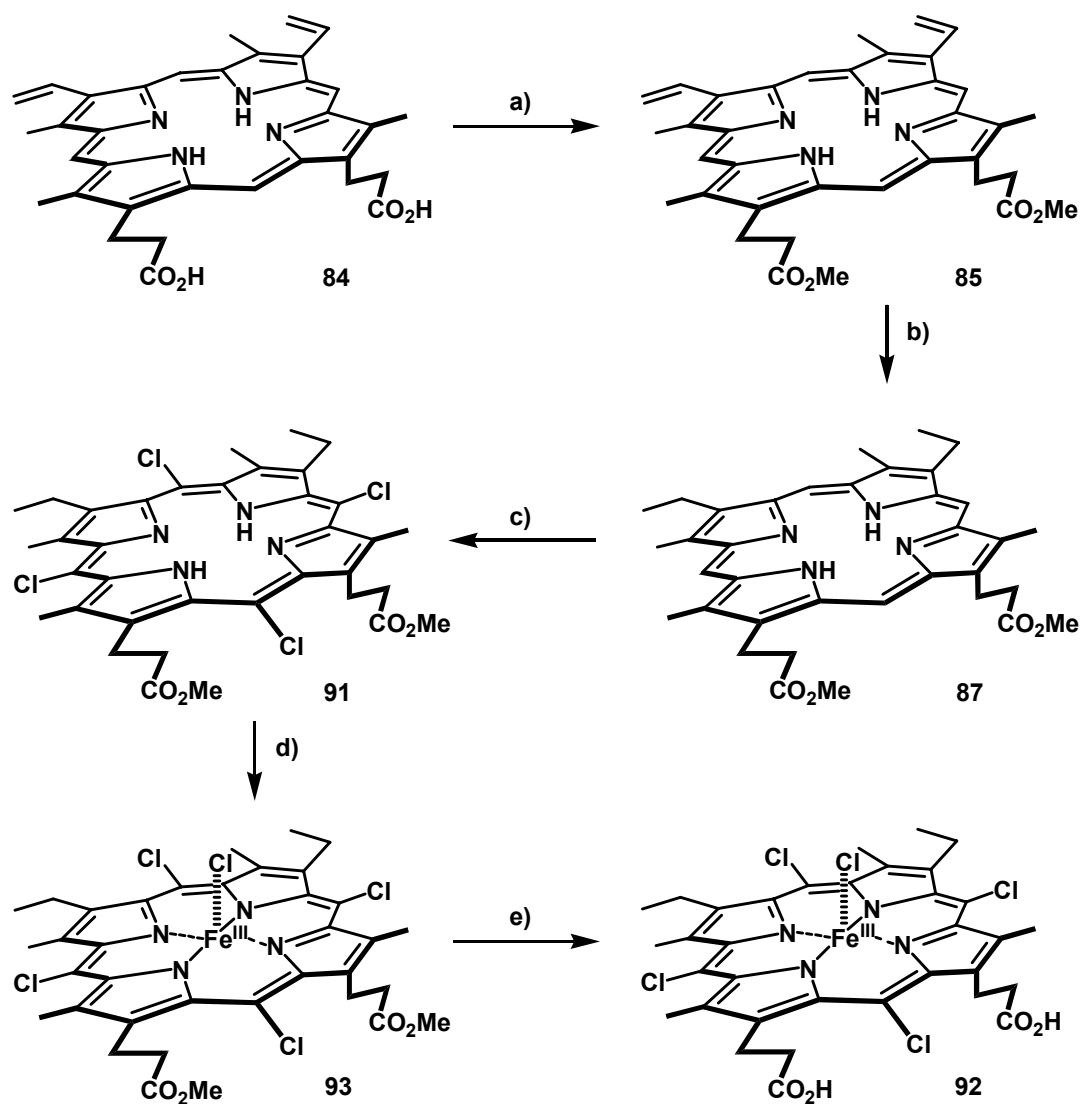
With this chlorinated precursor in hand, two possible routes lead to the desired free acid iron porphyrin **92** (scheme 33). Either by a) ester hydrolysis followed by iron insertion or b) iron insertion first and ester hydrolysis in the last step.



**Scheme 33:** The two possible routes to **92** starting from **91**, a) by first hydrolysis to **94** and b) by iron insertion to obtain **93** and subsequent hydrolysis.

Investigating both routes the latter, where iron insertion is done first, was found to be more fruitful, as the ester groups in iron-porphyrin **93** facilitate analysis of the iron complexes and because the free base acid **94** was found to be rather unstable and cumbersome to handle. Iron insertion was optimised to yield 65% of **93** (originally as its  $\mu$ -oxo dimer **95**, vide infra) by appliance of  $\text{FeCl}_2$  and 2,6-Lutidine in a  $\text{CH}_2\text{Cl}_2$ /acetonitrile mixture. (the same technique, when applied to unchlorinated **87** gave 73% of corresponding [Mesoporphyrin-dimethylester-iron(III)]Cl (**96**)) The latter could then finally be hydrolysed to the corresponding diacid **92** quantitatively in THF/1.0 M LiOH solution (2/1) overnight. Purity of **93** and **92** from other

porphyrinogenic compounds was again ensured by HPLC analysis. After the above procedure the newly obtained modified cofactor in principle is ready for incorporation into the apoprotein. A complete pathway of the final synthesis of **92** from pP-IX (**84**) is given in *scheme 34*.

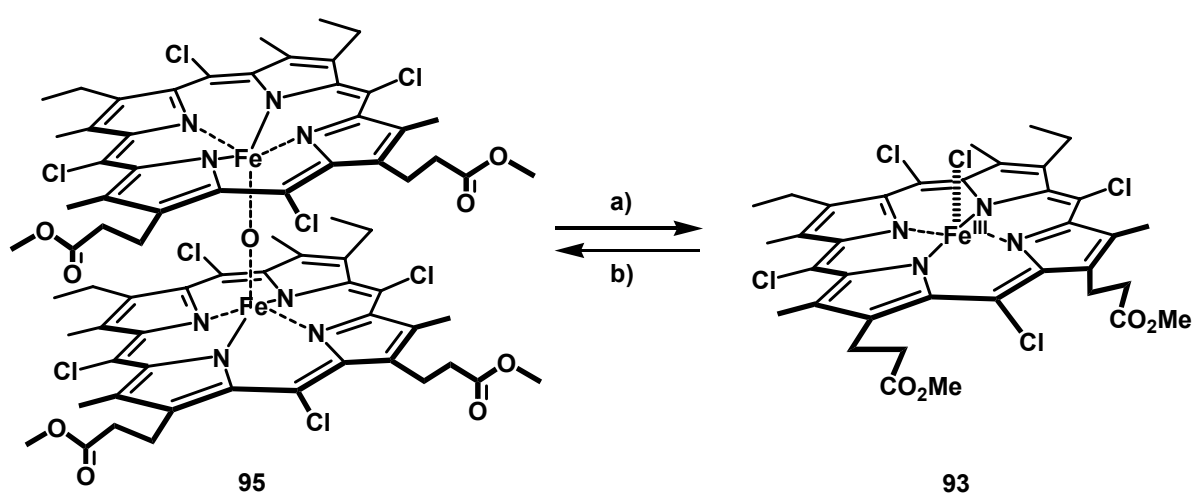


**Scheme 34:** The synthetic route to **92** starting from commercially available pP-IX **84**: a) TMOF/MeOH/H<sub>2</sub>SO<sub>4</sub>, 95% b) Pd/C, H<sub>2</sub>, CH<sub>2</sub>Cl<sub>2</sub> 92% c) 8 eq. NCS, CH<sub>2</sub>Cl<sub>2</sub>, r.t., 5d, then TMS-diazomethane/MeOH for 30 min, 20% d) FeCl<sub>2</sub>, 2,6-Lutidine, CH<sub>2</sub>Cl<sub>2</sub>/MeCN, 65% e) THF/1.0 M LiOH solution (2/1) overnight, quant.

## 3.8 Characterisation and Application of the modified Cofactor

### 3.8.1 Characterisation of Iron Complexes **92** and **93**

With the new iron complexes **92** and **93** synthesized, their properties were investigated by different analytic methods. It was observed that upon column chromatography (Alox B) **93** was originally obtained as its  $\mu$ -oxo dimer **95** (*scheme 35*), which in further workup treatment with 0.2 M HCl was finally converted to the desired product **93**. The two species are readily distinguished by their different UV/Vis and  $^1\text{H-NMR}$  spectra. **95** can be easily obtained from **93** by shaking a toluene solution of the latter with 20 mM NaOH solution or anew filtration over basic alox. Vice versa it is in principle possible to obtain a species of desired X<sup>-</sup>-ligation by shaking a solution of **95** with a solution of the corresponding acid HX.



**Scheme 35:** Conversion of **95** to **93** by a) washing with 0.2 M HCl, and of **93** to **95** by b) 20 mM NaOH or AloxB.

Characterisation of **93** and **95** was performed in comparison to analytical characteristics of the well-known nonchlorinated counterpart [Mesoporphyrin-dimethylester-iron(III)]Cl (**96**). The UV/Vis shift observed for the free bases upon chlorination is also reflected in the iron complexes. **93** shows a broad, split Soret band with  $\lambda_{\text{max}} = 396, 442$  nm in  $\text{CH}_2\text{Cl}_2$  compared to  $\lambda_{\text{max}} = 378$  nm for **96**. The  $\mu$ -oxo dimer **95** finally shows a broad absorption at  $\lambda_{\text{max}} = 415$  nm (*figure 31*). A split Soret band with poorly resolved Q-bands has also been observed for other sterically crowded, nonplanar iron(III)-porphyrins.<sup>112,113</sup>

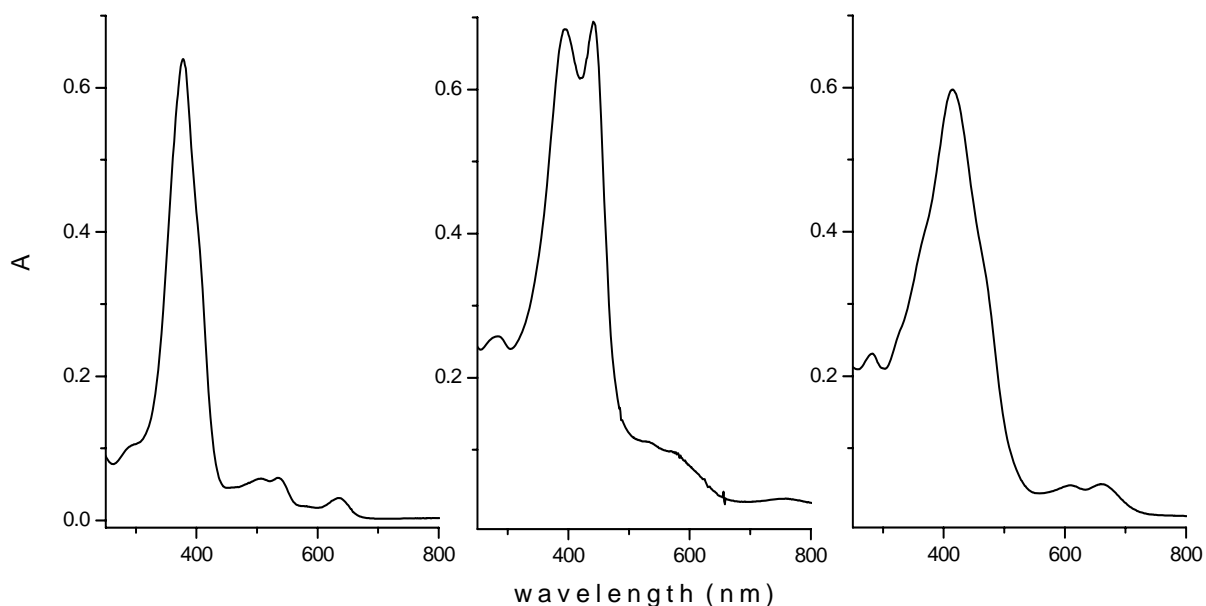


**Figure 31:** Electronic spectra of **96** (left), **93** (middle), and **95** (right) in  $\text{CH}_2\text{Cl}_2$ .

The  $^1\text{H-NMR}$  spectra of both **93** and **96** are characteristic of high spin iron(III) systems with signals spreading over a large range from 60 to -60 ppm due to the influence of the paramagnetic character of iron(III) (figure 32). Support for preservation of complete *meso*-chlorination upon iron insertion (besides MS analysis) comes from the fact, that the resonances for the *meso*-H at characteristically low ppm values are not observed in the spectrum of **93**, whereas they can be observed in the otherwise quite similar spectrum of **96**. These resonances as well as those at low field (30 to 60 ppm assigned to the Methyl-Hs of Methyl- and the  $-\text{CH}_2-$  of Ethyl-substituents in the  $\beta$ -positions respectively) can be assigned according to published spectra of **96**.<sup>114</sup> In contrast to the earlier two cases, the  $\mu$ -oxo dimer **95** does not show any signals in the “paramagnetic” regions at very high or low ppm. Its signals are all found within the range of “traditional” organic compounds from 0 to 10 ppm. This implies an antiferromagnetic coupling of the two iron atoms in the latter, again an effect known for other iron-porphyrin  $\mu$ -oxo-dimers.<sup>115,116</sup> This finding fits well to the EPR silent character of **95** observed in low temperature cw-EPR measurements (15K).

ESI-MS analysis of **93** in Methanol shows the coordination of MeOH and the isotopic distribution expected by calculation ( $m/z = 838$ ,  $[\text{M-Cl}+\text{NaOMe}]^+$ ). In the MALDI-TOF-MS analysis, the  $\text{Cl}^-$  ligation is seen. ( $m/z = 819$ ,  $[\text{M}]$ ). After ester hydrolysis, the MALDI-TOF-MS of **92** shows the corresponding signal  $[\text{M}]$  at  $m/z = 791$ , again displaying the characteristic isotopic pattern.

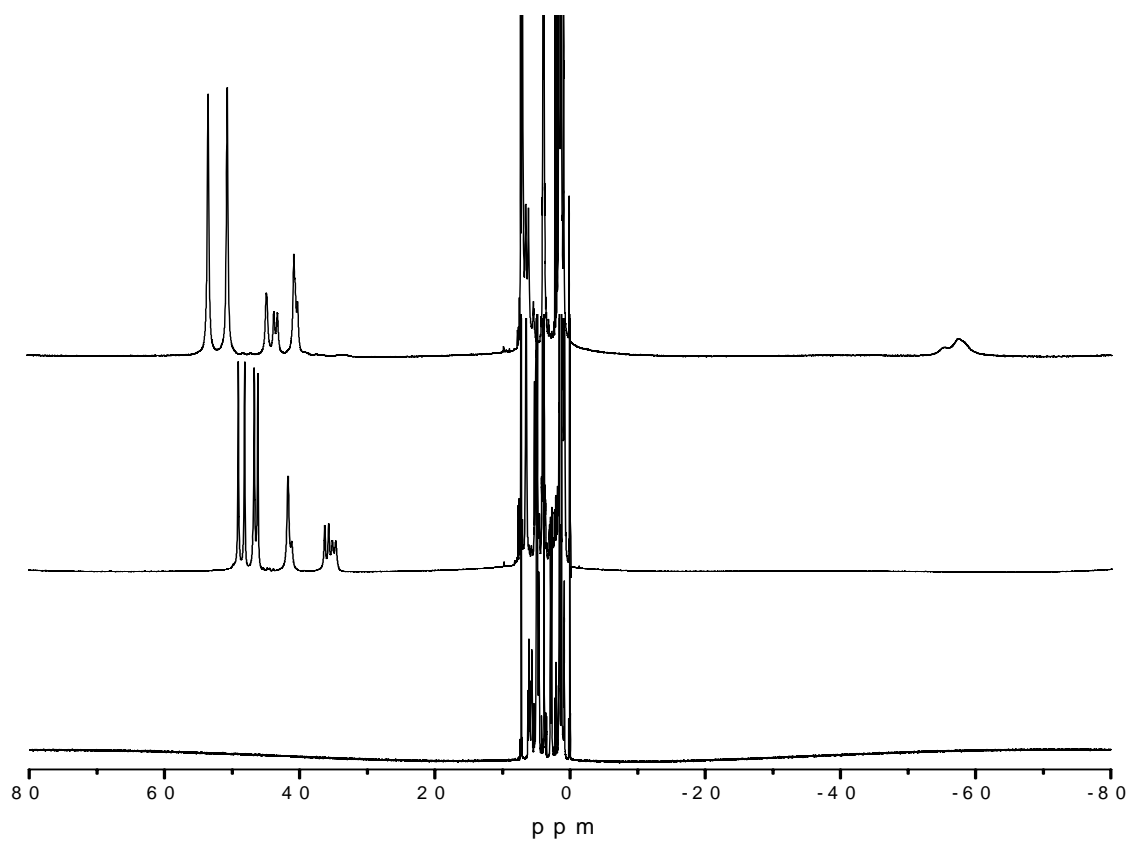


**Figure 32:** 80 to -80 ppm region of the <sup>1</sup>H-NMR spectra of **96** (upper), **93** (middle), and **95** (lower) in CDCl<sub>3</sub>.

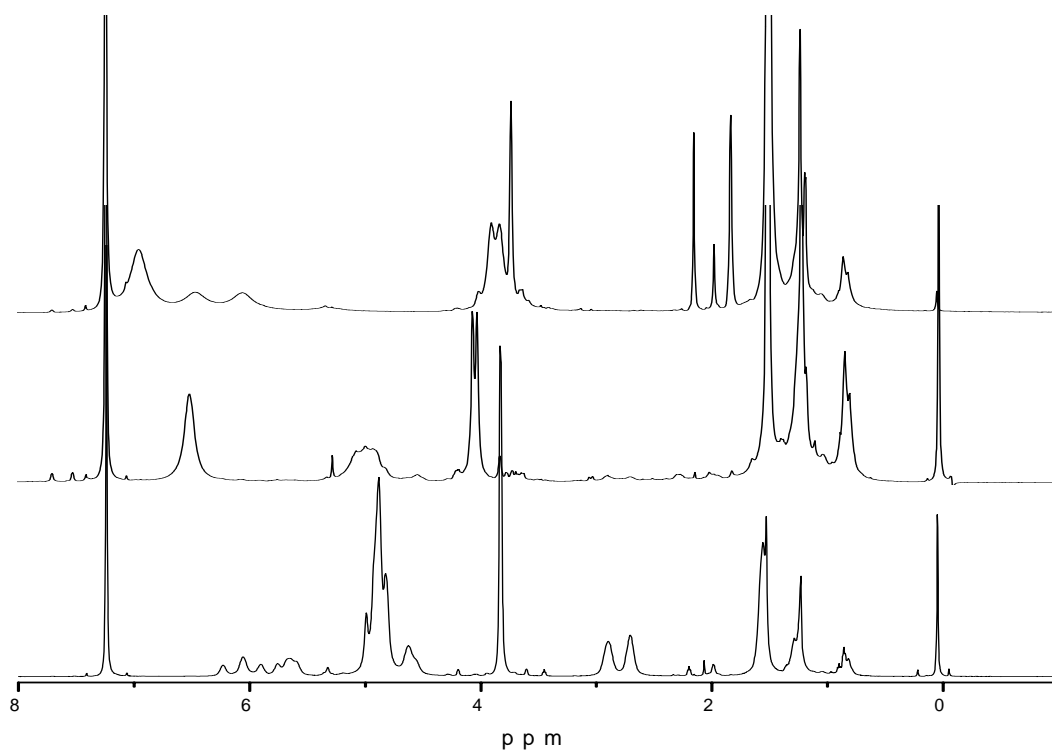


**Figure 33:** 8.0 to -1.0 ppm region of the <sup>1</sup>H-NMR spectra of **96** (upper), **93** (middle), and **95** (lower) in CDCl<sub>3</sub>.

The UV/Vis spectrum of **92** in  $\text{CH}_2\text{Cl}_2$  is practically superimposable with that of **93** showing a broad, split Soret band with  $\lambda_{\text{max}} = 395, 443 \text{ nm}$  and poorly resolved Q-bands. The  $^1\text{H-NMR}$  spectrum of **92** again is affected by huge shifts due to paramagnetic iron (*figure 34*). Further it shows disappearance of the signals at 4 ppm assigned<sup>114</sup> to the ester-methyl groups and occurrence of a new, broad signal at  $\sim 14 \text{ ppm}$  assigned to the carboxylic acid protons. Further proof for this assignment was obtained by  $\text{D}_2\text{O}$  exchange, whereupon the signal disappeared.

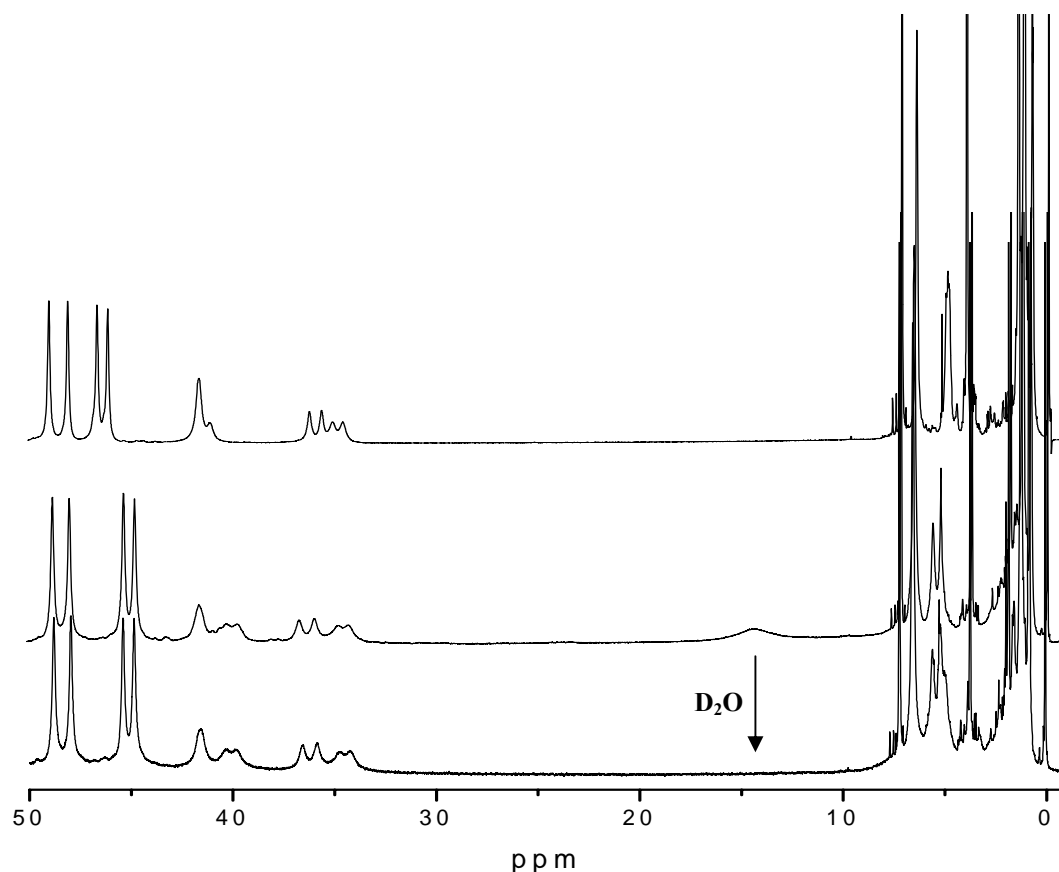


**Figure 34:** 50 to -1.0 ppm region of the  $^1\text{H-NMR}$  spectra of **93** (upper) and **92** (middle) in  $\text{CDCl}_3$ . The lowest trace shows the same sample of **92** after  $\text{D}_2\text{O}$  treatment.

The cw-EPR spectra for both **93** and **92** in  $\text{CH}_2\text{Cl}_2$  show very broad signals of low intensity even at very low temperatures (15K), a feature already observed earlier for Protoheme derivatives.<sup>117</sup> The spectra obtained could be drastically improved in a  $\text{CH}_2\text{Cl}_2/\text{THF}$  (1/1) mixture containing a tenfold excess of  $\text{Bu}_4\text{NCl}$ . For this solvent system, both complexes show rhombically distorted high spin iron(III) spectra ( $g = 6.20, 5.52$  and  $1.99$  for **93**, *figure 35*). In contrast, [Protoporphyrin-dimethylester-iron(III)]Cl was reported to display axial symmetry with  $g = 5.88$  and  $2.00$  under similar conditions.<sup>117</sup>

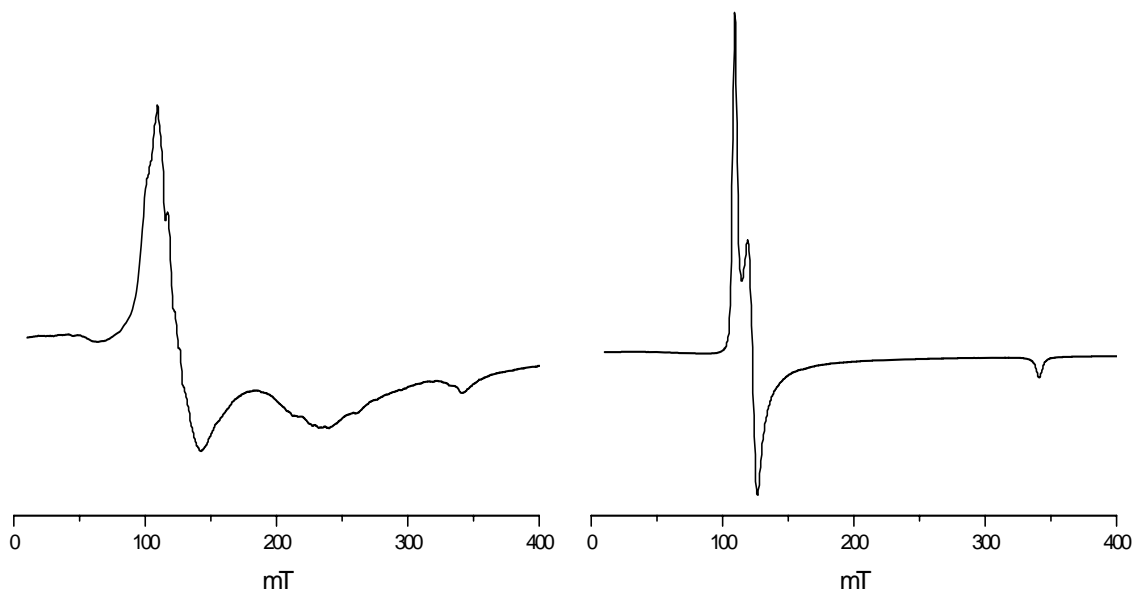
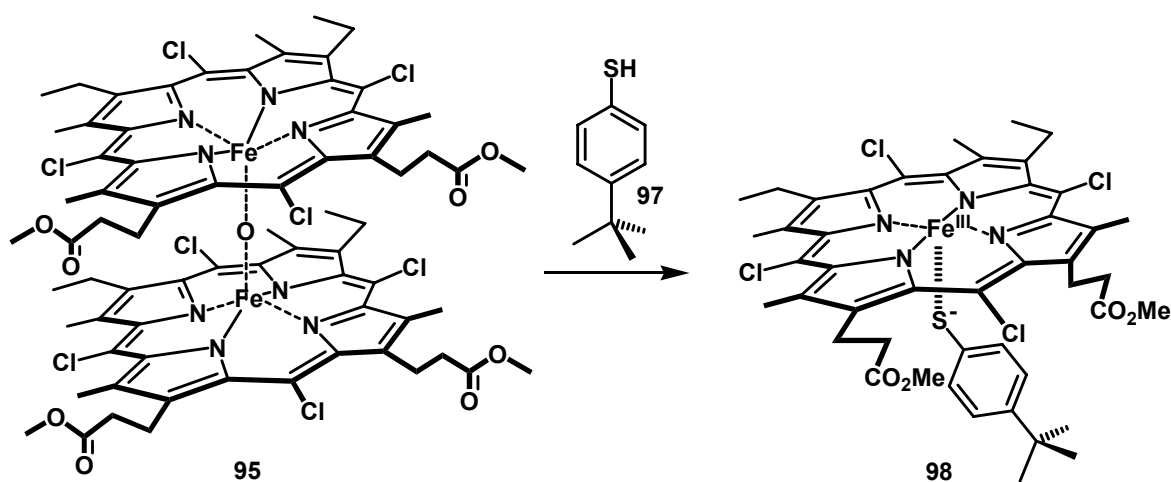


**Figure 35:** cw-EPR spectra of **93** 5.0 mM in  $\text{CH}_2\text{Cl}_2$  (left) and 2.5 mM in  $\text{CH}_2\text{Cl}_2/\text{THF}$  (1/1) with 25 mM  $\text{Bu}_4\text{NCl}$  (right;  $g = 6.20, 5.52$  and  $1.99$ ),  $T = 15\text{K}$ .

### 3.8.2 Sulfur Coordination

As in a correctly reconstituted enzyme system the modified cofactor is expected to coordinate to the thiolate of a cystein, it was of profound interest to know the spectroscopic properties of sulfur coordination. Therefore reaction of **95** with 4-*tert*-Butyl-thiophenol (**97**) in analogy to reported procedures for thiolate coordination<sup>118,119</sup> was performed under UV/Vis conditions in toluene (*scheme 36*).



**Scheme 36:** Thiolate ligation reaction of **95** forming two molecules of **98** and  $\text{H}_2\text{O}$ .



The spectral characterisation obtained under these conditions (apolar, noncoordinating solvent) was intended to reflect the analogous situation in the corresponding E·S complex after reconstitution.

Upon addition of an excess of **97** to **95** ( $\lambda_{\text{max}} = 420 \text{ nm}$ ), a new species was formed with clear isosbestic points within  $\sim 50 \text{ min}$  (*figure 36*). The so obtained species was stable for longer than 40 min without further changes in its spectrum ( $\lambda_{\text{max}} = 392, 447 \text{ nm}$ ). The so obtained spectrum is similar to that for the Cl<sup>-</sup>-complex **93** in the same solvent ( $\lambda_{\text{max}} = 392, 442 \text{ nm}$ ), indicating a similar coordinated species. Further insight into the nature of the obtained product was gained from <sup>1</sup>H-NMR measurements<sup>120</sup> of the same reaction in CDCl<sub>3</sub>, showing decrease of the signals of **95** with concomitant formation of a high spin iron(III) species with a spectrum again strongly resembling that of **93** (*figure 32, 33*). Additional evidence for formation of a high spin iron(III) species was obtained from EPR measurements upon addition of **97** to an EPR silent solution of **95** in toluene, showing a spectrum of close resemblance to the spectrum obtained for **93** in CH<sub>2</sub>Cl<sub>2</sub> (*figure 35*).

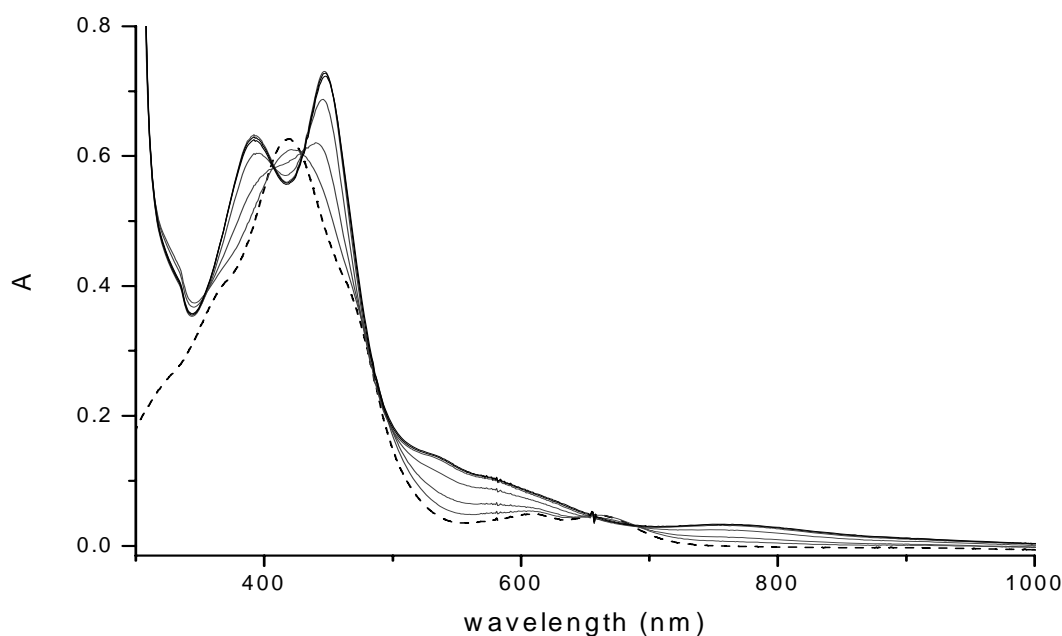


**Figure 36:** UV/Vis changes during 90 min upon addition of 20  $\mu\text{l}$  **97** to 2.0 ml of an 8  $\mu\text{M}$  solution of **95** (dashed line) in toluene.

All these findings together with earlier reports on similar reactions suggest the newly formed species to be thiolate ligated **98**. This leads to the proposal, that the enzyme system should display spectroscopic properties similar to **98** upon reconstitution.

### 3.8.3 Reactivity

As outlined earlier, the intention regarding the synthesis of the modified cofactor was to generate a more reactive species due to electron deficiency of the porphyrin macrocycle. To provide evidence for the consistency of the applied concept, the reactivity of **93** was compared to that of **96** in epoxidation reaction in solution. In succession of the earlier epoxidation reactions using model compound **29** and in allusion to epoxidation reactions performed with protoheme derivatives,<sup>121</sup> the epoxidation reaction of *cis*-stilbene with PhIO as a 'O'-source was chosen as a model reaction. As already discussed (*scheme 24*), *cis*-stilbene (**49**) is oxidized by iron porphyrins to the corresponding epoxides **50** and **51** and to ketone **52**. Formation of these products was followed for catalysis of **93** and **96** at similar conditions (CH<sub>2</sub>Cl<sub>2</sub>, r.t.) by GC-FID analysis. It was found that going from **96** to **93** the amount of products formed increased by a ~2.6 fold (*table 5*) while ensuring material balance in both cases. Blank reactions omitting the iron porphyrin catalyst resulted in no observable formation of products and quantitative recovery of **49**.

	<b>49</b> <sub>recovered</sub> (%) <sup>a</sup>	<b>50</b> (%)	<b>51</b> (%)	<b>52</b> (%)	total ox % <sup>b</sup>	TON <sup>c</sup>
<b>96</b>	97.6	1.4	0.8	0.1	10.8	1.5
<b>93</b>	89.7	4.1	1.5	0.4	28.5	4.0

**Table 5:** Products obtained after 1 h from epoxidation reactions of **49** by **96** respectively **93** and PhIO. Conditions: [**49**]: 226 mM, [PhIO]: 47 mM, [**96/93**]: 3.4 mM, CH<sub>2</sub>Cl<sub>2</sub>, r.t. a) calculated vs. int. standard (C-14 alkane). b) calculated vs. [PhIO] c) TON = turn over number.

This evident increase of potency for biomimetic catalysis supports our concept very clearly and lays the basis for employment of **92** in the field of biotechnological enzyme engineering.

## 4 Summary and Conclusions

Cytochromes P450 are heme-thiolate proteins abundant in nature. These monooxygenases catalyse a variety of reactions including alkene epoxidation, N-, O-, and S-dealkylation, C-C bond cleavage and hydrocarbon hydroxylation. This arsenal of interesting transformations, together with the importance of their biological functions has rendered them subject of intensive studies. In this context, two projects were pursued in the present work.

In a first project, two members of a new family of P450 model compounds, **28** and **29** (figure 37) were synthesized and characterized. The coordination of  $\text{SO}_3^-$  as a fifth ligand to iron in both compounds resembles the reduced charge density on the cystein thiolate coordinating in the enzyme case. This concept was confirmed by calculation results and X-ray crystallography as well as redox potentials of **28** and **29** and their reactivity in P450-catalysed reactions.

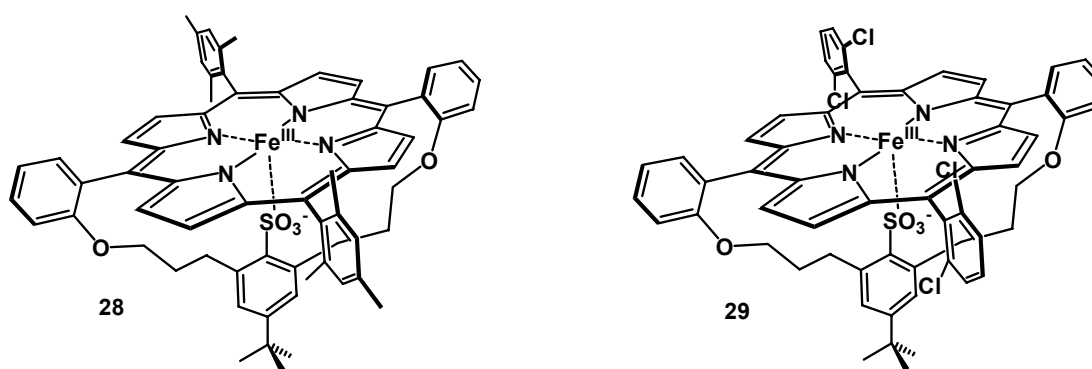


**Figure 37:** The two members of the new family of P450 model compounds

Both model compounds have been shown to generate an analogue of CpdI (the natural active species) upon shunt pathway reaction with external oxidant (*m*CPBA).

Model compound **29** was studied closely in its alkene epoxidation reaction in collaboration with van Eldik et al, wherefrom the complete catalytic cycle of this reaction could be visualised. Both compounds have been applied to biomimetic demethylation of amines, therein showing the influence of their different porphyrin substituents upon reactivity. Appliance of the upper systems to cleavage of vicinal diols has been accomplished by employing N-Oxides as 'O'-donors. Diol cleavage represents the last step in C-C bond cleavage by P450s, one of the reactions that illustrate best the power of P450 oxidative

transformations. With the above findings, a simple system for future studies on this interesting reaction has been elaborated. Furthermore the findings for this system suggest CpdI as the active species in diol cleavage reaction in similarity to alkene epoxidation and hydrocarbon hydroxylation, thereby confirming the unique role of this iron-oxo species in the field of P450 catalysis.

The field of appliance of the new model compounds has been further expanded in collaboration with van Eldik et al towards studies on binding of nitric oxide (NO). Binding of NO to **28** in toluene has therein been found to be an appropriate model for NO coordination of substrate bound P450<sub>cam</sub> studied by the van Eldik group earlier, displaying completely reversible binding of NO in mechanistic analogy to the enzyme case. Comparison of thermodynamic and kinetic factors for the two cases emphasise the role of the enzyme pocket in NO coordination of heme proteins.

In summary, the obtained results establish **28** and **29** as valuable models for diverse aspects of P450 research.

In a second project, modification of the natural cofactor of cytochromes P450 (heme *b*) was investigated. Additional substituents were introduced into the originally free *meso*-positions to alter the properties towards higher reactivity. By this strategy the tetrachlorinated cofactor **92** and its Dimethylester **93** (figure 38) were obtained and characterized.

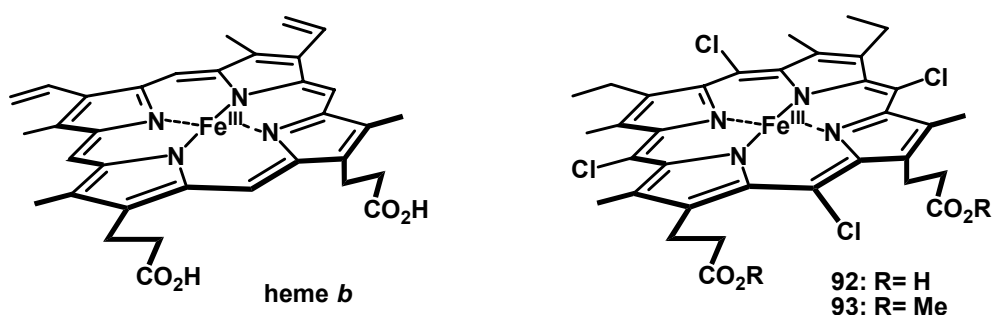


**Figure 38:** The natural cofactor of cytochromes P450, heme *b* (left) and its modified counterparts (right) synthesized in the present work.

The reactivity of **93** compared to its nonchlorinated counterpart **96** towards alkene epoxidation in solution indeed supported the applied strategy by ~2.6 fold increase of product formation for chlorinated **93**. With these findings, a new cofactor is available, which has promising properties for biotechnological applications once successfully incorporated into a cofactor free “apoprotein”.

## **Experimental Part**



## 5 Experimental Part

### 5.1 General Remarks

#### 5.1.1 Solvents and Reagents

Reagents were used as received from *Fluka AG* (Buchs, Switzerland), *Acros AG* (Basel, Switzerland), *Merck AG* (Darmstadt, Germany) and *Aldrich* (Buchs, Switzerland) unless otherwise stated. Chemicals of the quality *purum*, *purum p. a.* or >98% were used without further purification.

Solvents for chromatography and extractions were distilled prior to use. Dry CH<sub>2</sub>Cl<sub>2</sub> was distilled from CaH<sub>2</sub>. Et<sub>2</sub>O, THF and toluene were distilled from Na/benzophenone. Further solvents used for reactions corresponded to the quality *puriss p. a., abs., over Molecular Sieves* from *Fluka AG*. HPLC-grade solvents were purchased and used for analytical RP-HPLC. Degassed solvents for reactions under oxygen-free condition (*e.g.* in the glove box) were obtained by at least three freeze-pump-thaw cycles.

For an inert atmosphere *Argon 60* from *Carbagas AG* (Lenzburg, Switzerland) was used.

#### 5.1.2 Materials & Instruments

Solvents were removed with a *Büchi* (Switzerland) rotary evaporator.

For weighing compounds and reagents *Mettler* (Switzerland) balances P360 (> 1 g), AE163 (< 1 g), and AX205 (< 100 mg) were used.

A high-vacuum pump RV5 and E2M5 from *Edwards* (Sussex, England) was used for drying compounds and reagents.

For all non-aqueous reactions glassware was flame dried under vacuum and the atmosphere was exchanged by three cycles of evacuating and flushing with argon.

Reactions requiring strictly anaerobic conditions were carried out in a Labmaster 130 glove box (MBRAUN). The levels of oxygen (< 2 ppm) and water (< 0.1 ppm) were measured with a combined H<sub>2</sub>O/O<sub>2</sub>-analyser (MBRAUN). All solvents and reagents used in the glove box were dried and degassed in high-vacuum.

**Melting points (mp)** were determined on an apparatus by the *Werkstatt der Organischen Chemie der Universität Basel* and are uncorrected. For the porphyrins, the melting points are  $> 250^\circ$  and were not determined.

### 5.1.3 Chromatographic Methods

**Analytical thin layer chromatography (TLC)** was performed on precoated glass plates (5×10 cm, silica gel 60 F<sub>254</sub>, *Merck AG*, Darmstadt, Germany), on precoated glass plates (aluminium oxide 60 F<sub>254</sub>, *Merck AG*, Darmstadt, Germany), on precoated aluminium plates (25×25 cm, aluminium oxide neutral 60 F<sub>254</sub>, *Merck AG*, Darmstadt, Germany) or on precoated glass plates (5×10 cm, RP-18 F<sub>254s</sub>, *Merck AG*, Germany). Compounds were detected at 254 nm (UV) or at 366 nm (fluorescence). Description: TLC (solvent): *R<sub>f</sub>*.

**Preparative thin layer chromatography** was conducted on precoated glass plates (20×20 cm, silica gel 60 F<sub>254</sub>, *Merck AG*, Darmstadt, Germany).

For normal phase **column chromatography** silica gel 60 from *Merck* (0.043-0.06 mm, 230-400 mesh) or *Fluka* or basic or neutral aluminium oxide from *Fluka* (activity I, 0.05-0.15 mm) were used.

Analytical **reversed phase HPLC (RP-HPLC)** was performed on LiChrospher® 100 RP-18 silica gel from *Merck* (5 µm particle size, 4×250 mm column) or on Eclipse XDB-C8 silica gel from *Zorbax* (4.6×150 mm column) with nanopure water and HPLC-grade solvents. HPLC-System: *Agilent* 1100 Series 1100 HPLC system with Solvent degasser G1322A, Bin Pump G1312A, Auto sampler G1313A, Thermostatic column housing G1316A, Diode array UV detector G1315B).

**Gas chromatography (GC/MS)** was performed on a *Hewlett Packard* 5890 series II using a 25 m dimethyl silane column coupled with a *Hewlett Packard* 5971 series mass selective detector or a 5%phenyl-methyl silane column coupled with a *Hewlett Packard* 5970 series mass selective detector.



**Gas chromatography (GC-FID)** was performed on a *Finnigan Focus* using a 15 m Supelcowax column.

#### 5.1.4 Spectroscopic Methods

**Ultra violet – visible absorption spectra (UV/Vis)** were recorded on an *Agilent 8453* Diode Array spectrophotometer using optical 110-QS *Hellma* cuvettes (10 mm light path).

Description: UV/Vis (solvent): wavelength of maxima ( $\lambda_{\max}$ ) in nm (relative extinction coefficient in %). *sh* = shoulder.

Low temperature measurements were conducted using a vacuum-coated coolable *Hellma* 1X165.190-QS cuvette connected to a *JULABO* F70 recirculating cooler.

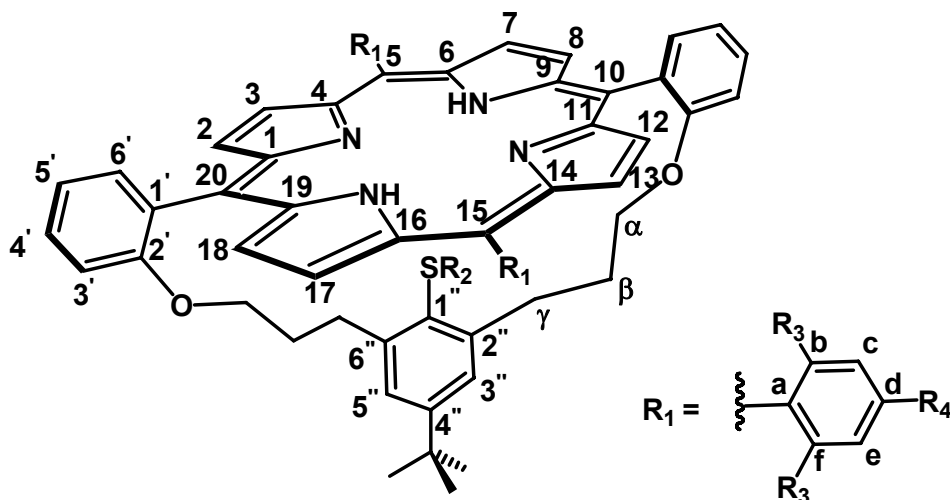
**Infrared spectra (IR)** were measured on a *FTIR-8400S* from *SHIMADZU*. Description: IR (medium): wave numbers of transmission maxima in  $\text{cm}^{-1}$ , intensity (*s* = strong, *m* = middle, *w* = weak, *br* = broad).

**$^1\text{H}$ -Nuclear magnetic resonance spectroscopy ( $^1\text{H}$ -NMR)** was performed using either a *Bruker* av250 (250 MHz), *Bruker* DPX-NMR (400 MHz), *Bruker* DRX-500 (500 MHz) or a *Bruker* DRX-600 (600 MHz) spectrometer. Solvents for NMR were obtained from *Dr. Glaser AG* (Basel, Switzerland) and *Cambridge Isotope Laboratories* (Andover, MA, USA).  $\text{CDCl}_3$  was filtered through basic alumina prior to use. If not otherwise stated all spectra were recorded at room temperature. If necessary for the interpretation correlated spectra like COSY, TOCSY, NOESY and ROESY were recorded also. The data for all peaks is given as observed from spectra and is not corrected for effects caused by higher order systems. Description:  $^1\text{H}$ -NMR (frequency, solvent):  $\delta_{\text{H}}$  in ppm relative to residual solvent peaks (peak multiplicity: *s* = singlet, *d* = doublet, *t* = triplet, *q* = quartet, *quin* = quintet, *sext* = sextet, *m* = multiplet, *br* = broad; coupling constants *J* in Hertz).

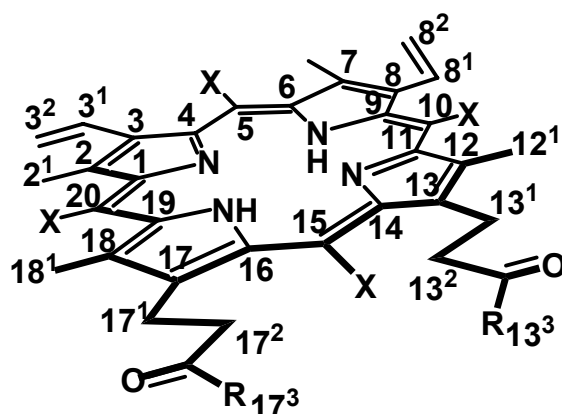
**$^{13}\text{C}$ -Nuclear magnetic resonance spectra ( $^{13}\text{C}$ -NMR)** were  $^1\text{H}$ -decoupled and recorded on a *Bruker* DPX-NMR (100 MHz) or *Bruker* DRX-500 (125 MHz) spectrometer. For the assignment of carbons APT, DEPT, HETCOR, HMQC and HMBC experiments were carried out if essential. Description:  $^{13}\text{C}$ -NMR (frequency, solvent):  $\delta_{\text{C}}$  in ppm relative to residual solvent peaks.

Porphyrin atom numbering for NMR assignment:

1) model compounds:



2) pP-IX derivatives:



**Electron impact mass spectra (EI-MS) and fast atom bombardment mass spectra (FAB-MS)** were measured by *Dr. H. Nadig* on a *Varian* double focussing VG-70-250 spectrometer in the mass spectrometry laboratory of the institute. As matrix for FAB-MS nitrobenzyl alcohol was used and if necessary KCl was added. **Electron spray ionisation mass spectra (ESI-MS)** were recorded on a Bruker Esquire 3000plus or a *Finnigan Mat* LCQ-700. For **matrix-assisted laser desorption/ionisation mass spectra** in conjunction with **time of flight mass analysis (MALDI-TOF-MS)** a *Perseptive Biosystems Vestec Mass Spectrometry Products Voyager™ Elite Biospectrometry™* Research Station was used. Porphyrin samples were prepared as follows: either 1-2  $\mu\text{l}$  of a diluted solution of porphyrin in dichloromethane

was mixed with a matrix solution of 4-Nitroaniline in dichloromethane on a 100-wells gold coated sample plate and left standing or the diluted porphyrin solution was placed directly on the sample plate and measured without matrix (**LDI-MS**). Description: MS (solvent): mass peaks in  $m/z$  (relative intensity in %). Peaks with an intensity of less than 5% were not considered.

**Continuous wave electron paramagnetic resonance spectroscopy (cw-EPR)** was carried out using a *Bruker* ESP-300 X-band ( $\nu_{\text{microwave}} = 9.485$  GHz) spectrometer equipped with a T<sub>102</sub> cell and an ER4111VT liquid nitrogen cryostat to assure low temperature during measurement. Sample concentration was typically 4mM and spectra were measured with a microwave power of 20 mW, modulation frequency of 100 kHz, and a modulation amplitude of 5.2 G. Samples were measured in dry and degassed toluene or dichloromethane Description: cw-EPR (solvent, temperature): g-values.

For more sensitive measurements a *Bruker* ElexSys E500 X-band ( $\nu_{\text{microwave}} = 9.6$  GHz) cw-spectrometer equipped with a liquid helium cryostat at the EPR labs at the ETHZ was used.

### 5.1.5 Elemental Analysis

The elemental analysis (**EA**) was carried out by Mr. *H. Kirsch* at the institute with a *Perkin-Elmer* 240 Analyser. Description: EA (chemical formula, molecular weight): calculated (calc.) abundance of C, H, O in %; found abundance of C, H, O in %.

### 5.1.6 Electrochemical methods

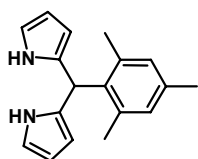
**Cyclic voltammetry (CV)** was carried out in collaboration with Dr. Egbert Figgemeier using a BAS 100 B electrochemical Analyzer controlled and analysed by BAS 100 W V 2.0 from Bioanalytical Systems, Inc. (West Lafayette, U.S.A.). A three electrode setup was used throughout. As a working electrode a glassy-carbon electrode was used. A platinum net was used as counter electrode and a silver wire as a reference electrode. The redox potentials were recorded versus ferrocene ( $\text{Fe}^{\text{II/III}}$ ) as an internal standard. These values might be calculated to the values versus SCE by appliance of the redox potential of the internal standard and corrections for solvent changes.

**Spectroelectrochemistry** was carried out with the above setup placed in a cuvette in an *Agilent* 8453 Diode Array spectrophotometer. Platinum net was used both for the working electrode and counter electrode and a silver wire as a reference electrode.

## 5.2 Syntheses

### 5.2.1 Porphyrin Model Compound Synthesis

#### (2,4,6-trimethyl)-bis (2-pyrryl)methane (**30**)



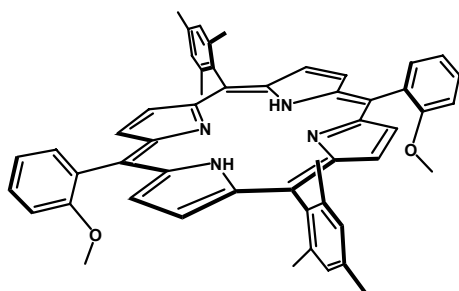
21.0 ml (302 mmol, 40 eq.) of freshly distilled pyrrole and 1.10 ml (7.59 mmol, 1.0 eq.) Mesitylaldehyde were mixed and purged with Argon for 15 min. Then 280  $\mu$ l (2.28 mmol, 0.3 eq.)  $\text{BF}_3 \cdot \text{OEt}_2$  were added. The resulting mixture was stirred at r.t. under exclusion of light for 1h. Then it was poured into a separation funnel with 40 ml of  $\text{CH}_2\text{Cl}_2$  and washed consecutive with 40 ml of 0.1 M NaOH-solution and twice with water. The organic layer was dried over  $\text{Na}_2\text{SO}_4$  and the solvent was removed. Chromatography of the resulting brown solid ( $\text{SiO}_2$ , hexane/EtOAc 3/1 + 1%  $\text{Et}_3\text{N}$ ) gave 1.40 g of a brown solid, which was washed three times with hexane to obtain 575 mg (29%) of white crystals. Since the compound was already described elsewhere<sup>64</sup> only selected data is given.

TLC ( $\text{SiO}_2$ ; hexane/EtOAc 3:1 + 1% $\text{Et}_3\text{N}$ ):  $R_f$  = 0.43.

$^1\text{H-NMR}$  (400 MHz,  $\text{CDCl}_3$ ): 7.97 (*br*, 2H, NH); 6.90 (*s*, 2H,  $\text{H}_{\text{aryl}}$ ); 6.72-6.68 (*m*, 2H,  $\text{H}_{\text{pyrrole}}$ ); 6.21 (*q*,  $J$  = 4.6, 2H,  $\text{H}_{\text{pyrrole}}$ ); 6.10-6.06 (*m*, 2H,  $\text{H}_{\text{pyrrole}}$ ); 5.96 (*s*, 1H, CH); 2.32 (*s*, 3H,  $\text{CH}_3$ ); 2.10 (*s*, 6H,  $\text{CH}_3$ ).

$^{13}\text{C-NMR}$  (125 MHz,  $\text{CDCl}_3$ ): 137.6, 136.6, 134.5, 131.2, 130.3, 116.1, 108.6, 106.5, 38.3, 20.8, 20.6.

#### 5,15-Bis-(2,4,6-trimethylphenyl)-10,20-bis(2-Methoxyphenyl)porphyrin (**39**)



132 mg (499  $\mu$ mol, 1.0 eq.) (2,4,6-trimethyl)-bis (2-pyrryl)methane (**30**) and 68.7 mg (505  $\mu$ mol, 1.0 eq.) 2-methoxybenzaldehyde were dissolved in 50 ml of  $\text{CH}_2\text{Cl}_2$  and 68.5 ml (922  $\mu$ mol, 1.8 eq.) of TFA were added. The reaction mixture was stirred at r.t. for 30 min and then 228 mg (1.00 mmol, 2.0 eq.) of DDQ

were added and the reaction heated to reflux for 1 h. Upon cooling to r.t. the mixture was filtrated over SiO<sub>2</sub> (CH<sub>2</sub>Cl<sub>2</sub> + 1% Et<sub>3</sub>N) and concentrated to give 70.3 mg of a purple solid which was chromatographed (SiO<sub>2</sub>, hexane/CH<sub>2</sub>Cl<sub>2</sub> 1/1 +1% Et<sub>3</sub>N) to yield 52.0 mg (27%) of a purple solid as a mixture of two atropisomers.

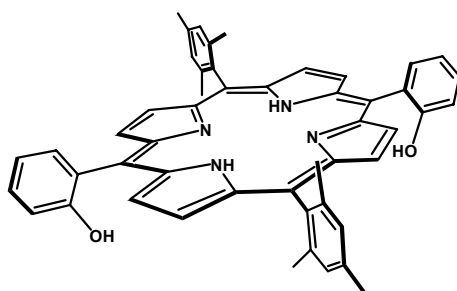
**TLC** (SiO<sub>2</sub>; hexane/ CH<sub>2</sub>Cl<sub>2</sub> 1:1 + 1% Et<sub>3</sub>N):  $R_f = 0.31$ ,  $R_f = 0.22$ .

**UV/Vis** (CHCl<sub>3</sub>): 419 (100, *Soret*); 514 (5); 550(2); 590 (1).

**<sup>1</sup>H-NMR** (500 MHz, CDCl<sub>3</sub>): 8.70 (*d*,  $J = 4.5$ , 4H, H 2,8,12,18); 8.62 (*d*,  $J = 4.5$ , 4H, H 3,7,13,17); 8.01 (*d*,  $J = 7.2$ , 2H, H 6'); 7.76 (*t*,  $J = 7.9$ , 2H, H 4'); 7.36-7.30 (*m*, 4H, H 3',5'); 7.26 (*s*, 4H, Hc,e); 3.60 (*s*, 6H, OCH<sub>3</sub>); 2.62 (*s*, 6H, CH<sub>3d</sub>); 1,84 (*s*, 6H, CH<sub>3b,f</sub>) (resp. 1.86 (*s*, 3H, CH<sub>3b</sub>); 1.83 (*s*, 3H, CH<sub>3f</sub>)); -2.55 (*br*, 2H, NH).

**ESI-MS** (MeCN): *Positive ion mode*: 759 (100, [M+H]<sup>+</sup>); 781 (100, [M+Na]<sup>+</sup>). *Negative ion mode*: 757 (100, [M-H]<sup>-</sup>).

#### 5,15-Bis-(2,4,6-trimethylphenyl)-10,20-bis(2-Hydroxyphenyl)porphyrin (40)



200 mg (264 μmol, 1.0 eq.) Dimethoxyporphyrin (**39**) were dissolved in 80 ml of CH<sub>2</sub>Cl<sub>2</sub> and cooled to 0 °C. 850 μl (8.82 mmol, 34 eq.) BBr<sub>3</sub> were added via syringe. After addition the cooling bath was removed and the mixture stirred at r.t. overnight. Then it was poured to 150 ml of sat. NaHCO<sub>3</sub>-solution. The water

phase was extracted twice with CH<sub>2</sub>Cl<sub>2</sub>. The combined organic layers were subsequently washed with sat. NaHCO<sub>3</sub>-solution and water and then dried over Na<sub>2</sub>SO<sub>4</sub>. Chromatography (SiO<sub>2</sub>, hexane/TBME 2/1) gave 153 mg (79%) of a purple solid as a mixture of two atropisomers.

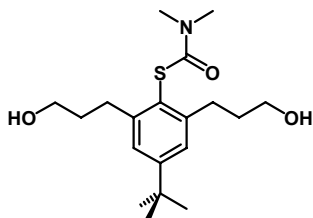
**TLC** (SiO<sub>2</sub>; hexane/ CH<sub>2</sub>Cl<sub>2</sub> 1:1 + 1% Et<sub>3</sub>N):  $R_f = 0.34$ ,  $R_f = 0.20$ .

**UV/Vis** (CHCl<sub>3</sub>): 418 (100, *Soret*); 514 (5); 549(2); 590 (2), 650 (1).

**<sup>1</sup>H-NMR** (500 MHz, CDCl<sub>3</sub>): 8.83 (*d*,  $J = 4.5$ , 4H, H 2,8,12,18); 8.73 (*d*,  $J = 4.5$ , 4H, H 3,7,13,17); 8.01 (*dx*,  $J = 7.4$ ,  $J' = 1.5$ , 2H, H 6') (resp. 7.99 (*dx*,  $J = 7.4$ ,  $J' = 1.5$ , 2H, H 6')); 7.72 (*tx*,  $J = 7.4$ ,  $J' = 1.5$ , 2H, H 4'); 7.38-7.31 (*m*, 4H, H 3',5'); 7.31- 7.27 (*m*, 4H, Hc,e); 4.98 (*s*, 2H, OH) (resp. 5.05 (*s*, 2H, OH)); 2.63 (*s*, 6H, CH<sub>3d</sub>); 1,83 (*s*, 6H, CH<sub>3b,f</sub>) (resp. 1.86 (*s*, 3H, CH<sub>3b</sub>); 1.81 (*s*, 3H, CH<sub>3f</sub>)); -2.63 (*br*, 2H, NH).

ESI-MS (MeCN): *Negative* ion mode: 729 (100,  $[M-H]^-$ ).

***S*-[4-(*tert*-Butyl)-2,6-bis(3-hydroxypropyl)-1-phenyl] N,N-dimethylthiocarbamate (**38**)**



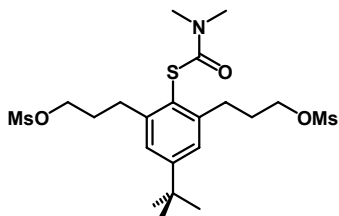
3.03 g (9.54 mmol, 1.0 eq.) of *S*-[2,6-Diallyl-4-(*tert*-Butyl)-1-phenyl] N,N-dimethylthiocarbamate (**37**) were dissolved in 100 ml of THF and cooled to 0 °C. 3.50 ml (35.0 mmol, 3.7 eq.)  $BH_3 \cdot SMe_2$  were added dropwise over 5 min via syringe pump. After addition, the mixture was stirred at r.t. for 3h during which increasing viscosity of the solution made addition of further THF (30 ml) necessary. Upon anew cooling 10 ml of 3 M NaOH-solution was added slowly and the mixture was afterwards allowed to come to r.t., 3.6 ml 30%  $H_2O_2$ -solution was added and the reaction was brought to reflux for 1 h. Then it was poured to ice-water and the resultant mixture was extracted three times with  $CH_2Cl_2$ . The combined organic layers were washed with water and brine and dried over  $Na_2SO_4$ . Chromatography ( $SiO_2$ ,  $CH_2Cl_2/MeOH$  95/5) gave 2.94 g (87%) of a colourless oil. Since the compound was already described elsewhere<sup>65</sup> only selected data is given.

TLC ( $SiO_2$ ;  $CH_2Cl_2/MeOH$  95:1 ):  $R_f = 0.22$ .

$^1H$ -NMR (400 MHz,  $CDCl_3$ ): 7.18 (s, 2H,  $H_{aryl}$ ); 3.63 (t,  $J = 6.1$ , 4H); 3.16 (br, 3H); 3.00 (br, 3H); 2.87 (t,  $J = 7.5$ , 4H); 1.91-1.83 (m, 6H); 1.29 (s, 9H).

ESI-MS (MeOH): *Positive* ion mode: 376 (100,  $[M+Na]^+$ ); 392 (11,  $[M+K]^+$ ).

***S*-[4-(*tert*-Butyl)-2,6-bis(3-methanesulfonylpropyl)-1-phenyl]N,N-dimethylthiocarbamate (**33**)**



769 mg (2.18 mmol, 1.0 eq.) diol (**38**) and 3.20 ml (22.9 mmol, 10 eq.)  $Et_3N$  were dissolved in 100 ml of  $CH_2Cl_2$  and the mixture was cooled to 0 °C. 1.05 ml (13.5 mmol, 6.2 eq.) Methanesulfonyl chloride in 60 ml  $CH_2Cl_2$  were added dropwise within 30 min. Then cooling was removed and the mixture stirred at r.t. for 2h. After anew cooling 60 ml 1 N HCl were added. The phases were separated and the water phase extracted two times with  $CH_2Cl_2$ . The combined organic layers were washed with sat.  $NaHCO_3$ -solution, water and brine and dried over  $Na_2SO_4$ . Chromatography ( $SiO_2$ ,

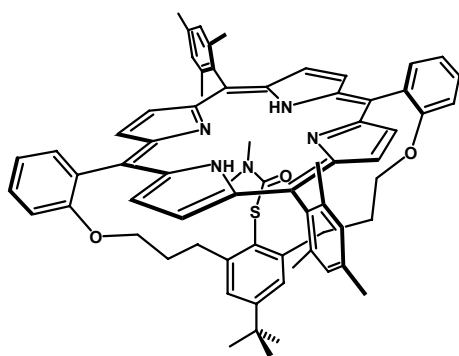
hexane/EtOAc 1/2) gave 1.01 g (92%) of a colourless oil which solidified upon standing at 4 °C. Since the compound was already described elsewhere<sup>65</sup> only selected data is given.

**TLC** (SiO<sub>2</sub>; hexane/EtOAc 1:2):  $R_f$  = 0.21.

**<sup>1</sup>H-NMR** (400 MHz, CDCl<sub>3</sub>): 7.19 (*s*, 2H, H<sub>aryl</sub>); 4.23 (*t*,  $J$  = 6.6, 4H); 3.18 (*br*, 3H); 2.99 (*br*, 9H); 2.89 (*t*,  $J$  = 7.8, 4H); 2.08-2.00 (*m*, 4H); 1.30 (*s*, 9H).

**ESI-MS** (MeOH): *Positive* ion mode: 532 (100, [M+Na]<sup>+</sup>); 548 (15, [M+K]<sup>+</sup>).

**5,15-({[5-(*t*-Butyl)-2-(*N,N*-dimethylcarbamoyl)thio-1,3-phenylene]bis(trimethyleneoxy)}-di-2,1-phenylene)-10,20-bis(2,4,6-trimethylphenyl) porphyrin (41)**



49.6 mg (67.9 μmol, 1.0 eq.) Dihydroxyporphyrin (**40**) and 650 mg (1.98 mmol, 30 eq.) Cs<sub>2</sub>CO<sub>3</sub> (previously dried at 100 °C in high vacuum overnight) were dissolved in 30 ml DMF and heated to 80 °C. After 30 min 56.1 mg (110 μmol, 1.6 eq.) Dimesylate (**33**) in 10 ml DMF were added via syringe pump during 3 h. After addition heating was continued for 1h. Then the mixture

was cooled in an ice bath and 17 ml 1 N HCl was added. After addition of 30 ml CH<sub>2</sub>Cl<sub>2</sub> the layers were separated and the water phase was extracted twice with CH<sub>2</sub>Cl<sub>2</sub>. The combined organic layers were washed with sat. NaHCO<sub>3</sub>-solution, water and brine and dried over Na<sub>2</sub>SO<sub>4</sub>. Chromatography (SiO<sub>2</sub>, hexane/CH<sub>2</sub>Cl<sub>2</sub> 5/1 + 1% Et<sub>3</sub>N) gave 53.1 mg (75%) of a purple solid.

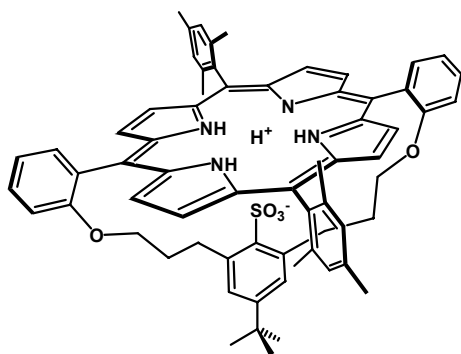
**TLC** (SiO<sub>2</sub>; hexane/ CH<sub>2</sub>Cl<sub>2</sub> 5:1 + 1% Et<sub>3</sub>N):  $R_f$  = 0.20.

**UV/Vis** (CHCl<sub>3</sub>): 424 (100, *Soret*); 519 (4); 554(2); 595 (2), 653 (1).

**<sup>1</sup>H-NMR** (500 MHz, CDCl<sub>3</sub>): 9.00 (*d*,  $J$  = 4.7, 2H, H 2,8); 8.70 (*d*,  $J$  = 4.7, 2H, H 3,7); 8.64 (*dxd*,  $J$  = 7.3,  $J'$  = 1.7, 2H, H 6'); 8.62 (*d*,  $J$  = 4.7, 2H, H 12,18); 8.40 (*d*,  $J$  = 4.7, 2H, H 13,17); 7.73 (*txd*,  $J$  = 8.1,  $J'$  = 1.8, 2H, H 4'); 7.51 (*txd*,  $J$  = 7.5,  $J'$  = 1.0, 2H, H 5'); 7.40 (*s*, 1H, H<sub>c2</sub>); 7.18 (*s*, 1H, H<sub>e2</sub>); 7.15 (*dxd*,  $J$  = 8.3,  $J'$  = 0.8, 2H, H 3'); 7.09 (*s*, 1H, H<sub>c1</sub>); 7.06 (*s*, 1H, H<sub>e1</sub>); 6.55 (*s*, 2H, H<sub>3''</sub>, H<sub>5''</sub>); 3.87-3.82 (*m*, 2H, H<sub>a</sub>); 3.73 (*txd*,  $J$  = 8.5,  $J'$  = 2.5, 2H, H<sub>a</sub>); 2.63 (*s*, 3H, CH<sub>3 d2</sub>); 2.53 (*s*, 3H, CH<sub>3 d1</sub>); 2.45 (*s*, 3H, CH<sub>3 b2</sub>); 1.49 (*br*, 6H, NCH<sub>3</sub>); 1.42 (*s*, 3H, CH<sub>3 f2</sub>); 1.37 (*s*, 3H, CH<sub>3 f1</sub>); 1.33-1.25 (*m*, 2H, H<sub>γ</sub>); 1.24 (*s*, 3H, CH<sub>3 b1</sub>); 1.14 (*s*, 9H, H<sub>tert-butyl</sub>); 1.02-0.85 (*m*, 4H, H<sub>β,γ</sub>); 0.68-0.58 (*m*, 2H, H<sub>β</sub>); -1.89 (*br*, 2H, NH).

**ESI-MS** (MeCN): *Positive ion mode*: 1048 (65,  $[M+H]^+$ ); 1070 (100,  $[M+Na]^+$ ); 1086 (16,  $[M+K]^+$ ).

**5,15-({[5-(*t*-Butyl)-2-sulfonato-1,3-phenylene]bis(trimethyleneoxy)}-di-2,1-phenylene)-10,20-bis(2,4,6-trimethylphenyl) porphyrin (**42**)**



**1)** A solution of 10.4 mg (9.92  $\mu\text{mol}$ , 1.0 eq.) Thiocarbamoylporphyrin (**41**) in 2.5 ml of dioxane was saturated with  $\text{O}_2$  and kept under  $\text{O}_2$ -atmosphere for 5 min before addition of 40.0 mg (571  $\mu\text{mol}$ , 58 eq.) KOMe (previously dried at 100  $^\circ\text{C}$  in high vacuum overnight). After addition the mixture was heated to reflux and stirred at that temperature overnight. After cooling to r.t., 2.5 ml sat.  $\text{NH}_4\text{Cl}$ -solution was added and the mixture poured into  $\text{CH}_2\text{Cl}_2/\text{H}_2\text{O}$ . The layers were separated, the water layer extracted twice with  $\text{CH}_2\text{Cl}_2$  and the combined organic layers washed with water and dried over  $\text{Na}_2\text{SO}_4$ . Chromatography ( $\text{SiO}_2$ , hexane/EtOAc 1/2 ) gave 4.10 mg (40%) of a purple solid.

**TLC** ( $\text{SiO}_2$ ; hexane/ EtOAc 1:2):  $R_f = 0.35$ .

**UV/Vis** ( $\text{CHCl}_3$ ): 424 (100, *Soret*); 548 (5); 582 (6), 635 (2).

**$^1\text{H-NMR}$**  (400 MHz,  $\text{CDCl}_3$ ): 9.01 (*d*,  $J = 4.8$ , 4H, H 2,8,12,18); 8.75 (*d*,  $J = 4.8$ , 4H, H 3,7,13,17); 8.44 (*dx*,  $J = 7.3$ ,  $J' = 1.5$ , 2H, H 6'); 7.80 (*txd*,  $J = 8.1$ ,  $J' = 1.8$ , 2H, H 4'); 7.52 (*txd*,  $J = 7.6$ ,  $J' = 1.0$ , 2H, H 5'); 7.25 (*t*, overlaid by solvent, 2H, H 3'); 7.25 (*s*, overlaid by solvent 2H, He); 7.23 (*s*, 2H, Hc); 6.08 (*s*, 2H, H3'',5''); 3.65 (*t*,  $J = 5.6$ , 4H, H $_{\alpha}$ ); 2.61 (*s*, 6H,  $\text{CH}_3$  d); 1.79 (*s*, 6H,  $\text{CH}_3$  f); 1.49 (*s*, 6H,  $\text{CH}_3$  b); 0.91 (*s*, 9H, H $_{\text{tert-butyl}}$ ); 0.91-0.78 (*m*, 4H, H $_{\gamma}$ ); 0.77-0.67 (*m*, 4H, H $_{\beta}$ ).

**ESI-MS** (MeCN): *Positive ion mode*: 1048 (65,  $[M+Na]^+$ ); 1064 (6,  $[M+K]^+$ ); 1070 (55,  $[M-H+2Na]^+$ ); 1086 (55,  $[M-H+Na+K]^+$ ). *Negative ion mode*: 1023 (100,  $[M-H]^-$ ).

Products of lower oxidation state on sulfur (obtained in the upper prescription **1**) as coloured fractions eluting before the  $\text{SO}_3$ -product) were converted to the desired product using prescription **2**)<sup>70</sup>.



**SH-product:**

**TLC** (SiO<sub>2</sub>; hexane/ EtOAc 4:1):  $R_f$  = 0.46.

**UV/Vis** (CHCl<sub>3</sub>): 422 (100, *Soret*); 517 (4); 551 (2); 595 (2), 650 (1).

**ESI-MS** (MeCN): *Positive* ion mode: 977 (100, [M+H]<sup>+</sup>); 999 (69, [M+Na]<sup>+</sup>); 1015 (4, [M+K]<sup>+</sup>); 1022 (4, [M-H+2Na]<sup>+</sup>). *Negative* ion mode: 975 (100, [M-H]<sup>-</sup>).

**SO<sub>2</sub>-product (43):**

**TLC** (SiO<sub>2</sub>; hexane/ EtOAc 1:2):  $R_f$  = 0.73.

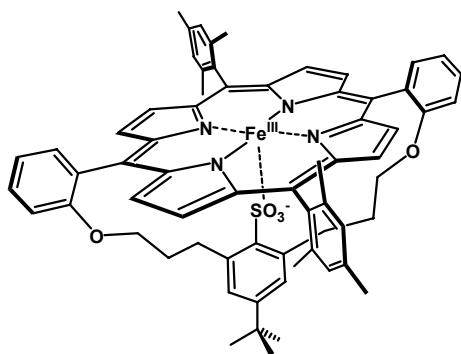
**UV/Vis** (CHCl<sub>3</sub>): 421 (100, *Soret*); 521 (4); 585 (2).

**ESI-MS** (MeCN): *Positive* ion mode: 1009 (100, [M+H]<sup>+</sup>); 1031 (70, [M+Na]<sup>+</sup>); 1047 (3, [M+K]<sup>+</sup>). *Negative* ion mode: 1007 (100, [M-H]<sup>-</sup>).

**2)** 3.60 mg (3.57 μmol, 1.0 eq.) SO<sub>2</sub>-porphyrin (**43**) were dissolved in 1.5 ml CH<sub>2</sub>Cl<sub>2</sub> and 2.00 mg nBu<sub>4</sub>NHSO<sub>5</sub> ( 5.63 μmol, 1.6 eq.) were added. The mixture was stirred at r.t. overnight and filtrated over SiO<sub>2</sub> eluting with EtOAc. Chromatography (SiO<sub>2</sub>, hexane/EtOAc 1/1) gave 2.20 mg (60%) of a purple solid

**2a)** nBu<sub>4</sub>NHSO<sub>5</sub> was obtained as follows: 4.02 g (6.50 mmol, 1.0 eq.) Oxon® was dissolved in 40 ml of water and 2.20 g (6.50 mmol, 1.0 eq.) nBu<sub>4</sub>NHSO<sub>4</sub> was added. The mixture was extracted six times with 100 ml of CH<sub>2</sub>Cl<sub>2</sub> and the combined organic layers were dried over Na<sub>2</sub>SO<sub>4</sub>. Removal of solvent gave 2.28 g (99%) of a white solid. The oxidative activity was determined to be 81% by iodometric titration.

**[5,15-([5-(*t*-Butyl)-2-sulfonato-1,3-phenylene]bis(trimethyleneoxy))-di-2,1-phenylene)-10,20-bis(2,4,6-trimethylphenyl) porphyrinato]iron (III) (**28**)**



66.4 mg (64.8 μmol, 1.0 eq.) SO<sub>3</sub>-porphyrin (**42**) were dissolved in 40 ml of toluene and 151 μl 2,6-lutidine (1.30 mmol, 20 eq.) were added. The mixture was heated to reflux for 5 min and upon cooling 143 mg FeBr<sub>2</sub> ( 663 μmol, 10 eq.) were added and heating was continued for 1 h. Upon cooling to r.t. the mixture was filtrated through celite and concentrated.

Chromatography (SiO<sub>2</sub>, hexane/CH<sub>2</sub>Cl<sub>2</sub>/EtOAc 5/5/1) gave 59,8 mg (86%) of a purple solid.

**TLC** (SiO<sub>2</sub>; hexane/CH<sub>2</sub>Cl<sub>2</sub>/EtOAc 5:5:1):  $R_f = 0.52$ .

**UV/Vis** (CHCl<sub>3</sub>): 416 (100, *Soret*); 512 (13); 581 (4), 670 (2).

**ESI-MS** (MeCN): *Positive* ion mode: 1078 (42, [M+H]<sup>+</sup>); 1100 (100, [M+Na]<sup>+</sup>); 1116 (7, [M+K]<sup>+</sup>).

**cw-EPR** (toluene, 94 K): 5.67, 2.03 (axial, high spin).

**HPLC** (NC-04, 250 x 4.0 mm, heptane/EtOAc 1/1 for 30 min, flow 1.0 ml/min, DAD ( $\lambda_{\text{det}} = 420$  nm, T = 25 °C):  $R_t = 5.2$  min.

#### **Iron(II)-state (44):**

UV/Vis spectra of **44** were obtained by treating 2.50 ml of a 5.00  $\mu\text{M}$  solution of **28** in degassed toluene in a UV/Vis cuvette with aliquots of a KH (15.0 mM) / 18-crown-6 (30.0 mM) toluene solution under constant control of UV/Vis spectrum changes.

cw-EPR samples were prepared by treating 500  $\mu\text{l}$  of a 4.00 mM solution of **28** in toluene in a glove box with aliquots of a KH (15.0 mM) / 18-crown-6 (30.0 mM) solution under continuous control of UV/Vis spectra of samples taken from the reaction solution. The obtained solutions of **44** were transferred to EPR-tubes and sealed directly in the glove box. Purification of **44** via chromatography failed in several attempts.

**UV/Vis** (toluene): 422 (100, *Soret*); 579 (8).

(DMF, 0.1 M LiClO<sub>4</sub>): 425 (100, *Soret*); 526 (5).

**cw-EPR** (toluene, 96 K): silent (trace signal of **28**  $g = 5.94$ ).

#### **CO-complex 44(CO):**

UV/Vis cuvette-samples of **44** in toluene obtained above were saturated with CO by bubbling a stream of CO-gas through the solution. No spectral changes were observed.

#### **CpdI analogue 45:**

UV/Vis spectra of **45** were obtained by cooling 1.50 ml of a 8.00  $\mu\text{M}$  solution of **28** in degassed CH<sub>2</sub>Cl<sub>2</sub> to -50 °C in a vacuum-coated coolable UV/Vis cuvette and subsequent treating with 16  $\mu\text{l}$  (18.6 nmol, 1.5 eq.) of a 1.16 mM solution of *m*CPBA in CH<sub>2</sub>Cl<sub>2</sub>.

**UV/Vis** (CH<sub>2</sub>Cl<sub>2</sub>): 408 (100, *Soret*); 664 (7) *broad*.

**MeOH-complex 68:**

570  $\mu\text{g}$  (529 nmol) of **28** were dissolved in 100  $\mu\text{l}$  of degassed toluene in an EPR tube equipped with a septum and EPR spectra were measured upon subsequent addition of degassed MeOH.

In another experiment, 520  $\mu\text{g}$  (482 nmol) of **28** were dissolved in 100  $\mu\text{l}$  of degassed MeOH and EPR spectra were measured upon subsequent addition of toluene.

**cw-EPR** (toluene, 100 K): 5.57, 2.04 (axial, high spin).

**Methylate-complex 28(MeO<sup>-</sup>):**

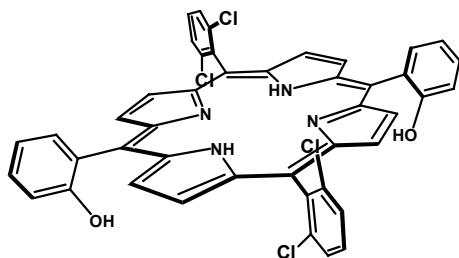
560  $\mu\text{g}$  (519 nmol) of **28** were dissolved in 100  $\mu\text{l}$  degassed toluene in an EPR tube equipped with a septum and treated with 50  $\mu\text{l}$  of a sat. KOMe/MeOH solution.

**cw-EPR** (toluene, 94 K):  $g = 2.42, 2.15, 1.93$ .

**NO-complex 28(NO):**

590  $\mu\text{g}$  (547 nmol) of **28** were dissolved in 120  $\mu\text{l}$  of degassed toluene in an EPR tube. After a first EPR measurement displaying the corresponding high spin signals for **28**, the solution was saturated with NO by bubbling through a stream of NO for 10 min (NO was cleaned from trace amounts of higher nitrogen oxides by passing it through an Ascarite column and a gas scrubbing bottle containing 5 M NaOH-solution). To regain **28** from these solutions after EPR measurements, they were bubbled with argon for 20 min upon which the samples showed the restored EPR-Signals of **28**.

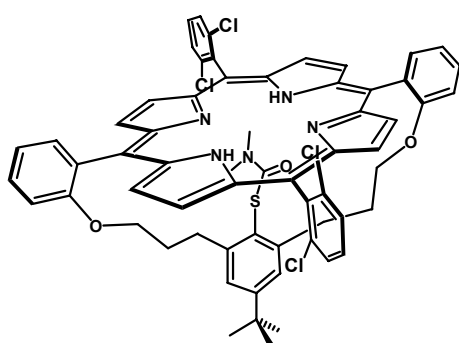
Samples of NO saturated toluene for comparison were obtained by bubbling a stream of NO through 200  $\mu\text{l}$  of degassed toluene in an EPR tube equipped with a septum for 10 min (NO was cleaned from trace amounts of higher nitrogen oxides by passing it subsequently through an Ascarite column and a gas scrubbing bottle containing 5 M NaOH).

**5,15-Bis-(2,6-dichlorophenyl)-10,20-bis(2-Hydroxyphenyl)porphyrin (40b)**

532 mg (655  $\mu\text{mol}$ , 1.0 eq.) of the Dichloro-dimethoxy-Porphyrin (Cpd. **51** in reference 63) were dissolved in 200 ml of  $\text{CH}_2\text{Cl}_2$  and cooled to 1  $^\circ\text{C}$ . Then 2.10 ml (21.8 mmol, 33 eq.)  $\text{BBr}_3$  were added. The mixture was allowed to come to r.t. and stirred at r.t. overnight. Then it was poured to sat.  $\text{NaHCO}_3$ -solution. The water phase was extracted two times with  $\text{CH}_2\text{Cl}_2$  and the combined organic layers washed with sat.  $\text{NaHCO}_3$ -solution and water. Drying over  $\text{Na}_2\text{SO}_4$  and evaporation of solvent gave 496 mg (97%) of a purple solid, which was used for the next step without further purification. Since the compound was already described elsewhere<sup>62,63</sup> only selected data is given.

TLC ( $\text{SiO}_2$ ;  $\text{CH}_2\text{Cl}_2$ ):  $R_f = 0.65$ ,  $R_f = 0.13$ .

ESI-MS (MeOH): Positive ion mode: 783 (100,  $[M+H]^+$ ).

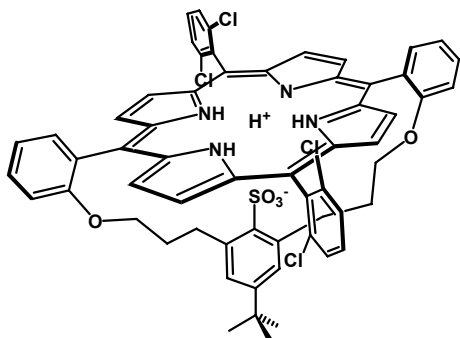
**5,15-({[5-(*t*-Butyl)-2-(*N,N*-dimethylcarbamoyl)thio-1,3-phenylene]bis(trimethyleneoxy)}-di-2,1-phenylene)-10,20-bis(2,6-dichlorophenyl) porphyrin (41b)**

489 mg (623  $\mu\text{mol}$ , 1.0 eq.) of crude Dihydroxy-porphyrin (**40b**) and 7.50 g (23.0 mmol, 37 eq.)  $\text{Cs}_2\text{CO}_3$  (previously dried at 100  $^\circ\text{C}$  in high vacuum overnight) were dissolved in 300 ml DMF and heated to 80  $^\circ\text{C}$ . After 30 min 473 mg (928  $\mu\text{mol}$ , 1.5 eq.) Dimesylate (**33**) in 100 ml DMF were added via syringe pump during 3 h. After addition heating was continued for 1 h. Then the mixture was cooled in an ice bath and 200 ml 1 N HCl was added. After addition of  $\text{CH}_2\text{Cl}_2$  the layers were separated and the water phase was extracted twice with  $\text{CH}_2\text{Cl}_2$ . The combined organic layers were washed with sat.  $\text{NaHCO}_3$ -solution, water and brine and dried over  $\text{Na}_2\text{SO}_4$ . Chromatography ( $\text{SiO}_2$ ,  $\text{CH}_2\text{Cl}_2$  + 1%  $\text{Et}_3\text{N}$ ) gave 511 mg (74%) of a purple solid. Since the compound was already described elsewhere<sup>62,63</sup> only selected data is given.

TLC (SiO<sub>2</sub>; CH<sub>2</sub>Cl<sub>2</sub> + 1% Et<sub>3</sub>N):  $R_f = 0.36$ .

ESI-MS (MeOH): *Positive ion mode*: 1100 (28, [M+H]<sup>+</sup>); 1122 (100, [M+Na]<sup>+</sup>). *Negative ion mode*: 1098 (100, [M-H]<sup>-</sup>).

**5,15-({[5-(*t*-Butyl)-2-sulfonato-1,3-phenylene]bis(trimethyleneoxy)}-di-2,1-phenylene)-10,20-bis(2,6-dichlorophenyl) porphyrin (42b)**



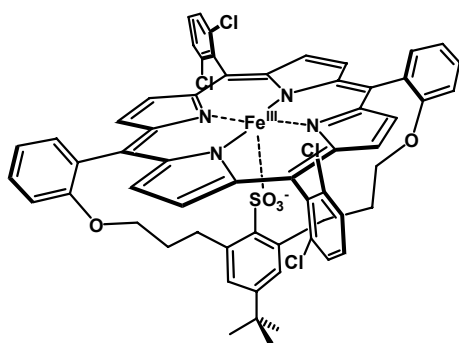
A solution of 473 mg (429 μmol, 1.0 eq.) Thiocarbamoylporphyrin (**41b**) in 100 ml of dioxane was saturated with O<sub>2</sub> and kept under O<sub>2</sub>-atmosphere for 10 min before addition of 2.00 g (28.6 mmol, 67 eq.) KOMe (previously dried at 100 °C in high vacuum overnight). After addition the mixture was heated to reflux and stirred at that temperature overnight. After cooling to r.t.

100 ml sat. NH<sub>4</sub>Cl-solution was added and the mixture poured into CH<sub>2</sub>Cl<sub>2</sub>/H<sub>2</sub>O. The layers were separated, the water layer extracted twice with CH<sub>2</sub>Cl<sub>2</sub> and the combined organic layers washed with water and dried over Na<sub>2</sub>SO<sub>4</sub>. Chromatography (SiO<sub>2</sub>, hexane/EtOAc 1/10 to EtOAc/MeOH 9/1) gave 270 mg (58%) of a crude purple solid. Since the compound was already described elsewhere<sup>62,63</sup> only selected data is given.

TLC (SiO<sub>2</sub>; hexane/ EtOAc 1:5):  $R_f = 0.16$ .

ESI-MS (MeOH): *Positive ion mode*: 1101 (100, [M+Na]<sup>+</sup>); 1123 (79, [M-H+2Na]<sup>+</sup>).

**[5,15-({[5-(*t*-Butyl)-2-sulfonato-1,3-phenylene]bis(trimethyleneoxy)}-di-2,1-phenylene)-10,20-bis(2,6-dichlorophenyl) porphyrinato]iron (III) (29)**



265 mg (246 μmol, 1.0 eq.) of crude SO<sub>3</sub>-porphyrin (**42b**) were dissolved in 170 ml of toluene and 580 μl 2,6-lutidine (5.00 mmol, 20 eq.) were added. The mixture was heated to reflux for 5 min and upon cooling 543 mg (2.52 mmol, 10 eq.) FeBr<sub>2</sub> were added and heating was continued for 1 h. Upon cooling to r.t. the mixture was filtrated through celite and

concentrated. Chromatography (SiO<sub>2</sub>, hexane/CH<sub>2</sub>Cl<sub>2</sub>/EtOAc 5/5/1) gave 60.6 mg (22%) of a

purple solid. Since the compound was already described elsewhere<sup>62,63</sup> only selected data is given.

**TLC** (SiO<sub>2</sub>; hexane/CH<sub>2</sub>Cl<sub>2</sub>/EtOAc 5:5:1):  $R_f = 0.34$ .

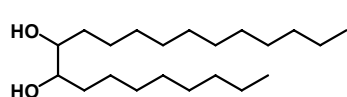
**UV/Vis** (CHCl<sub>3</sub>): 416 (100, *Soret*); 513 (11); 590 (2), 656 (2).

**ESI-MS** (MeOH): *Positive* ion mode: 1152 (100, [M+Na]<sup>+</sup>).

**HPLC** (XDB-C8, 150 x 4.6 mm, NH<sub>4</sub>OAc-buffer (1.0M, pH 4.62) / MeOH 1/3 to pure MeOH in 25 min, flow 1.0 ml/min, DAD ( $\lambda_{\text{det}} = 416$  nm, T = 25 °C)) :  $R_t = 18.5$  min.

## 5.2.2 Synthesis of Substrates, Co-oxidants and References for Catalytic Experiments

### 9,10-heneicosan-diol (56)



299 mg (1.02 mmol, 1.0 eq.) of *cis*-9-heneicosen were dissolved in 4 ml of H<sub>2</sub>O/*t*-Butanol 1/1. 158 mg (752  $\mu$ mol, 0.7 eq.) of citric acid monohydrate, 3.13 mg (8.50  $\mu$ mol, 0.8 mol%) of K<sub>2</sub>OsO<sub>2</sub>(OH)<sub>4</sub> and 152 mg (1.29 mmol, 1.3 eq.) of NMO were subsequently added. The resulting mixture was stirred at r.t. for 7 d, partially concentrated and acidified with 1 N HCl to pH 2. Two extractions with CH<sub>2</sub>Cl<sub>2</sub> and drying of the combined organic layers over Na<sub>2</sub>SO<sub>4</sub> gave 322 mg of crude product, which was crystallised from EtOAc to yield 274 mg (82%) of a white solid.

**TLC** (SiO<sub>2</sub>; hexane/TBME 1:1):  $R_f = 0.50$ .

**mp**: 124-126 °C

**IR** (neat): 3279*br*, 2957*w*, 2915*s*, 2849*s*, 1467*m*, 1070*m*, 1042*w*.

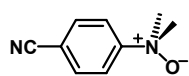
**<sup>1</sup>H-NMR** (400 MHz, CDCl<sub>3</sub>): 3.60 (*m*, 2H, H 9,10); 1.85 (*br*, 2H, -OH); 1.50 (*m*, 2H, H 7,12); 1.43 (*q*,  $J = 6.6$ , 4H, H 8,11); 1.25 (*m*, 28 H, H 2-7 and 12-20); 0.88 (*t*,  $J = 6.8$ , 6H, H1,21)

**<sup>13</sup>C-NMR** (100 MHz, CDCl<sub>3</sub>): 75.1, 32.3, 31.6, 30.1, 30.0, 29.8, 29.7, 26.4, 23.1, 14.5.

**EI-MS** (70 eV): 185 (12); 166 (7); 143 (15); 124 (17); 111 (24); 97 (42); 83 (72); 69 (100); 57 (32); 55 (37); 43 (22); 41 (15).

**FAB-MS**: 657 (7); 482 (10); 327 (11, [M-H]); 311 (100, [M-OH]); 293 (9); 111 (14); 97 (39); 83 (52); 69 (54); 55 (60); 43 (54).

**EA** calc. for C<sub>21</sub>H<sub>44</sub>O<sub>2</sub> (328.58): C 76.76, H 13.50, O 9.74; found: C 76.55, H 13.26, O 9.78.

**4-cyano-N,N-dimethylbenzenamine oxide(24)**

922 mg (3.74 mmol, 1.1 eq.) *m*CPBA in 7 ml of CH<sub>2</sub>Cl<sub>2</sub> were added to 502 mg (3.43 mmol, 1.0 eq.) of 4-cyano-N,N-dimethylbenzenamine (**53**) in 20 ml of CH<sub>2</sub>Cl<sub>2</sub> precooled to -4 °C such that the temperature stayed below 0 °C. After addition the cooling bath was removed and the solution was stirred at r.t. for 4 h. The crude reaction mixture was poured onto basic alox and remaining starting material was eluted with CH<sub>2</sub>Cl<sub>2</sub>. Elution with CH<sub>2</sub>Cl<sub>2</sub>/MeOH 3/1 gave 625 mg of a yellowish solid which was recrystallised from acetone/hexane to obtain 419 mg (75%) of colourless crystals.

**TLC** (Alox B; CH<sub>2</sub>Cl<sub>2</sub>/MeOH 20:1): *R<sub>f</sub>* = 0.25.

**mp**: 146-148 °C

**UV/Vis** (CH<sub>2</sub>Cl<sub>2</sub>): 231 (100); 263 (19); 270 (19); 278 (17).

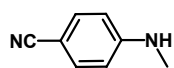
**IR** (neat): 3500-2800 *br*, 3356*w*, 3101*w*, 3024 *m*, 2978*w*, 2230*s*, 1497*s*, 972*s*, 849*s*.

**<sup>1</sup>H-NMR** (400 MHz, CDCl<sub>3</sub>): 8.17 (*d*, *J* = 9.1, 2H, H<sub>aryl</sub>); 7.80 (*d*, *J* = 9.1, 2H, H<sub>aryl</sub>); 3.60 (*s*, 6H, H<sub>methyl</sub>).

**<sup>13</sup>C-NMR** (100 MHz, CDCl<sub>3</sub>): 158.4, 133.7, 121.8, 117.9, 113.8, 63.8.

**EI-MS** (70 eV): 162 (57); 145 (100); 131 (22); 119 (39); 102 (34); 90 (11); 75 (11); 64 (8); 51 (7); 44 (43); 42 (21).

**FAB-MS**: 325 (8, [2*M*+H]); 316 (10); 163 (100, [*M*+H]); 146 (42).

**4-cyano-N-methylbenzenamine (54)**

5.68 g (48.1 mmol, 1.0 eq.) 4-aminobenzonitrile (**55**) were dissolved in 15 ml of MeOH and 2.60 ml (41.8 mmol, 0.9 eq.) MeI in 15 ml of MeOH were added over 1 h via syringe-pump. The mixture was heated to reflux overnight. Then the solvent was removed and the residuum redissolved in CH<sub>2</sub>Cl<sub>2</sub>. two times washing with 1 N NaOH-solution and drying over Na<sub>2</sub>SO<sub>4</sub> gave 5.84 g of a yellowish oil which solidified upon cooling overnight at 4 °C. Chromatography (Alox B, hexane/CH<sub>2</sub>Cl<sub>2</sub> 3/2) of the latter gave three products eluting in the order: 4-cyano-N,N-Dimethylbenzenamine (**53**)(718 mg, 10%); 4-cyano-N-methylbenzenamine (**54**)(1.66 g, 26 %); 4-aminobenzonitrile (**55**) (2.49 g, 44%).

As the title compound was obtained according to earlier prescriptions<sup>84</sup>, only selected data is given.

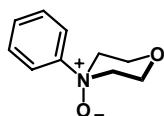
**TLC** (Alox B; hexane/ CH<sub>2</sub>Cl<sub>2</sub> 3:2):  $R_f$  = 0.15.

**mp**: 89-92 °C

**<sup>1</sup>H-NMR** (400 MHz, CDCl<sub>3</sub>): 7.42 (*d*,  $J$  = 8.8, 2H, H<sub>aryl 3,5</sub>); 6.55 (*d*,  $J$  = 8.6, 2H, H<sub>aryl 2,6</sub>); 4.30 (*br*, 1H, NH); 2.87 (*s*, 3H, H<sub>methyl</sub>).

**<sup>13</sup>C-NMR** (100 MHz, CDCl<sub>3</sub>): 152.6, 134.1, 121.0, 112.2, 98.9, 30.4.

#### 4-phenylmorpholine-4-oxide (60)



502 mg (3.08 mmol, 1.0 eq.) of 4-phenylmorpholine (**62**) were dissolved in 20 ml of dry CH<sub>2</sub>Cl<sub>2</sub> and cooled to 3 °C. 910 mg (3.69 mmol, 1.2 eq.) of *m*CPBA were added and the cooling bath removed to bring the solution to r.t. at which it was stirred overnight. Chromatography on basic alox was run with first CH<sub>2</sub>Cl<sub>2</sub> to remove remaining starting material. Further elution with CH<sub>2</sub>Cl<sub>2</sub>/MeOH 10/1 gave 533 mg of a yellowish solid which was recrystallised from acetone/hexane to yield 298 mg (54%) of colourless crystals.

**TLC** (Alox B; CH<sub>2</sub>Cl<sub>2</sub>/MeOH 20:1):  $R_f$  = 0.22.

**mp**: 189-192 °C

**UV/Vis** (CH<sub>2</sub>Cl<sub>2</sub>): 229 (100).

**IR** (neat):, 3103*w*, 3084*w*, 3048*m*, 3028*m*, 3000*m*, 2960*w*, 2949*w*, 2939*m*, 2922*m*, 2990*m*, 2878*w*, 2867*m*, 1490*m*, 1267*m*, 1108*s*, 963*s*, 850*s*, 755*s*.

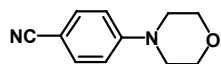
**<sup>1</sup>H-NMR** (400 MHz, CDCl<sub>3</sub>): 8.02 (*d*,  $J$  = 7.8, 2H, H<sub>aryl</sub>); 7.50 (*t*,  $J$  = 8.4, 2H, H<sub>aryl</sub>); 7.41 (*t*,  $J$  = 7.3, 1H, H<sub>aryl</sub>); 4.73 (*dxt*,  $J$  = 1.5,  $J'$  = 11.6, 2H, H<sub>2,6axial</sub>); 3.94 (*dxt*,  $J$  = 3.5,  $J'$  = 11.6, 2H, H<sub>3,5eq</sub>); 3.87 (*dxt*,  $J$  = 3.5,  $J'$  = 12.1, 2H, H<sub>2,6eq</sub>); 3.08 (*d*,  $J$  = 11.4, 2H, H<sub>3,5axial</sub>).

**<sup>13</sup>C-NMR** (100 MHz, CDCl<sub>3</sub>): 155.2, 129.7, 129.6, 120.7, 68.1, 62.7.

**EI-MS** (70 eV): 163 (36); 161 (14); 132 (5); 122 (17); 105 (100); 91 (13); 86 (99); 77 (73); 65 (13); 56 (84); 51 (25).

**FAB-MS**: 359 (8, [2*M*+H]); 333 (5); 180 (100, [*M*+H]); 163 (45); 105 (7); 86 (13); 77 (7); 63 (5); 57 (8); 51 (8); 43 (8); 41 (8).



**4-(4-cyanophenyl)morpholine (61)**

1.00 g (8.26 mmol, 1.0 eq.) 4-fluorobenzonitrile were dissolved in 14 ml DMSO and 1.50 ml (17.2 mmol, 2.1 eq.) morpholine were added via syringe. The mixture was heated to 100 °C and stirred for 7 h. Then it was cooled to r.t. and poured to 50 ml of H<sub>2</sub>O. Formation of a white solid occurred which was taken up in TBME. The water phase was extracted three more times with TBME and the combined organic layers were washed twice with brine, dried over Na<sub>2</sub>SO<sub>4</sub> and evaporated to yield 1.44 g of yellowish crystals. Chromatography (SiO<sub>2</sub>, hexane/EtOAc yielded 1.44 g (92%) of colourless crystals.

**TLC** (SiO<sub>2</sub>; hexane/EtOAc 1:1):  $R_f$  = 0.46.

**mp**: 87-89 °C

**UV/Vis** (CH<sub>2</sub>Cl<sub>2</sub>): 291 (100).

**IR** (neat): 3099<sub>w</sub>, 2982<sub>w</sub>, 2832<sub>m</sub>, 2216<sub>s</sub>, 1604<sub>s</sub>, 1515<sub>s</sub>, 1383<sub>s</sub>, 1244<sub>s</sub>, 1180<sub>s</sub>, 1111<sub>s</sub>, 927<sub>s</sub>, 834<sub>s</sub>, 815<sub>s</sub>.

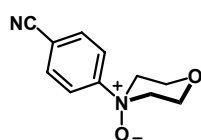
**<sup>1</sup>H-NMR** (400 MHz, CDCl<sub>3</sub>): 7.51 (*d*,  $J$  = 8.8, 2H, H<sub>aryl 3,5</sub>); 6.86 (*d*,  $J$  = 8.8, 2H, H<sub>aryl 2,6</sub>); 3.85 (*t*,  $J$  = 4.8, 4H, H<sub>2,6</sub>); 3.27 (*t*,  $J$  = 5.0, 4H, H<sub>3,5</sub>).

**<sup>13</sup>C-NMR** (100 MHz, CDCl<sub>3</sub>): 153.9, 133.9, 120.3, 114.5, 101.4, 66.9, 47.7.

**EI-MS** (70 eV): 188 (71); 130 (100); 129 (29); 102 (16).

**FAB-MS**: 189 (100, [*M*+H]); 188 (100); 187 (39); 130 (14); 77 (7); 57 (5); 51 (5); 41 (5); 39 (5).

**EA** calc. for C<sub>11</sub>H<sub>12</sub>N<sub>2</sub>O (188.23): C 70.19, H 6.43, N 14.88, O 8.50; found: C 70.24, H 6.54, N 14.81, O 8.46.

**4-(4-cyanophenyl)morpholine-4-oxide (59)**

1.01 g (5.32 mmol, 1.0 eq.) of 4-(4-cyanophenyl)morpholine (**61**) were dissolved in 30 ml of CH<sub>2</sub>Cl<sub>2</sub> and cooled in an ice bath. 1.31 g (5.32 mmol, 1.0 eq.) of *m*CPBA in 45 ml of CH<sub>2</sub>Cl<sub>2</sub> were added over 5 min. After further 5 min the cooling was removed to let the reaction mixture come to r.t. where it was stirred for 7 h. The crude mixture was poured onto basic alox from which remaining starting material was eluted with CH<sub>2</sub>Cl<sub>2</sub>. Subsequent elution using CH<sub>2</sub>Cl<sub>2</sub>/MeOH 3/1 yielded 1.07 g (98%) of a white solid.

**TLC** (Alox B; CH<sub>2</sub>Cl<sub>2</sub>/MeOH 20:1):  $R_f$  = 0.22.

**mp**: 180-182 °C

**UV/Vis** (CH<sub>2</sub>Cl<sub>2</sub>): 230 (100) 262 (20).

**IR** (neat):, 3097 $w$ , 3023 $m$ , 2981 $m$ , 2939 $m$ , 2226 $s$ , 1602 $m$ , 1500 $s$ , 1115 $s$ , 1106 $s$ , 1036 $m$ , 1014 $m$ , 965 $m$ , 927 $m$ , 902 $m$ , 865 $m$ , 855 $s$ , 851 $s$ .

**<sup>1</sup>H-NMR** (400 MHz, CDCl<sub>3</sub>): 8.21 ( $d$ ,  $J$  = 8.8, 2H, H<sub>aryl 3,5</sub>); 7.83 ( $d$ ,  $J$  = 8.8, 2H, H<sub>aryl 2,6</sub>); 4.76 – 4.66 ( $m$ , 2H, H<sub>2,6axial</sub>); 3.98 – 3.86 ( $m$ , 4H, H<sub>3,5axial,2,6eq</sub>); 3.08 ( $d$ ,  $J$  = 11.1, 2H, H<sub>3,5eq</sub>).

**<sup>13</sup>C-NMR** (100 MHz, CDCl<sub>3</sub>): 158.7, 133.8, 122.2, 117.9, 114.1, 68.2, 62.6.

**EI-MS** (70 eV): 204 (5); 188 (38); 186 (9); 147 (12); 130 (100); 129 (55); 119 (11); 116 (10); 102 (58); 90 (9); 86 (61); 75 (12); 56 (84).

**FAB-MS**: 409 (9, [2M+H]); 358 (8); 205 (100, [M+H]); 188 (42); 130 (10); 86 (13); 77 (7); 63 (5); 57 (12); 51 (8); 43 (11); 41 (10).

### 5.2.3 Catalytic Experiments applying Model Compounds

#### N-Dealkylation reactions

In a dry 5 ml Flask 100  $\mu$ l of a 46 mM solution of N-Oxide (**24**) was added to 0.46  $\mu$ mol (0.1 eq.) of Porphyrin (**28** or **29**) in 200  $\mu$ l degassed and anhydrous CH<sub>2</sub>Cl<sub>2</sub> at -50 °C. Then cooling was removed and the reaction stirred for 90 min at r.t. under the exclusion of light. After filtration through silica undecanal was added as a standard and the volume of the resulting solution was partially reduced. Analysis of the products was performed on GC-FID and GC-MS and the yields quantified relative to added N-Oxide in reference to the standard.

#### Diol cleavage reactions

In a dry 5 ml Flask 4.60  $\mu$ mol (10 eq.) of the oxidant and the diol (**56**) were added to 460 nmol (1.0 eq.) of Porphyrin (**28** or **29**) in 300  $\mu$ l degassed and anhydrous CH<sub>2</sub>Cl<sub>2</sub> at -50 °C. Then cooling was removed and the reaction stirred for 90 min at r.t. under the exclusion of light. After filtration through silica undecanal was added as a standard and the volume of the resulting solution was partially reduced. Analysis of the products was performed on GC-FID and GC-MS and the yields quantified relative to added oxidant in reference to the standard.

For determination of potentially formed acids, the reaction mixture was treated with an excess of TMS-CHN<sub>2</sub> and MeOH for 20 min prior to filtration.

For determination of unreacted diol, the reaction mixture was treated with p-TsOH and an excess of Acetone dimethyl acetal for 20 min prior to filtration.

### Control experiments

Control experiments were performed identical to the catalytic experiments described above under omission of either the porphyrin (**28/29**) or the co-oxidant.

### Epoxidation reactions

4.80 ml of a solution of **29** in MeCN were cooled to -35 °C (acetone/dry ice bath) in a dry 10 ml two necked flask containing a steering bar and a low temperature thermometer. 100 µl of a *m*CPBA-solution in MeCN was added and reacted with the former for at least 0.5 min (changes in optical properties of the reaction solution from brownish to green were observed during this period). After that, 3.50 µl of *cis*-stilbene (**49**) were added and samples (~1.5 ml) were taken after additional 1.5, 5 and 20 min. The latter were filtrated through basic alox to remove *m*CPBA, partially concentrated at reduced pressure and injected into GC-FID for analysis.

The concentrations of the solutions where chosen such that in the final reaction mixture the concentrations were: *m*CPBA:  $1.6 \times 10^{-4}$  M, *cis*-stilbene:  $4.0 \times 10^{-3}$  M, **29**:  $8.6 \times 10^{-6}$  M.

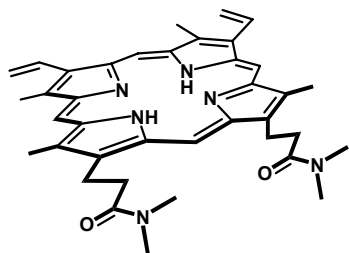
Additional experiments were performed under similar conditions, where upon *cis*-stilbene addition, the complete reaction was quickly brought to r.t. after 5 min and filtrated over basic alox, concentrated at reduced pressure and injected into GC-FID. Yields where calculated therefrom upon addition of known quantities of *cis*-stilbene.

Control experiments were performed by cooling 4.90 ml of a solution of *m*CPBA in MeCN to -35 °C (acetone/dry ice bath) in a dry 10 ml two necked flask containing a steering bar and a low temperature thermometer. 3.50 µl of *cis*-stilbene (**49**) were added and either samples (~1.5 ml) were taken after 1.5, 5 and 20 min, or the complete reaction volume was brought to r.t. quickly 5 min after addition of *cis*-stilbene. The so obtained samples were filtrated through basic alox to remove *m*CPBA, partially concentrated at reduced pressure and injected into GC-FID for analysis.

Again the concentrations were chosen to be the same as in the former experiments. (*m*CPBA:  $1.6 \times 10^{-4}$  M, *cis*-stilbene:  $4.0 \times 10^{-3}$  M)

## 5.2.4 Protoporphyrin Derivative Synthesis

### Protoporphyrin di-(N,N-dimethyl)-amide (**86**)



1.00 g (1.78 mmol, 1.0 eq.) of Protoporphyrin-IX were dissolved in 180 ml of THF, 759 mg (3.97 mmol, 2.2 eq.) EDCI and 607 mg (3.97 mmol, 2.2 eq.) HOBt·H<sub>2</sub>O were added and the mixture heated to 50 °C for 2 h. Then 2.50 ml (5.00 mmol, 2.8 eq.) of a 2 M solution of Dimethylamine in THF and 660 μl (3.92 mmol, 2.2 eq.) Hünigs-base were added and the mixture stirred at r.t.

overnight. The solvent was removed and the residue chromatographed (SiO<sub>2</sub>, CH<sub>2</sub>Cl<sub>2</sub>/MeOH 20/1) to obtain 942 mg (86%) of a purple solid.

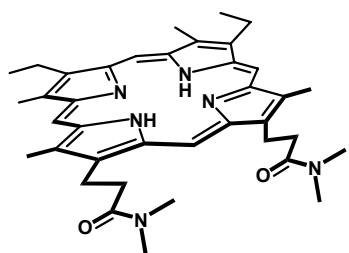
Since the compound was already described elsewhere<sup>108</sup> only selected data is given.

**TLC** (SiO<sub>2</sub> ; CH<sub>2</sub>Cl<sub>2</sub>/MeOH 20:1): *R<sub>f</sub>* = 0.26.

**<sup>1</sup>H-NMR** (400 MHz, CDCl<sub>3</sub>): 10.23 (*s*, 1H, H5,10,15,20); 10.17 (*s*, 1H, H5,10,15,20); 10.09 (*s*, 1H, H5,10,15,20); 10.04 (*s*, 1H, H5,10,15,20); 8.30 (*dxd*, *J* = 17.7, *J'* = 11.4, 2H, H 3<sup>1</sup>,8<sup>1</sup>); 6.38 (*d*, *J* = 17.7, H 3<sup>2</sup>,8<sup>2</sup>); 6.20 (*d*, *J* = 11.6, 2H, H 3<sup>2</sup>,8<sup>2</sup>); 4.42 (*t*, *J* = 7.8, 4H, H 13<sup>1</sup>,17<sup>1</sup>); 3.72 (*s*, 3H, H 2<sup>1</sup>,7<sup>1</sup>,12<sup>1</sup>,18<sup>1</sup>); 3.71 (*s*, 3H, H 2<sup>1</sup>,7<sup>1</sup>,12<sup>1</sup>,18<sup>1</sup>); 3.64 (*s*, 3H, H 2<sup>1</sup>,7<sup>1</sup>,12<sup>1</sup>,18<sup>1</sup>); 3.62 (*s*, 3H, H 2<sup>1</sup>,7<sup>1</sup>,12<sup>1</sup>,18<sup>1</sup>); 3.27 (*t*, *J* = 7.8, 4H, H13<sup>2</sup>,17<sup>2</sup>); 2.90 (*s*, 6H, H 13<sup>3</sup>,17<sup>3</sup>); 2.66 (*s*, 6H, H 13<sup>3</sup>,17<sup>3</sup>); -3.71 (*s*, 2H, NH).

**ESI-MS** (CH<sub>2</sub>Cl<sub>2</sub>/MeOH): *Positive* ion mode: 617 (42, [M+H]<sup>+</sup>); 639 (100, [M+Na]<sup>+</sup>); 1255 (26, [2M+Na]<sup>+</sup>).

### Mesoporphyrin di-(N,N-dimethyl)-amide (**88**)



940 mg (1.52 mmol, 1.0 eq.) of pP-DMA (**86**) were dissolved in 60 ml of CH<sub>2</sub>Cl<sub>2</sub> and 94.1 mg Pd/C (10%Pd) were added. The atmosphere was changed to H<sub>2</sub> and the mixture stirred vigorously at r.t. overnight. Filtration over celite and chromatography (SiO<sub>2</sub>, CH<sub>2</sub>Cl<sub>2</sub>/MeOH 20/1) gave 860 mg (91%) of a purple solid.

**TLC** (SiO<sub>2</sub>; CH<sub>2</sub>Cl<sub>2</sub>/MeOH 10:1):  $R_f$  = 0.41.

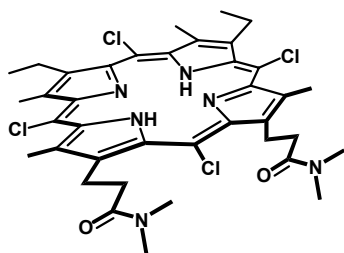
**UV/Vis** (CH<sub>2</sub>Cl<sub>2</sub>): 397 (100, *Soret*); 498 (8); 531 (6), 566 (5), 620 (3).

**<sup>1</sup>H-NMR** (400 MHz, CDCl<sub>3</sub>): 10.11-10.09 (*m*, 4H, H 5,10,15,20); 4.45 (*t*,  $J = 7.4$ , 4H, H 13<sup>1</sup>,17<sup>1</sup>); 4.10 (*q*,  $J = 7.6$ , 4H, H 3<sup>1</sup>,8<sup>1</sup>); 3.70-3.58 (*m*, 12H, H 2<sup>1</sup>,7<sup>1</sup>,12<sup>1</sup>,18<sup>1</sup>); 3.28 (*t*,  $J = 7.4$ , 4H, H13<sup>2</sup>,17<sup>2</sup>); 2.90 (*s*, 3H, H 13<sup>3</sup>,17<sup>3</sup>); 2.88 (*s*, 3H, H 13<sup>3</sup>,17<sup>3</sup>); 2.66 (*s*, 3H, H 13<sup>3</sup>,17<sup>3</sup>); 2.60 (*s*, 3H, H 13<sup>3</sup>,17<sup>3</sup>); 1.87 (*t*,  $J = 7.6$ , 6H, H3<sup>2</sup>,8<sup>2</sup>); -3.79 (*s*, 2H, NH).

**ESI-MS** (MeOH): *Positive* ion mode: 621 (19, [M+H]<sup>+</sup>); 643 (100, [M+Na]<sup>+</sup>); 1263 (12, [2M+Na]<sup>+</sup>).

**HPLC** (LiChrospher® 100 RP-18 (5 μm particle size, 4×250 mm), H<sub>2</sub>O/MeOH 1/9 to pure MeOH in 50 min, flow 1.0 ml/min, DAD (λ<sub>det</sub> = 400, T = 25 °C)):  $R_t$  = 16.4 min.

### 5,10,15,20-tetrachloromesoporphyrin di-(N,N-dimethyl)-amide (**89**)



102 mg (161 μmol, 1.0 eq.) of MP-DMA (**88**) were dissolved in 5 ml of CH<sub>2</sub>Cl<sub>2</sub> and 175 mg (1.31 mmol, 8.1 eq.) NCS were added. The mixture was stirred for 5 d at r.t. under the exclusion of light and controlled via HPLC (small aliquots was taken and filtrated over SiO<sub>2</sub> in a Pasteur pipette. CH<sub>2</sub>Cl<sub>2</sub> was used to

remove apolar components and CH<sub>2</sub>Cl<sub>2</sub>/MeOH 20/1 eluted the desired porphyrin band, which was concentrated in vacuo, redissolved in MeOH and filtrated to be analysed by HPLC: LiChrospher® 100 RP-18 (5 μm particle size, 4×250 mm), H<sub>2</sub>O/ MeOH 1/9 to pure MeOH in 50 min, then pure MeOH for 20 min, flow 1.0 ml/min, DAD (λ<sub>det</sub> = 400,450 nm, T = 25 °C). Chromatography (SiO<sub>2</sub>, CH<sub>2</sub>Cl<sub>2</sub>/MeOH 20/1) gave 96.0 mg (77%) of a dark green solid. Unfortunately different purification methods including chromatography and crystallisation could not separate the product from impurities evident by NMR.

**TLC** (SiO<sub>2</sub>; CH<sub>2</sub>Cl<sub>2</sub>/MeOH 20:1):  $R_f$  = 0.23.

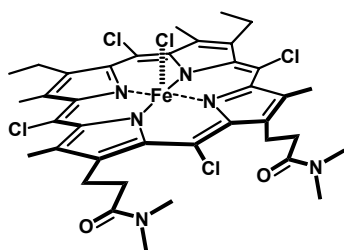
**UV/Vis** (CH<sub>2</sub>Cl<sub>2</sub>): 444 (100, *Soret*); 548 (7), 593 (7), 684 (6).

**<sup>1</sup>H-NMR** (400 MHz, CDCl<sub>3</sub>): no interpretable spectra were obtained in several attempts.

**ESI-MS** (MeOH): *Positive* ion mode: 757 (100, [M+H]<sup>+</sup>), 779 (42, [M+Na]<sup>+</sup>) 787 (24); 809 (20).

**HPLC** (LiChrospher® 100 RP-18 (5  $\mu\text{m}$  particle size, 4 $\times$ 250 mm), H<sub>2</sub>O/MeOH 1/9 to pure MeOH in 50 min, flow 1.0 ml/min, DAD ( $\lambda_{\text{det}} = 450$ , T = 25 °C)):  $R_t = 33.9$  min (main impurities: 22.1, 23.6, 28.1 min).

### Chloro(5,10,15,20-tetrachloromesoporphyrinato di-(N,N-dimethyl)-amide) iron (III) (90)



475 mg (max. 627  $\mu\text{mol}$ , 1.0 eq.) of crude Cl<sub>4</sub>-MP-DMA (**89**) were dissolved in 425 ml of toluene and 1.90 ml 2,6-lutidine (16.4 mmol, 26 eq.) were added. The mixture was heated to reflux for 5 min and upon cooling 1.74 g (8.01 mmol, 12 eq.) FeBr<sub>2</sub> were added and heating was continued for 1 h. Upon cooling to r.t. the mixture was filtrated through celite and concentrated.

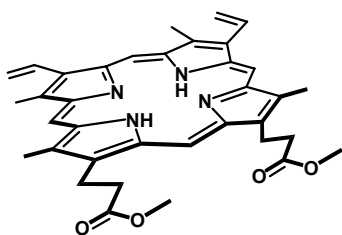
Chromatography (SiO<sub>2</sub>, CH<sub>2</sub>Cl<sub>2</sub>/MeOH 20/1) gave 51.0 mg (10%) of a dark green solid.

**TLC** (SiO<sub>2</sub>; CH<sub>2</sub>Cl<sub>2</sub>/MeOH 10:1):  $R_f = 0.49$ .

**UV/Vis** (CH<sub>2</sub>Cl<sub>2</sub>): 405 (100, *Soret*); 433 (95, sh, *Soret*); poorly resolved bands at 576 (6), 656 (5), 752 (2).

**ESI-MS** (MeOH): *Positive ion mode*: 810 (100, [M-Cl]<sup>+</sup>); 841 (15, [M-Cl+MeOH]<sup>+</sup>); 864 (85, [M-Cl+NaOMe]<sup>+</sup>); 878 (13).

### Protoporphyrin dimethyl ester (85)



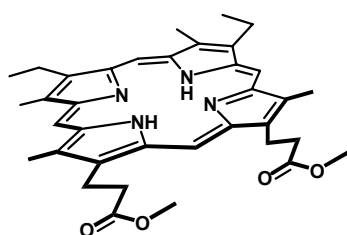
1.04 g (1.85 mmol, 1.0 eq.) of Protoporphyrin-IX were dissolved in 50 ml of MeOH and 50 ml of TMOF were added. After cooling to 0 °C 10 ml of conc. H<sub>2</sub>SO<sub>4</sub> was added such that T  $\leq$  5 °C and the cooling bath was removed afterwards to let the reaction come to r.t., where it was stirred for 90 min. Then it was

poured to a water/ice mixture and neutralised with 3 M NaOH after addition of CH<sub>2</sub>Cl<sub>2</sub>. the water phase was extracted two more times with CH<sub>2</sub>Cl<sub>2</sub> and the combined organic layers were dried over Na<sub>2</sub>SO<sub>4</sub> and concentrated in vacuo. Chromatography (SiO<sub>2</sub>, CH<sub>2</sub>Cl<sub>2</sub> to CH<sub>2</sub>Cl<sub>2</sub>/MeOH 97/3) gave 1.03 g (95%) of a brownish solid. Since the compound was already described elsewhere<sup>108, 122, 123</sup> only selected data is given.

**TLC** (SiO<sub>2</sub>; CH<sub>2</sub>Cl<sub>2</sub>/MeOH 100:1):  $R_f = 0.34$ .

**<sup>1</sup>H-NMR** (400 MHz, CDCl<sub>3</sub>): 10.17 (*s*, 1H, H<sub>5,10,15,20</sub>); 10.13 (*s*, 1H, H<sub>5,10,15,20</sub>); 10.03 (*s*, 1H, H<sub>5,10,15,20</sub>); 10.00 (*s*, 1H, H<sub>5,10,15,20</sub>); 8.29 (*dxd*, *J* = 11.6, *J'* = 2.0, 1H, H 3<sup>1</sup>,8<sup>1</sup>); 8.24 (*dxd*, *J* = 11.4, *J'* = 2.0, 1H, H 3<sup>1</sup>,8<sup>1</sup>); 6.37 (*dxd*, *J* = 17.9, *J'* = 1.5, 2H, H 3<sup>2</sup>,8<sup>2</sup>); 6.18 (*d*, *J* = 11.6, 2H, H 3<sup>2</sup>,8<sup>2</sup>); 4.39 (*t*, *J* = 7.8, 4H, H 13<sup>1</sup>,17<sup>1</sup>); 3.69 (*s*, 3H, H 2<sup>1</sup>,7<sup>1</sup>,12<sup>1</sup>,18<sup>1</sup>); 3.68 (*s*, 3H, H 2<sup>1</sup>,7<sup>1</sup>,12<sup>1</sup>,18<sup>1</sup>); 3.66 (*s*, 6H, H 13<sup>3</sup>,17<sup>3</sup>); 3.61 (*s*, 3H, H 2<sup>1</sup>,7<sup>1</sup>,12<sup>1</sup>,18<sup>1</sup>); 3.60 (*s*, 3H, H 2<sup>1</sup>,7<sup>1</sup>,12<sup>1</sup>,18<sup>1</sup>); 3.27 (*t*, *J* = 7.8, 4H, H<sub>13<sup>2</sup>,17<sup>2</sup></sub>); -3.78 (*s*, 2H, NH).

### Mesoporphyrin dimethyl ester (**87**)



1.06 g (1.79 mmol, 1.0 eq.) of pP-DME (**85**) were dissolved in 100 ml of CH<sub>2</sub>Cl<sub>2</sub> and 106 mg Pd/C (10%Pd) were added. The atmosphere was changed to H<sub>2</sub> and the mixture stirred vigorously at r.t. overnight. Filtration over celite and chromatography (SiO<sub>2</sub>, CH<sub>2</sub>Cl<sub>2</sub> to CH<sub>2</sub>Cl<sub>2</sub>/ MeOH 97/3) gave 981 mg (92%) of a purple solid.

**TLC** (SiO<sub>2</sub>; hexane/ EtOAc 1:2): *R<sub>f</sub>* = 0.28.

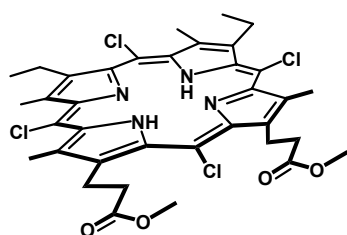
**UV/Vis** (THF): 397 (100, *Soret*); 498 (10); 529 (7), 569 (5), 623 (5).

**<sup>1</sup>H-NMR** (400 MHz, CDCl<sub>3</sub>): 10.11-10.08 (*m*, 4H, H<sub>5,10,15,20</sub>); 4.44 (*t*, *J* = 7.6, 4H, H 13<sup>1</sup>,17<sup>1</sup>); 4.09 (*q*, *J* = 7.3, 4H, H 3<sup>1</sup>,8<sup>1</sup>); 3.67 (*s*, 6H, H 2<sup>1</sup>,7<sup>1</sup>,12<sup>1</sup>,18<sup>1</sup>); 3.66 (*s*, 6H, H 13<sup>3</sup>,17<sup>3</sup>); 3.64 (*s*, 3H, H 2<sup>1</sup>,7<sup>1</sup>,12<sup>1</sup>,18<sup>1</sup>); 3.63 (*s*, 3H, H 2<sup>1</sup>,7<sup>1</sup>,12<sup>1</sup>,18<sup>1</sup>); 3.30 (*t*, *J* = 7.6, 4H, H<sub>13<sup>2</sup>,17<sup>2</sup></sub>); 1.87 (*t*, *J* = 7.6, 6H, H<sub>3<sup>2</sup>,8<sup>2</sup></sub>); -3.77 (*s*, 2H, NH).

**ESI-MS** (MeCN): *Positive ion mode*: 595 (100, [M+H]<sup>+</sup>); 617 (98, [M+Na]<sup>+</sup>).

**HPLC** (XDB-C8, 150 x 4.6 mm, NH<sub>4</sub>OAc-buffer (1.0M, pH 4.62) / MeOH 1/4 to pure MeOH in 20 min, flow 1.0 ml/min, DAD (λ<sub>det</sub> = 400 nm, T = 25 °C)): *R<sub>t</sub>* = 10.1 min.

### 5,10,15,20-tetrachloromesoporphyrin dimethyl ester (**91**)



1.01 g (1.68 mmol, 1.0 eq.) of MP-DME (**87**) were dissolved in 90 ml of CH<sub>2</sub>Cl<sub>2</sub> and 1.82 g (13.6 mmol, 8.1 eq.) NCS were added. The mixture was stirred for 6 d at r.t. under the exclusion of light and controlled via HPLC (small aliquots was taken and filtrated over SiO<sub>2</sub> in a Pasteur pipette. CH<sub>2</sub>Cl<sub>2</sub> was used to remove polar components and CH<sub>2</sub>Cl<sub>2</sub>/MeOH 20/1 eluted the desired porphyrin band, which

was concentrated in vacuo, redissolved in THF/MeOH/ NH<sub>4</sub>OAc-buffer (1.0M, pH 4.62) and filtrated to be analysed by HPLC: XDB-C8, 150 x 4.6 mm, NH<sub>4</sub>OAc-buffer (1.0M, pH 4.62) / MeOH 1/4 to pure MeOH in 20 min, flow 1.0 ml/min, DAD ( $\lambda_{\text{det}} = 400,450 \text{ nm}$ , T = 25 °C). Upon completion 10 ml of MeOH and 4 ml of 2 N TMS-diazomethane in hexane were added and the stirring continued for 30 min. removal of solvent and chromatography (Alox B, hexane/CH<sub>2</sub>Cl<sub>2</sub>/EtOAc 12/8/1) gave 252 mg (20%) of a dark green solid.

**TLC** (Alox B; hexane/CH<sub>2</sub>Cl<sub>2</sub>/EtOAc 12:8:1):  $R_f = 0.61$ .

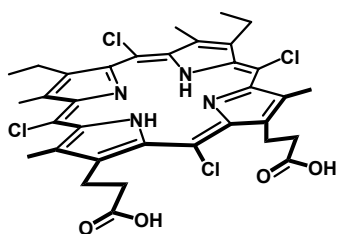
**UV/Vis** (THF): 442 (100, *Soret*); 547 (6), 595 (5), 690 (3).

**<sup>1</sup>H-NMR** (400 MHz, CDCl<sub>3</sub>): 3.93-3.84 (*m*, 4H, H 13<sup>1</sup>,17<sup>1</sup>); 3.71 (*s*, 6H, H 13<sup>3</sup>,17<sup>3</sup>); 3.59-3.50 (*m*, 4H, H 3<sup>1</sup>,8<sup>1</sup>); 3.09 (*s*, 3H, H12<sup>1</sup>,18<sup>1</sup>); 3.08 (*s*, 3H, H 12<sup>1</sup>,18<sup>1</sup>); 3.06 (*s*, 3H, H 2<sup>1</sup>,7<sup>1</sup>); 3.05 (*s*, 3H, H 2<sup>1</sup>,7<sup>1</sup>); 3.00-2.92 (*m*, 4H, H13<sup>2</sup>,17<sup>2</sup>); 1.56-1.48 (*m*, 6H, H3<sup>2</sup>,8<sup>2</sup>); -1.28 (*s*, 2H, NH).

**ESI-MS** (MeCN): *Positive ion mode*: 731 (100, [M+H]<sup>+</sup>).

**HPLC** (XDB-C8, 150 x 4.6 mm, NH<sub>4</sub>OAc-buffer (1.0M, pH 4.62) / MeOH 1/4 to pure MeOH in 20 min, flow 1.0 ml/min, DAD ( $\lambda_{\text{det}} = 450 \text{ nm}$ , T = 25 °C) :  $R_t = 15.2 \text{ min}$ .

### 5,10,15,20-tetrachloromesoporphyrin (94)



100 mg (137  $\mu\text{mol}$ , 1.0 eq.) of Cl<sub>4</sub>-MP-DME (**91**) in 44 ml of THF (unstabilized) were added to 44 ml of a 2 N KOH solution and stirred at r.t. overnight. The reaction mixture was diluted with water and extracted three times with CH<sub>2</sub>Cl<sub>2</sub>. After acidification with 130 ml of 1 M HCl the product was taken up in CH<sub>2</sub>Cl<sub>2</sub> and

the water phase extracted once more with a mixture of CH<sub>2</sub>Cl<sub>2</sub>/THF. The combined organic layers were washed with 0.2 M HCl, filtrated through celite and concentrated in vacuo to obtain 112 mg of a green solid. Unfortunately different purification methods including chromatography (RP-18, THF/H<sub>2</sub>O 3/1 to pure THF) could not produce a very pure compound, HPLC always showing polar contaminations. Nevertheless purity was good enough to obtain reasonable data from most analytic methods.

**TLC** (RP-18; THF/H<sub>2</sub>O 3:1):  $R_f = 0.58$ .

**UV/Vis** (THF): 441 (100, *Soret*); 545 (8), 595 (8).

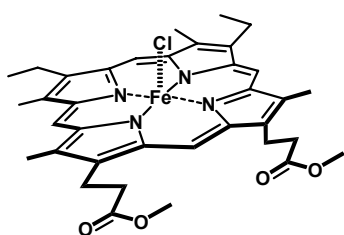


**<sup>1</sup>H-NMR** (600 MHz, pyridine): 4.14-4.10 (*m*, 4H, H 13<sup>1</sup>,17<sup>1</sup>); 3.48-3.41 (*m*, 4H, H 3<sup>1</sup>,8<sup>1</sup>); 3.29-3.23 (*m*, 4H, H13<sup>2</sup>,17<sup>2</sup>); 3.10 (*s*, 6H, H12<sup>1</sup>,18<sup>1</sup>); 3.00 (*s*, 6H, H 2<sup>1</sup>,7<sup>1</sup>); 1.54-1.49 (*m*, 6H, H3<sup>2</sup>,8<sup>2</sup>); -0.22 (*br*, 2H, NH).

**ESI-MS** (THF): *Positive* ion mode: 703 (100, [M+H]<sup>+</sup>).

**HPLC** (XDB-C8, 150 x 4.6 mm, NH<sub>4</sub>OAc-buffer (1.0M, pH 4.62) / MeOH 2/3 to 1/19 in 40 min, flow 1.0 ml/min, DAD (λ<sub>det</sub> = 450 nm, T = 25 °C) : R<sub>t</sub> = 22 min.

### Chloro(mesoporphyrinato dimethyl ester) iron (III) (96)



40.7 mg (68.4 μmol, 1.0 eq.) of MP-DME (**87**) were dissolved in 8.0 ml of CH<sub>2</sub>Cl<sub>2</sub> and 80.0 μl (697 μmol, 10 eq.) of 2,6-Lutidine were added. 30.0 mg (235 μmol, 3.4 eq.) of FeCl<sub>2</sub> were dissolved in 8.0 ml acetonitrile by heating to reflux for 5 min.

After cooling to r.t. the above obtained porphyrin solution was added via syringe. The mixture was stirred at r.t. for 50 min and then filtered through celite and concentrated. After chromatography (Alox N, CH<sub>2</sub>Cl<sub>2</sub>/MeOH 191/1) the solvent was removed and the residue redissolved in CH<sub>2</sub>Cl<sub>2</sub> and washed two times with 0.2 M HCl to obtain 32.2 mg (73%) of a brown solid.

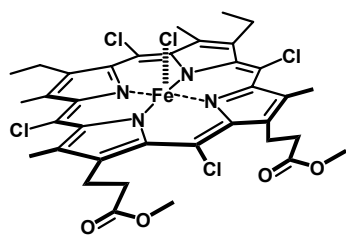
**TLC** (Alox N; CH<sub>2</sub>Cl<sub>2</sub>/MeOH 99:1): R<sub>f</sub> = 0.66

**UV/Vis** (CH<sub>2</sub>Cl<sub>2</sub>): 378 (100, *Soret*); 507 (10), 534 (10), 634 (5).

**<sup>1</sup>H-NMR** (600 MHz, CDCl<sub>3</sub>): 53.3 (*s*, 6H, H 2<sup>1</sup>,7<sup>1</sup>); 50.5 (*s*, 6H, H 12<sup>1</sup>,18<sup>1</sup>); 44.7 (*s*, 2H, H 3<sup>1</sup>,8<sup>1</sup>,13<sup>1</sup>,17<sup>1</sup>); 43.6 (*s*, 1H, H 3<sup>1</sup>,8<sup>1</sup>,13<sup>1</sup>,17<sup>1</sup>); 43.1 (*s*, 1H, H 3<sup>1</sup>,8<sup>1</sup>,13<sup>1</sup>,17<sup>1</sup>); 41.3-39.4 (*m*, 4H, H 3<sup>1</sup>,8<sup>1</sup>,13<sup>1</sup>,17<sup>1</sup>); 6.95 (*s*, 6H, H 3<sup>2</sup>,8<sup>2</sup>); 6.47 (*s*, 2H, H 13<sup>2</sup>,17<sup>2</sup>); 6.06 (*s*, 2H, H 13<sup>2</sup>,17<sup>2</sup>); 3.91 (*s*, 3H, H13<sup>3</sup>,17<sup>3</sup>); 3.84 (*s*, 3H, H13<sup>3</sup>,17<sup>3</sup>); -54.0- -60.0 (*br*, 4H, H 5,10,15,20).

**ESI-MS** (MeOH/ CH<sub>2</sub>Cl<sub>2</sub>): *Positive* ion mode: 648 (100, [M-Cl]<sup>+</sup>), 721 (27).

**HPLC** (XDB-C8, 150 x 4.6 mm, NH<sub>4</sub>OAc-buffer (1.0M, pH 4.62) / MeOH 2/3 to 1/19 in 40 min, flow 1.0 ml/min, DAD (λ<sub>det</sub> = 400 nm, T = 25 °C) : R<sub>t</sub> = 26.0 min.

**Chloro(5,10,15,20-tetrachloromesoporphyrinato dimethyl ester) iron (III) (93)**

41.5 mg (56.6  $\mu\text{mol}$ , 1.0 eq.) of Cl<sub>4</sub>-MP-DME (**91**) were dissolved in 8.0 ml of CH<sub>2</sub>Cl<sub>2</sub> and 65.0  $\mu\text{l}$  (566  $\mu\text{mol}$ , 10 eq.) of 2,6-Lutidin were added. 25.3 mg (198  $\mu\text{mol}$ , 3.5 eq.) of FeCl<sub>2</sub> were dissolved in 8.0 ml acetonitrile by heating to reflux for 5 min. After cooling to r.t. the above obtained porphyrin solution was added via syringe. The mixture was stirred at r.t. for 50 min and then filtered through celite and concentrated. After chromatography (Alox N, hexane/CH<sub>2</sub>Cl<sub>2</sub>/EtOAc 12/8/1 to CH<sub>2</sub>Cl<sub>2</sub>/EtOAc 1/1) the solvent was removed and the residue redissolved in CH<sub>2</sub>Cl<sub>2</sub> and washed two times with 0.2 M HCl to obtain 30.2 mg (65%) of a dark green solid.

**TLC** (Alox N; hexane/CH<sub>2</sub>Cl<sub>2</sub>/EtOAc 5:5:1):  $R_f$  = 0.65 ( $\mu$ -oxo dimer).

**UV/Vis** (toluene): 392 (84, *Soret*); 442 (100, *Soret*); poorly resolved bands at 527 (13), 568 (11), 752 (3).

(CH<sub>2</sub>Cl<sub>2</sub>): 396 (98, *Soret*); 442 (100, *Soret*); poorly resolved bands at 528 (14), 567 (11), 755 (4).

**<sup>1</sup>H-NMR** (600 MHz, CDCl<sub>3</sub>): 49.0 (*s*, 3H, H 2<sup>1</sup>,7<sup>1</sup>,12<sup>1</sup>,18<sup>1</sup>); 48.1 (*s*, 3H, H 2<sup>1</sup>,7<sup>1</sup>,12<sup>1</sup>,18<sup>1</sup>); 46.6 (*s*, 3H, H 2<sup>1</sup>,7<sup>1</sup>,12<sup>1</sup>,18<sup>1</sup>); 46.1 (*s*, 3H, H 2<sup>1</sup>,7<sup>1</sup>,12<sup>1</sup>,18<sup>1</sup>); 42.5-40.5 (*m*, 4H, H 3<sup>1</sup>,8<sup>1</sup>,13<sup>1</sup>,17<sup>1</sup>); 36.5-34.3 (*m*, 4H, H 3<sup>1</sup>,8<sup>1</sup>,13<sup>1</sup>,17<sup>1</sup>); 6.52 (*s*, 6H, H 3<sup>2</sup>,8<sup>2</sup>); 5.20-4.80 (*m*, 4H, H 13<sup>2</sup>,17<sup>2</sup>); 4.08 (*s*, 3H, H13<sup>3</sup>,17<sup>3</sup>); 4.04 (*s*, 3H, H13<sup>3</sup>,17<sup>3</sup>).

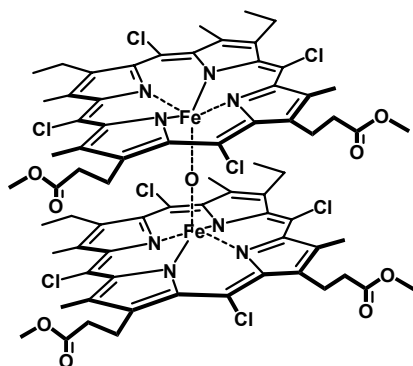
**ESI-MS** (MeOH): *Positive* ion mode: 838 (100, [M-Cl+NaOMe]<sup>+</sup>).

**MALDI-TOF-MS** (4-Nitroaniline): 784 (100, [M-Cl]); 819 (24, [M]).

**cw-EPR** (25mM Bu<sub>4</sub>NCl in CH<sub>2</sub>Cl<sub>2</sub>/THF 1/1, 15 K): 6.20, 5.52, 1.99 (high spin with slight rhombic distortion).

**HPLC** (XDB-C8, 150 x 4.6 mm, pure MeOH, flow 0.2 ml/min, DAD ( $\lambda_{\text{det}}$  = 450 nm, T = 25 °C)):  $R_t$  = 18.4 min.

(XDB-C8, 150 x 4.6 mm, Imidazole/HCl-buffer (500 mM, pH 7.00) / MeOH 1/3 for 30 min, flow 1.0 ml/min, DAD ( $\lambda_{\text{det}}$  = 430 nm, T = 25 °C) :  $R_t$  = 10.8 min.

**( $\mu$ -Oxo)-bis[(5,10,15,20-tetrachloromesoporphyrinato dimethyl ester)iron (III)] (**95**)**

The  $\mu$ -oxo dimer was obtained in the iron insertion step after chromatography.

To obtain it in a very pure form, 6.90 mg (8.40  $\mu$ mol, 1.0 eq.) of Fe(Cl<sub>4</sub>-MP-DME)Cl (**93**) were dissolved in 50 ml CH<sub>2</sub>Cl<sub>2</sub> and washed with 50 ml of a 20 mM NaOH-solution twice. The organic layer was dried over Na<sub>2</sub>SO<sub>4</sub> and concentrated. Filtration (Alox N, CH<sub>2</sub>Cl<sub>2</sub> to CH<sub>2</sub>Cl<sub>2</sub>/EtOAc 20/1) gave 4.69 mg (70%) of a dark green solid.

**TLC** (Alox N; hexane/CH<sub>2</sub>Cl<sub>2</sub>/EtOAc 5:5:1):  $R_f$  = 0.65.

**UV/Vis** (CH<sub>2</sub>Cl<sub>2</sub>): 415 (100, *Soret, broad*); 609 (8), 660 (8).

**<sup>1</sup>H-NMR** (600 MHz, CDCl<sub>3</sub>): 6.28-5.60 (*m*, 4H, H 3<sup>1</sup>,8<sup>1</sup>,13<sup>1</sup>,17<sup>1</sup>); 5.05-4.45 (*m*, 16H, H 2<sup>1</sup>,3<sup>1</sup>,7<sup>1</sup>,8<sup>1</sup>,12<sup>1</sup>,13<sup>1</sup>,17<sup>1</sup>,18<sup>1</sup>); 3.83 (*s*, 6H, H 13<sup>3</sup>,17<sup>3</sup>); 2.90 (*s*, 2H, H 13<sup>2</sup>,17<sup>2</sup>); 2.71 (*s*, 2H, H 13<sup>2</sup>,17<sup>2</sup>); 1.56 (*s*, 6H, H 3<sup>2</sup>,8<sup>2</sup>).

**ESI-MS** (CH<sub>2</sub>Cl<sub>2</sub>): *Positive ion mode*: 1588 (100, [ $M_{\text{highest isotopic peak}}$ ]<sup>+</sup>).

**MALDI-TOF-MS** (4-Nitroaniline): 784 (85, [1/2( $M$ -O)]); 1584 (100, [ $M$ ]).

**HPLC** (XDB-C8, 150 x 4.6 mm, pure MeOH, flow 1.0 ml/min, DAD ( $\lambda_{\text{det}}$  = 400 nm, T = 25 °C)) :  $R_t$  = 19.5 min.

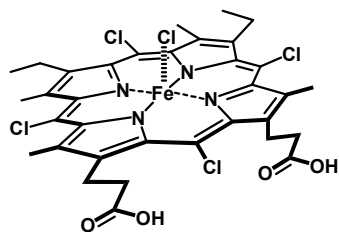
**Thiolate-Complex 98:**

UV/Vis spectra of **98** were obtained by addition of 20.0  $\mu$ l of 4-*tert*-butyl-thiophenol (**97**) to 2.0 ml of a 8.00  $\mu$ M solution of **95** in toluene in a UV/Vis cuvette.

<sup>1</sup>H-NMR tracking of the reaction of **95** to **98** was performed upon addition of 2.00  $\mu$ l (11.9  $\mu$ mol, 9.5 eq.) of **97** to 2.00 mg (1.26  $\mu$ mol, 1.0 eq.) of **98** in 500  $\mu$ l of CDCl<sub>3</sub>.

cw-EPR spectra of **98** were obtained after addition of 2.00  $\mu$ l (11.9  $\mu$ mol, 23 eq.) of **97** to an EPR silent sample of 0.82 mg (514 nmol, 1.0 eq.) of **95** in 200  $\mu$ l of toluene and standing at r.t. for 3h.

**UV/Vis** (toluene): 392 (86, *Soret*); 447 (100, *Soret*); very poorly resolved bands at ~530 (19), 580 (14) and 760 (5).

**Chloro(5,10,15,20-tetrachloromesoporphyrinato) iron (III) (92)**

30.2 mg (36.7  $\mu\text{mol}$ , 1.0 eq.)  $\text{Fe}(\text{Cl}_4\text{-MP-DME})\text{Cl}$  (**93**) were dissolved in 6.0 ml THF and 3.0 ml 1 M LiOH-solution were added. The mixture was stirred vigorously at r.t. overnight. Then it was poured to 40 ml of  $\text{CH}_2\text{Cl}_2$  and 50 ml of 0.2 M HCl. The organic layer was washed with further 50 ml of 0.2 M HCl and the solvent removed in vacuo to obtain 31.0 mg (quant.) of a dark green solid.

UV/Vis ( $\text{CH}_2\text{Cl}_2$ ): 395 (97, *Soret*); 443 (100, *Soret*); poorly resolved bands at 534 (14), 582 (11), 758 (4).

$^1\text{H-NMR}$  (600 MHz,  $\text{CDCl}_3$ ): 48.8 (*s*, 3H, H 2<sup>1</sup>,7<sup>1</sup>,12<sup>1</sup>,18<sup>1</sup>); 47.9 (*s*, 3H, H 2<sup>1</sup>,7<sup>1</sup>,12<sup>1</sup>,18<sup>1</sup>); 45.3 (*s*, 3H, H 2<sup>1</sup>,7<sup>1</sup>,12<sup>1</sup>,18<sup>1</sup>); 44.7 (*s*, 3H, H 2<sup>1</sup>,7<sup>1</sup>,12<sup>1</sup>,18<sup>1</sup>); 41.8-39.2 (*m*, 4H, H 3<sup>1</sup>,8<sup>1</sup>,13<sup>1</sup>,17<sup>1</sup>); 37.0-33.5 (*m*, 4H, H 3<sup>1</sup>,8<sup>1</sup>,13<sup>1</sup>,17<sup>1</sup>); 14.4 (*br*, 2H, H 13<sup>3</sup>,17<sup>3</sup>); 6.59 (*s*, 6H, H 3<sup>2</sup>,8<sup>2</sup>); 5.90-5.10 (*m*, 4H, H 13<sup>2</sup>,17<sup>2</sup>).

MALDI-TOF-MS (4-Nitroaniline): 756 (100, [*M-Cl*]); 791 (17, [*M*]).

HPLC (XDB-C8, 150 x 4.6 mm, Imidazole/HCl-buffer (500 mM, pH 7.00) / MeOH 1/3 for 20 min, flow 1.0 ml/min, DAD ( $\lambda_{\text{det}} = 430 \text{ nm}$ , T = 25 °C):  $R_t = 7.3 \text{ min}$ .

**5.2.5 Catalytic Experiments applying the Modified Cofactor****Epoxidation reactions**

5.60 mg (6.81  $\mu\text{mol}$ , 1.0 eq.) of **93** (resp. 4.66 mg of **96**) were dissolved in 1 ml of  $\text{CH}_2\text{Cl}_2$  and 10.0  $\mu\text{l}$  (38.4  $\mu\text{mol}$ , 5.6 eq.) of internal standard (C-14 alkane), 80.0  $\mu\text{l}$  (452  $\mu\text{mol}$ , 66 eq.) of *cis*-stilbene (**49**) and 20.6 mg (93.8  $\mu\text{mol}$ , 13.8 eq.) of PhIO were consecutively added and washed down with an additional 1 ml of  $\text{CH}_2\text{Cl}_2$ . The mixture was vigorously stirred at r.t. under the exclusion of light and aliquots were consecutively taken. The latter were filtrated over silica to separate PhIO, partially evaporated at reduced pressure and injected into GC-FID. Yields were determined relative to the internal standard. Product identification was ensured by coinjection of commercially available product compounds.

Blank reactions were performed under identical conditions omitting iron porphyrin catalysts (**93/96**).

# **Appendix**



## 6 Appendix

### 6.1 Abbreviations

$\mu\text{g}$	micrograms
$\mu\text{l}$	microliters
Alox B	basic aluminiumoxide
Alox N	neutral aluminiumoxide
$\text{BF}_3 \cdot \text{OEt}_2$	Boron trifluoride diethyl etherate
$\text{BH}_3 \cdot \text{SMe}_2$	Borane dimethyl sulfide complex
BMP	heme domain of soluble P450 <sub>BM-3</sub>
BMR	reductase domain of soluble P450 <sub>BM-3</sub>
BNAH	1,2-benzyl-3-carbamoyl-1,4-dihydropyridine
conc.	concentrated
Cpd0	Compound 0
CpdI	Compound I
CV	cyclic voltametry
cw	contiuous wave
Cys	Cystein
d	days
DDQ	2,3-Dichloro-5,6-dicyano- <i>p</i> -benzoquinone
DFT	Density function theory
DMF	dimethylformamide
DMSO	Dimethylsulfoxide
e.g.	for example (exempli gratia)
EA	elemental analysis
EDCI	1-(3-Dimethylaminopropyl)-3-ethylcarbodiimide hydrochloride
EI	electron impact
EPR	electron paramagnetic resonance
eq.	equivalents
ESI	electron spray ionisation
$\text{Et}_3\text{N}$	Triethylamine
EtOAc	ethylacetate
FAD	Flavin adenin dinucleotide
FID	Flame ionisation detection
FMN	Flavin mononucleotide
FT	Fourier transformation
g	grams
GC	Gas chromatography
h	hours
HAT	hydrogen atom transfer
HCl	hydrochloric acid
His	Histidine
HOMO	highest occupied molecular orbital
HPLC	high performance liquid chromatography
HS	high spin
IR	Infrared

---

K	Kelvin
KOMe	potassium methoxide
LDI	laser desorption ionisation
LS	low spin
LUMO	lowest unoccupied molecular orbital
M	molar
MALDI	Matrix-assisted laser desorption ionisation
<i>m</i> CPBA	<i>m</i> -chloroperbenzoic acid
MeCN	acetonitrile
MeI	Methyliodide
MeOH	Methanol
mg	milligrams
MHz	Megahertz
min	minutes
ml	milliliters
MS	Mass spectroscopy
MsCl	Methanesulfonylchloride
mV	millivolt
N	normal
NAD <sup>+</sup>	Nicotinamide adenine dinucleotide
NADP <sup>+</sup>	Nicotinamide adenine dinucleotide phosphate
NaOH	Sodium hydroxide
NaOMe	sodium methoxide
<i>n</i> Bu <sub>4</sub> NHSO <sub>5</sub>	Tetra- <i>n</i> -butylammonium-peroxymonosulfate
NCS	N-chlorosuccinimide
NH <sub>4</sub> OAc	ammoniumacetate
NMO	N-Methyl-morpholine
NMR	nuclear magnetic resonance
PhIO	Iodosobenzene
pP-IX	protoporphyrin IX
ppm	parts per million
quant.	quantitatively
r.t.	room temperature
sat.	saturated
SCE	standard callomel electrode
sec	seconds
SET	single electron transfer
SHE	standard hydrogen electrode
SiO <sub>2</sub>	silica gel
T	Temperature
TBPH	2,4,6-tri- <i>tert</i> -butylphenol
TFA	Trifluoroacetic acid
THF	tetrahydrofurane
TLC	thin layer chromatography
TMOF	Trimethyl orthoformate
TMS	trimethylsilyl-
TOF	Time of flight
TON	Turn over number
UV/Vis	Ultra violet - visible light absorption
vs.	versus



## 6.2 References

1. Klingenberg, M., *Arch. Biochem. Biophys.* **1958**, 75, 376.
2. Omura, T.; Sato, R., *J. Biol. Chem.* **1962**, 237, 1375.
3. Ortiz de Montellano, P. R., *Cytochrome P450 Structure, Mechanism, and Biochemistry*. third edition ed.; Plenum press: New York, 2005.
4. Meunier, B.; de Vissier, S. P.; Shaik, S., *Chem. Rev.* **2004**, 104, (9), 3947-3980.
5. G. A. Roberts, G. G., A. Greter, S. L. Flitsch, N. J. Turner, *J. Bacteriol.* **2002**, 184, 3893.
6. Poulos, T. L.; Finzel, B. C.; Howard, A. J., *Biochemistry* **1986**, 25, 5314-5322.
7. Fulco, A. J., *Annu. Rev. Pharmacol. Toxicol.* **1991**, 31, 177-203.
8. Munro, A. W.; Leys, D.; McLean, K. L.; Marshall, K. R.; Ost, T. W. B.; Daff, S.; Miles, C. S.; Chapman, S. K.; Lysek, D. A.; Moser, C. C.; Page, C. C.; Dutton, P. L., *Trends Biochem. Sci.* **2002**, 27, (5), 250.
9. M. Hecker, V. U., *J. Biol. Chem.* **1989**, 264, 141.
10. W. C. Song, A. R. B., *science* **1991**, 253, 781.
11. S. Adachi, T. L., A. Nakagawa, K. Nakahara, H. Nakamura, E. Obayashi, S.-Y. Park, H. Shimizu, Y. Shiro, H. Shoun, I. Tanaka, *Nat. Struct. Biol.* **1997**, 4, 827.
12. D. R. Nelson, <http://drnelson.utmem.edu/CytochromeP450.html>.
13. Groves, J. T., *J. Chem. Educ.* **1985**, 62, 928-931.
14. Bangcharoenpaupong, O.; Rizos, A.; Champion, P.; Jollie, D.; Sligar, S. G., *J. Biol. Chem.* **1986**, 261, 8089-8090.
15. Sharrock, M.; Münck, E.; Debrunner, P. G.; Marshall, V.; Lipscomb, J. D.; Gunsalus, I. C., *Biochemistry* **1973**, 12, (2), 258-265.
16. Newcomb, M.; Shen, R.; Choi, S.-Y.; Toy, P. H.; Hollenberg, P. F.; Vaz, A. D. N.; Coon, M. J., *J. Am. Chem. Soc.* **2000**, 122, (12), 2677-2686.
17. Newcomb, M.; Toy, P. H., *Acc. Chem. Res.* **2000**, 33, 449-455.
18. Shaik, S.; Filatov, M.; Schröder, D.; Schwarz, H., *Chem. Eur. J.* **1998**, 4, (2), 193-199.
19. Shaik, S.; de Visser, S. P.; Ogliaro, F.; Schwarz, H.; Schröder, D., *Curr. Opin. Chem. Biol.* **2002**, 6, 556-567.
20. Sbaragli, L.; Woggon, W.-D., *Synthesis* **2005**, 9, 1538.
21. Walker, F. A., *Encyclopedia of Inorganic Chemistry*. John Wiley&Sons: Chichester, 1987; Vol. 4.
22. Collman, J. P.; Groh, S. E., *J. Am. Chem. Soc.* **1982**, 104, 1391.
23. Patzelt, H.; Woggon, W.-D., *Helv. Chim. Acta* **1992**, 75, 523.
24. Wagenknecht, H.-A.; Woggon, W.-D., *angew. Chem. Int. Ed.* **1997**, 36, 390.
25. Poulos, T. L., *J. Biol. Inorg. Chem.* **1996**, 1, 356-359.
26. Ueyama, N.; Nishikawa, N.; Yamada, Y.; Okamura, T.-a.; Nakamura, A., *J. Am. Chem. Soc.* **1996**, 118, 12826-12827.
27. Omura, T.; Sato, R.; Cooper, D. Y.; Rosenthal, O.; Estabrook, R. W., *Federation Proc.* **1965**, 24, 1181.
28. Shikita, M.; Hall, P. F., *proc. Nat. Acad. Sci. U. S. A.* **1974**, 71, (4), 1441.

29. Lieberman, S.; Lin, Y. Y., *J. Steroid Biochem. Mol. Biol.* **2001**, 78, 1.
30. Stock, J. E.; De Voss, J. J., *Arch. Biochem. Biophys.* **2000**, 384, 351.
31. Cryle, M. J.; De Voss, J. J., *Chem. Commun.* **2004**, 86.
32. Murray, R. I.; Sligar, S. G., *J. Am. Chem. Soc.* **1985**, 107, (7), 2186-7.
33. Okamoto, T.; Sasaki, K.; Shimada, M.; Oka, S., *Chem. Commun.* **1985**, (7), 381-3.
34. Okamoto, T.; Sasaki, K.; Oka, S., *J. Am. Chem. Soc.* **1988**, 110, (4), 1187-96.
35. Okamoto, T.; Sasaki, K.; Takano, M.; Oka, S., *Chem. Lett.* **1988**, (3), 415-16.
36. Ito, Y., *Chem. Commun.* **1991**, (9), 622-4.
37. Ito, Y.; Kunimoto, K.; Miyachi, S.; Kako, T., *Tetrahedron Lett.* **1991**, 32, (32), 4007-10.
38. Warman, A. J.; Roitel, O.; Neeli, R.; Girvan, H. M.; Seward, H. E.; Murray, S. A.; McLean, K. L.; Joyce, M. G.; Toogood, H.; Holt, R. A.; Leys, D.; Scrutton, N. S.; Munro, A. W., *Biochem. Soc. Trans.* **2005**, 33, (4), 747.
39. Ravichandran, K. G.; Boddupalli, S. S.; Hasemann, C. A.; Peterson, J. A.; Deisenhofer, J., *Science* **1993**, 261, 731-736.
40. Li, H.; Poulos, T. L., *Nat. Struct. Biol.* **1997**, 4, 140.
41. Noble, M. A. e. a., *Biochem. J.* **1999**, 339, 371.
42. Oliver, C. F.; Modi, S.; Sutcliffe, M. J.; Primrose, W. U.; Lian, L. Y.; Roberts, G. C., *biochemistry* **1997**, 36, 1567.
43. Li, Q.-S.; Schwaneberg, U.; Fischer, P.; Schmid, R. D., *Chem. Eur. J.* **2000**, 6, (9), 1531-1536.
44. Wong, T. S.; Arnold, F. H.; Schwaneberg, U., *Biotechnol. Bioeng.* **2004**, 85, (3), 351.
45. Neeli, R.; Roitel, O.; Scrutton, N. S.; Munro, A. W., *J. Biol. Chem.* **2005**, 280, 17634.
46. Udit, A. K.; Arnold, F. H.; Gray, H. B., *J. Inorg. Biochem.* **2004**, 98, 1547.
47. Meinhold, P.; Peters, M. W.; Hartwick, A.; Hernandez, A. R.; Arnold, F. H., *Adv. Synth. Catal.* **2006**, 348, 763.
48. Graham-Lorence, S. e. a., *J. Biol. Chem.* **1997**, 272, 1127.
49. Cirino, P. C.; Arnold, F. H., *Angew. Chem. Int. Ed.* **2003**, 42, 3299.
50. Salazar, O.; Cirino, P. C.; Arnold, F. H., *ChemBioChem* **2003**, 4, 891.
51. Lu, Y.; Berry, S. M.; Pfister, T. D., *Chem. Rev.* **2001**, 101, 3047-3080.
52. Wagner, G. C.; Perez, M.; Toscano, W. A.; Gunsalus, I. C., *J. Biol. Chem.* **1981**, 256, (12), 6262.
53. Pikuleva, I. A.; Lapko, A. G.; L., C., *J. Biol. Chem.* **1992**, 267, (3), 1438.
54. Modi, S.; Primrose, W. U.; Lian, L. Y.; Roberts, C. K., *Biochem. J.* **1995**, 310, 939.
55. Peterson, J. A., *unpublished results*.
56. Yamamoto, Y.; Hirai, Y.; Suzuki, A., *J. Biol. Inorg. Chem.* **2000**, 5, 455.
57. Makris, T. M.; von Koenig, K.; Schlichting, I.; Sligar, S., G., *J. Inorg. Biochem.* **2006**, 100, 507.
58. Woggon, W.-D., *Acc. Chem. Res.* **2005**, 38, 127.
59. Kozuch, S.; Leifels, T. R.; Meyer, D.; Sbaragli, L.; Shaik, S.; Woggon, W.-D., *Synlett* **2005**, 4, 675.
60. Murray, K. S., *Coord. Chem. Rev.* **1974**, 12, 1.
61. Stäubli, B. *Synthese von Modellverbindungen von Cytochrome P-450*, PhD thesis, University of Zürich, 1989.
62. Leifels, T. R. *Cytochrom P450 -Synthese von Modellverbindungen-*, PhD thesis, University of Basel, 2003.

63. Sbaragli, L. Radical Clock Investigation with a MetalloPorphyrin Enzyme Model, PhD Thesis, University of Basel, 2005.
64. Lee, C.-H.; Lindsey, J. S., *Tetrahedron* **1994**, 50, (39), 11427.
65. Stäubli, B.; Fretz, H.; Piantini, U.; Woggon, W.-D., *Helv. Chim. Acta* **1987**, 70, 1173-1193.
66. Arsenault, G. P.; Bullock, E.; MacDonald, S. F., *J. Am. Chem. Soc.* **1960**, 82, 4384.
67. Littler, B. J.; Ciringh, Y.; Lindsey, J. S., *J. Org. Chem.* **1999**, 64, 2864-2872.
68. McOmie, J. F. W.; Watts, M. L.; West, D. E., *Tetrahedron* **1968**, 24, 2289.
69. Lochner, M. Synthesis and Characterisation of Iron Porphyrin Model Compounds Mimicking the Resting State of Cytochrome P450cam (CYP101), PhD thesis, University of Basel, 2003.
70. Travis, B. R.; Ciaramitaro, B. P.; Borhan, B., *Eur. J. Org. Chem.* **2002**, 3429.
71. Meyer, D.; W.-D., W., *Chimia* **2005**, 59, 85.
72. *Crystallographic data (excluding structure factors) for the structures of 26 and 27 have been deposited with the Cambridge Crystallographic Data Center, the deposition numbers being 279642 and 279643. Copies of the data can be obtained, free of charge, on application to the CCDC, 12 Union Road, Cambridge CB2 1EZ, UK [fax: +44-1223-336033 or e-mail: deposit@ccdc.cam.ac.uk].*
73. Pavlishchuk, V. V.; Addison, A. W., *Inorg. Chim. Acta* **2000**, 298, 97.
74. Noviadri, I.; Brown, K. N.; Fleming, D. S.; Gulyas, P. T.; Lay, P. A.; Masters, A. F.; Phillips, L., *J. Phys. Chem. B* **1999**, 103, 6713.
75. Groves, J. T.; Watanabe, Y., *J. Am. Chem. Soc.* **1988**, 110, 8443.
76. Weiss, R.; Gold, A.; Trautwein, A. X.; Turner, J., *The Porphyrin Handbook*. Academic Press: 2000; Vol. 4.
77. Hessenauer-Illicheva, N.; Franke, A.; Meyer, D.; Woggon, W.-D.; van Eldik, R., *paper in preparation*.
78. Yamaguchi, K.; Watanabe, Y.; Morishima, I., *Inorg. Chem.* **1992**, 31, (2), 156-7.
79. Meyer, D.; Leifels, T. R.; Sbaragli, L.; Woggon, W.-D., *Biochem. Biophys. Res. Commun.* **2005**, 338, 372.
80. Pan, Z.; Zhang, R.; Newcomb, M., *J. Inorg. Biochem.* **2006**, (100), 524.
81. Shannon, P.; Bruice, T. C., *J. Am. Chem. Soc.* **1981**, 103, (15), 4580.
82. Nee, M. W.; Bruice, T. C., *J. Am. Chem. Soc.* **1982**, 104, (22), 6123.
83. Powell, M. F.; Pai, E. F.; Bruice, T. C., *J. Am. Chem. Soc.* **1984**, 106, (11), 3277.
84. Dicken, C. M.; Lu, F. L.; Nee, M. W.; Bruice, T. C., *J. Am. Chem. Soc.* **1985**, 107, (20), 5776.
85. Woon, T. C.; Dicken, C. M.; Bruice, T. C., *J. Am. Chem. Soc.* **1986**, 108, (25), 7990.
86. Dicken, C. M.; Woon, T. C.; Bruice, T. C., *J. Am. Chem. Soc.* **1986**, 108, (7), 1636.
87. Ostovic, D.; Knobler, C. B.; Bruice, T. C., *J. Am. Chem. Soc.* **1987**, 109, (11), 3444.
88. Bruice, T. C.; Dicken, C. M.; Balasubramanian, P. N.; Woon, T. C.; Lu, F. L., *J. Am. Chem. Soc.* **1987**, 109, (11), 3436.
89. Heimbrook, D. C.; Murray, R. I.; Egeberg, K. D.; Sligar, S. G.; Nee, M. W.; Bruice, T. C., *J. Am. Chem. Soc.* **1984**, 106, (5), 1514-15.
90. Dowers, T. S.; Rock, D. A.; Rock, D. A.; Jones, J. P., *J. Am. Chem. Soc.* **2004**, 126, (29), 8868-8869.
91. Shaffer, C. L.; Harriman, S.; Koen, Y. M.; Hanzlik, R. P., *J. Am. Chem. Soc.* **2002**, 124, (28), 8268-8274.
92. Bhakta, M. N.; Wimalasena, K., *J. Am. Chem. Soc.* **2002**, 124, (9), 1844-1845.

93. Dupau, P.; Epple, R.; Thomas, A. A.; Fokin, V. V.; Sharpless, K. B., *Adv. Synth. Catal.* **2002**, 344, 421.
94. Hashimoto, N.; Aoyama, T.; Shioiri, T., *Chem. Pharm. Bull.* **1981**, 29, (5), 1475-1478.
95. Szacilowski, K.; Chmura, A.; Stasicka, Z., *Coord. Chem. Rev.* **2005**, 249, 2408.
96. Hoshino, M.; Laverman, L.; Ford, P. C., *Coord. Chem. Rev.* **1999**, 187, 75.
97. Franke, A.; Hessnauer-Illicheva, N.; Meyer, D.; Stochel, G.; Woggon, W.-D.; Van Eldik, R., *J. Am. Chem. Soc.* **2006**, 128, 13611.
98. Franke, A.; Stochel, G.; Jung, C.; Van Eldik, R., *J. Am. Chem. Soc.* **2004**, 126, 4181.
99. Watan, A.; Wolak, M.; Orzel, L.; Brindell, M.; Van Eldik, R.; Stochel, G., *Coord. Chem. Rev.* **2002**, 229, 37.
100. Dolphin, D.; Traylor, T. G.; Xie, L. Y., *Acc. Chem. Res.* **1997**, 30, 251.
101. Mansuy, D., *Coord. Chem. Rev.* **1993**, 125, 129.
102. Fischer, H.; Röse, H., *Ber.* **1913**, 46, 2460.
103. Bonnett, R.; Gale, I. A. D.; Stephenson, G. F., *J. Chem. Soc. (C)* **1966**, 1600.
104. Gong, L.-C.; Dolphin, D., *Can. J. Chem.* **1985**, 63, 401.
105. Forrer, O. Beeinflussung der Redoxpotentiale von P450 Enzymmodellen durch substitution mit NO<sub>2</sub>-Gruppen am Porphyrin und den Liganden, PhD Thesis, University of Basel, 1998.
106. Haddad, R. E.; Gazeau, S.; Pecaut, J.; Marchon, J.-C.; Medforth, C. J.; Shelnutt, J. A., *J. Am. Chem. Soc.* **2003**, 125, (5), 1253.
107. Andrews, L. E.; Bonnett, R.; Kozyrev, A. N.; Appelman, E. V., *J. Chem. Soc., Perkin Trans. 1* **1988**, 1735.
108. Soydaner, M. A. U. Synthesis and Computational Study of *Meso*-perhalogenated Protoporphyrin-IX Complexes-towards Hybrid CYP Enzymes, diploma thesis, University of Basel, 2005.
109. Podstawka, E.; Proniewicz, L. M., *J. Inorg. Biochem.* **2004**, 98, 1502.
110. Mie, Y.; Kishita, M.; Neya, S.; Funasaki, N.; Mizutani, F.; Nishiyama, K.; Taniguchi, I., *J. Electroanal. Chem.* **2006**, 588, 226.
111. Monroe, M. <http://ncrr.pnl.gov/software/MWCalculator.stm>.
112. Sparks, L. D.; Medforth, C. J.; Park, M. S.; Chamberlain, J. R.; Ondrias, M. R.; Senge, M. O.; Smith, K. M.; Shelnutt, J. A., *J. Am. Chem. Soc.* **1993**, 115, (2), 581-92.
113. Cheng, R.-J.; Chen, P.-Y.; Gau, P.-R.; Chen, C.-C.; Peng, S.-M., *J. Am. Chem. Soc.* **1997**, 119, 2563.
114. Budd, D. L.; La Mar, G. N.; Langry, K. C.; Smith, K. M.; Nayyir-Mazhir, R., *J. Am. Chem. Soc.* **1979**, 101, (20), 6091.
115. La Mar, G. N.; Eaton, G. R.; Holm, R. H.; Walker, F. A., *J. Am. Chem. Soc.* **1973**, 95, (1), 63-75.
116. Wicholas, M.; Mustacich, R.; Jayne, D., *J. Am. Chem. Soc.* **1972**, 94, (13), 4518.
117. Van Camp, H. L.; Scholes, C. P.; Mulks, C. F., *J. Am. Chem. Soc.* **1976**, 98, (14), 4094.
118. Tang, S. C.; Koch, S.; Papaefthymiou, G. C.; Foner, S.; Frankel, R. B.; Ibers, J. A.; Holm, R. H., *J. Am. Chem. Soc.* **1976**, 98, (9), 2414.
119. Ueyama, N.; Nishikawa, N.; Yamada, Y.; Okamura, T.-a.; Oka, S.; Sakurai, H.; Nakamura, A., *Inorg. Chem.* **1998**, 37, 2415-2421.
120. Arasasingham, R. D.; Balch, A. L.; Cornman, C. R.; de Ropp, J. S.; Eguchi, K.; La Mar, G. N., *Inorg. Chem.* **1990**, 29, 1847-1850.
121. Groves, J.; Nemo, T. E., *J. Am. Chem. Soc.* **1983**, 105, 5786.

122. Becker, E. D.; Bradley, R. B.; Watson, C. J., *J. Am. Chem. Soc.* **1961**, 83, 3743.
123. Grinstein, M., *J. Biol. Chem.* **1947**, 167, 515.



## 6.3 Curriculum Vitae

### *Personalien*

Name	Dominik Büttiker (geb. Meyer)
Geburtsdatum	18. April 1977
Zivilstand	verheiratet
Nationalität	Schweizer
Heimatort	Basel

### *Ausbildung*

<b>1984-1993</b>	Rudolf Steiner Schule Basel
<b>1993-1997</b>	Mathematisch-Naturwissenschaftliches Gymnasium Basel
<b>Juni 1997</b>	Matura Typus C (Maturandenpreis der Novartis)
<b>Juli-Nov. 1997</b>	Rekrutenschule
<b>Jan.-Mai 1998</b>	Unteroffiziersschule und Abverdienen des Unteroffiziergrades
<b>Okt. 1998</b>	Beginn des Chemiestudiums an der Universität Basel
<b>Sept.-Okt. 2001</b>	Forschungsarbeiten an der Universität Cardiff (Wales)
<b>2002</b>	Diplom in Chemie
<b>2003-2007</b>	Doktorarbeit in der Forschungsgruppe von Prof. Dr. W.-D. Woggon am Departement Chemie der Universität Basel

### *Weitere Tätigkeiten*

<b>2003-2007</b>	Assistierenden-Vertreter in Departement Chemie
<b>2004-2007</b>	Assistierenden-Vertreter in der Philosophisch-Naturwissenschaftlichen Fakultät und deren Prüfungskommission
<b>2005-2007</b>	Assistenz im organisch-chemischen Praktikum für Studierende der Nanowissenschaften
<b>2006</b>	Assistenz Übungen: Einführung in die Chemie II für Studierende der Naturwissenschaften

## 6.4 Publications and Presentations

- 1 C. Meyer, D. Meyer, T. A. Bickle, B. Giese, "Chemical Restriction: Strand Cleavage by Ammonia Treatment at 8-Oxoguanine Yields Biologically Active DNA", *ChemBioChem*, **2003**, 4, 610.
- 2 A. Boye, D. Meyer, C. Ingison, A. French, T. Wirth, "Novel Lactonization with Phenonium Ion Participation Induced by Hypervalent Iodine Reagents", *Org. Lett.*, **2003**, 5(12), 2157.
- 3 D. Meyer, W.-D. Woggon, "Synthesis and Characterization of a New Family of Iron Porphyrins", Posterpräsentation im Rahmen des 24. Regiosymposiums über Organische und Bioorganische Chemie, 29. Sept. -01. Okt. **2004**, Lucelle (FR).
- 4 D. Meyer, W.-D. Woggon, "Synthesis and Characterization of a New Family of Iron Porphyrins" Vortrag im Rahmen der Herbstversammlung der Schweizerischen Chemischen Gesellschaft, 07. Okt. **2004**, Universität Zürich. Mettler Toledo Award for Best Oral Presentation.
- 5 D. Meyer, W.-D. Woggon, "Synthesis and Characterization of a New Family of Iron Porphyrins", *Chimia*, **2005**, 59(3), 85.
- 6 S. Kozuch, T. Leifels, D. Meyer, L. Sbaragli, S. Shaik, W. -D. Woggon, "New Synthetic Models of Cytochrome P450: How Different Are They from the Natural Species?", *Synlett*, **2005**, 4, 675.
- 7 D. Meyer, T. Leifels, L. Sbaragli, W. -D. Woggon, „Reactivity of a new Class of P450 enzyme models“, *Biochem. Biophys. Res. Commun.*, **2005**, 338, 372.
- 8 D. Meyer, T. Leifels, L. Sbaragli, W. -D. Woggon, „Reactivity of a new Class of P450 enzyme models“, Posterpräsentation im Rahmen des 25. Regiosymposiums über Organische und Bioorganische Chemie, 28.-30. Sept. **2005**, Sornetan (CH). 1. Rang in der Poster-Preisverleihung.



- 9 D. Meyer, Wolf-D. Woggon, "New P450 Enzyme Models – Characterization, NO-binding and Reactivity", Vortrag im Rahmen des 1. Workshop of the International Research Training Group "Catalysts and Catalytic Reactions for Organic Synthesis" (GRK 1038), 24.-25. März **2006**, Universität Freiburg i. Br. (D).
- 10 A. Franke, N. Hessenauer-Ilicheva, D. Meyer, G. Stochel, W.-D. Woggon, R. van Eldik, "Thermodynamic and Kinetic Studies on the Binding of Nitric Oxide to a New Enzyme Mimic of Cytochrome P450", *J. Am. Chem. Soc.* **2006**, 128, 13611.
- 11 N. Hessenauer-Ilicheva, A. Franke, D. Meyer, W.-D. Woggon, R. Van Eldik, „Low Temperature Rapid-Scan Detection of Reactive Intermediates in Epoxidation Reactions Catalyzed by New Enzyme Mimic of Cytochrome P450”, *in preparation*.

## **6.5 Eidesstattliche Erklärung**

Hiermit erkläre ich an Eides statt, dass ich meine Dissertation selbständig und nur mit den darin angegebenen Hilfsmitteln verfasst habe. Ich erkläre ausserdem, dass ich diese Dissertation bei keiner anderen Universität und keiner anderen Fakultät der Universität Basel eingereicht habe.

Basel, den 10. April. 2007

Dominik Büttiker